International Scientific-Technical and Production Journal

The Paton WELDING JOURNAL

September 2012 # 9

English translation of the monthly «Avtomaticheskaya Svarka» (Automatic Welding) journal published in Russian since 1948

Founders: *E.O. Paton Electric Welding Institute of the NAS of Ukraine*
International Association «Welding»

Publisher: *International Association «Welding»*

Address:
E.O. Paton Electric Welding Institute,
International Association «Welding»,
11, Bozhenko str., 03680, Kyiv, Ukraine
Tel.: (38044) 200 82 77
Fax: (38044) 200 81 45
E-mail: journal@paton.kiev.ua
URL: www.rucont.ru

State Registration Certificate
KV 4790 of 09.01.2001

Subscriptions:
$324, 12 issues per year,
postage and packaging included.
Back issues available.

CONTENTS

FRICTION WELDING OF PIM HEAT-RESISTANT STEEL TO STEEL 40Kh

I.V. ZYAKHOR and **S.I. KUCHUK-YATSENKO**
E.O. Paton Electric Welding Institute, NASU, Kiev Ukraine

Experimental data are given on evaluation of structure of heat-resistant steel AISI310 produced by the powder injection moulding technology. The investigation results are presented on peculiarities of formation of dissimilar joints between steel AISI310 and structural steel 40Kh under different thermal-deformation cycles of friction welding in manufacture of bimetal shafts for automotive engine turbocharger rotors.

Keywords: *friction welding, bimetal joints, powder injection moulding, welded joints, turbocharger rotor shafts*

One of the new powder metallurgy methods is powder injection moulding [1–5], which in the English technical literature is collectively known as the PIM-technology. Powder injection moulding has been gaining an increasingly wider acceptance in the last years owing to a number of advantages over traditional methods of metal processing, first of all in manufacture of complex-geometry and mass-production parts. According to the data given in [3], density of the finished parts produced by the PIM-technology is 96 to 100 % of its theoretical value, while the detected pores and non-metallic inclusions have small sizes and a spherical shape, and are uniformly distributed in the bulk.

The promising market for the parts produced by the PIM-technology is the automotive engine construction industry. The issue of current importance in terms of technology and economy is application of the PIM-technology to manufacture complex-configuration parts. For example, these are wheels of bimetal shafts for automotive engine turbocharger rotors (TCR). Compared to the currently applied investment casting method, the PIM-technology provides an increased productivity, minimal possible deviations of sizes and a high quality of the surface of the wheels for the TCR shafts.

The technological cycle of manufacture of the bimetal TCR shafts provides for the use of friction welding (FW) of a heat-resistant alloy wheel to a structural steel shank. Friction welding is applied to advantage to join materials produced by the casting, thermo-mechanical deformation and powder metallurgy methods [6–8]. However, no information on application of FW for the parts produced by the PIM-technology has been found in technical literature so far. Therefore, it is of scientific and practical interest to study the effect of structure of the PIM-materials on the possibility of joining them to structural steel to manufacture bimetal TCR shafts.

The purpose of this study was to investigate formation of dissimilar joints between heat-resistant steel AISI310 produced by the PIM-technology and structural steel 40Kh under different thermal-deformation cycles of FW for manufacture of bimetal TCR shafts.

General view of the TCR shaft wheels made by the PIM-technology from steel AISI310 (feed stock — BASF «Catamold» [3]) is shown in Figure 1. Chemical composition of the materials welded, as well as their mechanical properties are given in the Table.

Austenitic stainless steel AISI310 (domestically produced analogue — steel 20Kh25N20S2 (EI283)) combines satisfactory heat resistance and high oxidation resistance at high temperatures. Bimetal TCR shafts were produced by join-

Chemical composition and mechanical properties of materials welded

Steel grade	Content of elements, wt.%							Mechanical properties			
	C	Cr	Nb	Si	Mn	Fe	Ni	σ_y, MPa	σ_t, MPa	δ, %	ψ, %
AISI310	<0.2	24–26	<0.2	1.5–2.0	1.0–1.4	Base	18–21	>205	>515	>40	>50
40Kh	0.36–0.40	0.8–1.1	–	<0.35	0.5–0.8	Same	<0.3	>720	>860	<14	<60

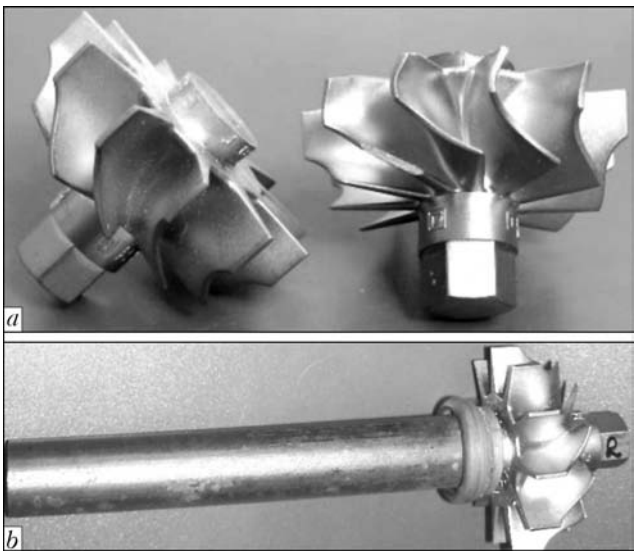

Figure 1. Wheels for TCR shafts of steel AISI310 produced by the PIM technology (*a*), and welded TCR shaft (*b*)

ing wheels of steel AISI310 to shanks of structural steel 40Kh under different conditions of conventional and combined FW [7, 8].

Experiments on FW were carried out by using machine ST120, which was upgraded to implement different thermal-deformation cycles corresponding to conventional, inertia and combined FW [9]. Structure of the materials welded and of the bimetal joints was examined by optical microscopy («Neophot-32», Germany) and by scanning electron microscopy (SEM) (JSM-35CA, JEOL, Japan). X-ray spectrum microanalysis (EDS-analyser INCA-459, «Oxford Instruments», Great Britain; probe diameter — approximately 1 μm) was conducted, and microhardness of the joining zone metal was measured under a load of 1–5 N (microhardness meter M400, LECO, USA).

Parameters of the FW process were varied within the following ranges: heating pressure P_h = 50–150 MPa, forge pressure P_f = 150–300 MPa, peripheral velocity v = 0.5–2.5 m/s,

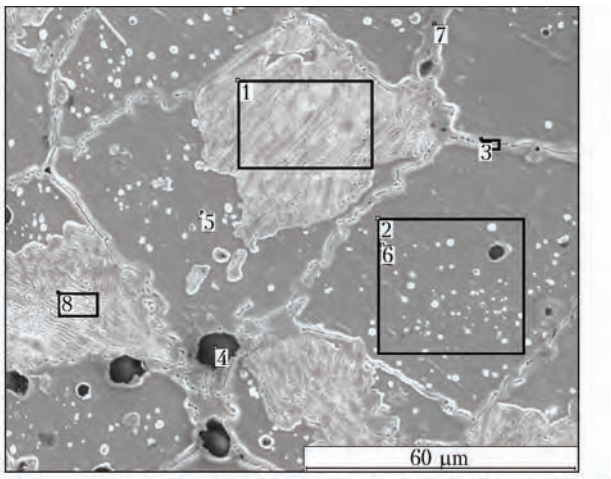

Spectrum	C	Si	Cr	Mn	Fe	Ni	Nb
1	0.14	0.63	19.13	0.69	52.76	24.19	2.44
2	0.11	1.19	24.30	0.10	50.18	21.69	2.43
3	0.18	0.88	21.40	1.12	53.87	22.57	0
4	0.42	83.91	8.49	1.61	2.97	1.46	1.14
5	0.40	1.02	24.65	0.94	51.73	21.18	0.08
6	0.12	0.72	24.37	1.12	52.62	20.15	0.90
7	0.16	0.28	24.49	0.29	53.16	21.61	0
8	0.20	0.90	18.35	1.30	56.84	21.45	0.96

Figure 3. Microstructure of the base metal of steel AISI310 (SEM), and results of X-ray spectrum microanalysis of metal of the investigated regions (wt.%)

heating time t_h = 5–30 s, deceleration time t_d = = 0.2–2.5 s, and burn-off rate v_b = 0.1–1.0 m/s. Diameter of the billets welded was 15 mm.

Microstructures of the base metal of steel AISI310 and compositions of structural components are shown in Figures 2 and 3. Steel AISI310 has equiaxed crystalline structure with grain size of about 60 μm. Optical microscopy allows revealing dark and light grains (Figure 2, *a*), individual pores with a size of up to 15 μm located along the grain boundaries, and randomly arranged particles of non-metallic SiO_2 inclusions with a size of 2–10 μm (Figure 3, spectrum 4).

Structure of the dark grains (see Figure 3, spectra 1 and 8) is lamellar, consisting of alternate light- and dark-etchable laminae less than 1 μm thick. The content of chromium in the grains

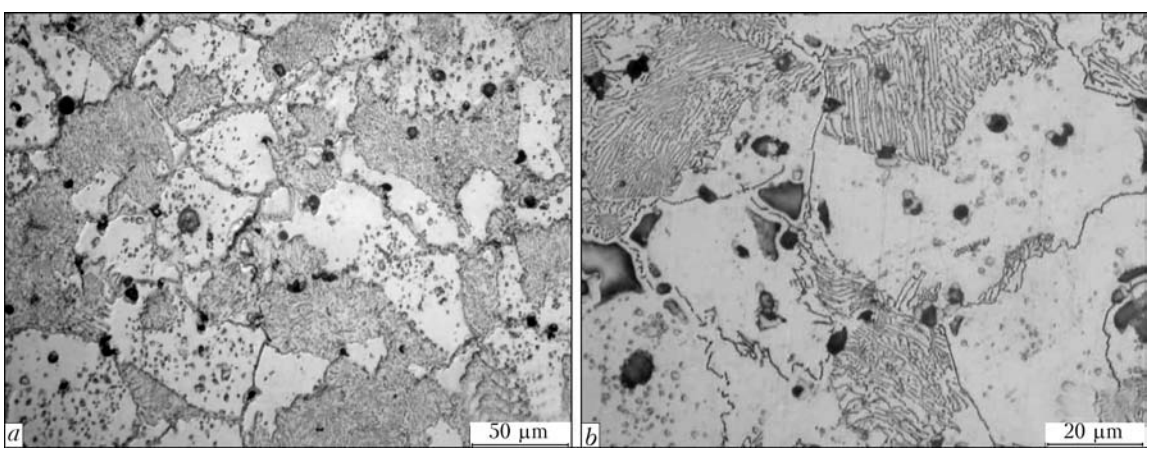

Figure 2. Microstructures of steel AISI310 (optical microscopy)

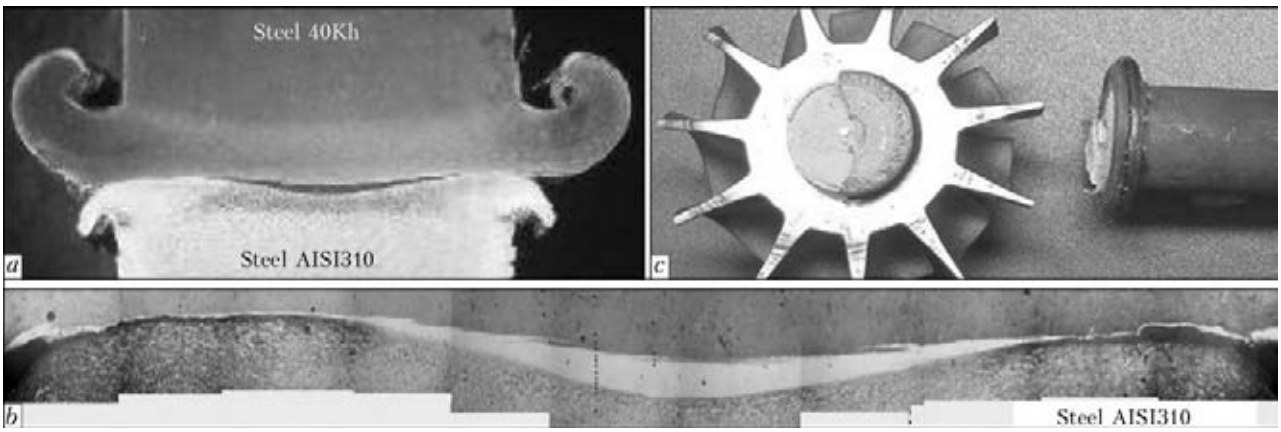

Figure 4. Macrosection of the AISI310–40Kh steel joint made in mode 1 (*a*), panoramic view of section of the welded joint (*b*), and welded TCR shaft after tensile tests (*c*)

with a lamellar structure is somewhat lower, compared to its content in the light grains. Chemical composition of the light grains (spectrum 2) corresponds to the requirements of standard AISI, except for the increased niobium content. Dispersed (1–2 μm) particles of a round shape (spectra 5 and 6) can be distinguished in the bulk of the light grains. These particles do not differ in chemical composition from those in the bulk of the dark grains. However, they have lower niobium content. No substantial liquation of alloying elements and impurities along the grain boundaries is fixed (spectra 3 and 7). Presence of the grains with a lamellar structure evidences that the sintering process was performed at a temperature close to T_S [10–12].

Formation of the dissimilar joints between steels AISI310 and 40Kh was investigated under different thermal-deformation cycles corresponding to conventional and combined FW.

Mode 1 («soft» mode) was conventional friction welding (CFW) [7, 8] with the minimal values of P_h, P_f and t_d, and the maximal values of v and t_h in the ranges under investigation. Mode 2 («rigid» mode) was CFW with the maximal values of P_h and P_f, and the minimal values of v, t_h and t_d in the ranges under investigation. Mode 3 was the technology developed by the E.O. Paton Electric Welding Institute for combined FW with controlled deformation. For this technology the values of v and P_h were set proceeding from the requirement to provide the certain deformation rate (burn-off rate) in heating, which was varied during the heating process within the $v_b = 0.1–1.0$ m/s range, forge pressure being applied at a stage of rotation deceleration regulated following the preset program [9]. In combined FW the values of t_h and t_d were set on the basis of the results of preliminary experiments, so that the total length loss for all the modes investigated was $\Delta_w = 6$ mm.

As seen from Figure 4, *a*, deformation of the billets during welding in mode 1 occurs mainly due to steel 40Kh. The transition zone with a width varying from 25 μm in the peripheral part of a section to about 500 μm at the centre, which

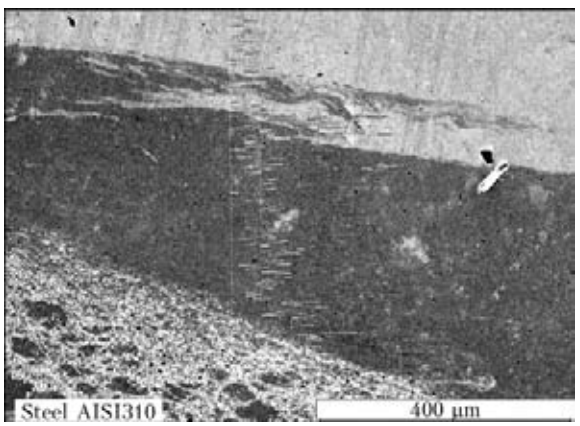

Figure 5. Microstructure of the AISI310–40Kh steel joint (mode 1)

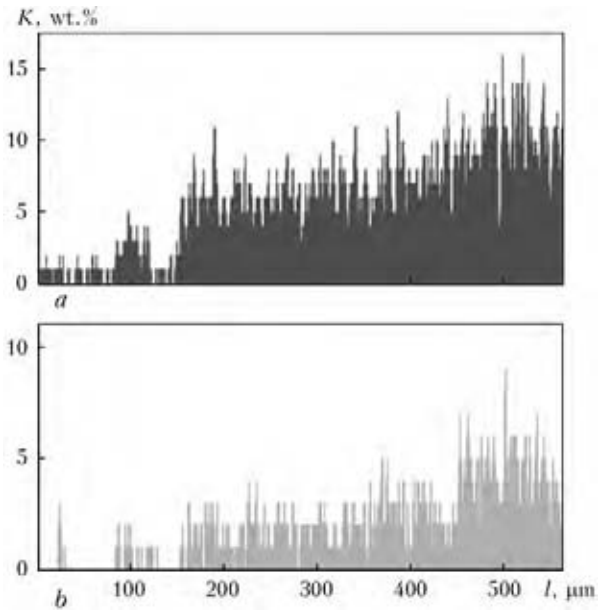

Figure 6. Distribution of chromium (*a*) and nickel (*b*) across the joining zone between steels AISI310 and 40Kh (mode 1)

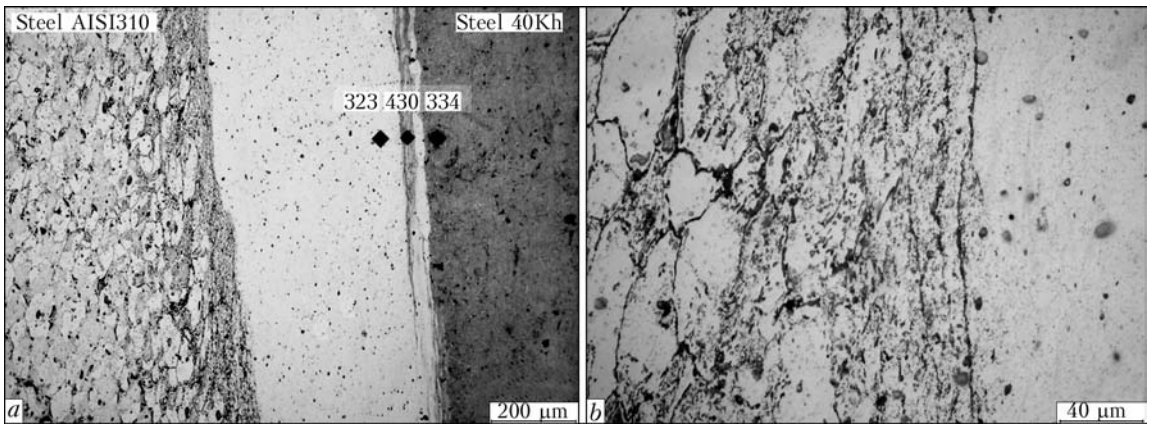

Figure 7. Microstructures of the transition zone (*a*) (indentations *HV*3, MPa·10^{-1}) and metal of the joint on the side of steel AISI310

is non-uniform across the sections of the billets, can be seen within the joining zone (see Figure 4, *b*).

X-ray spectrum microanalysis fixed a variable composition of the transition zone across the width (see Figures 5 and 6). The presence of uniformly distributed non-metallic SiO_2 inclusions in the transition zone proves that the latter forms on the side of steel AISI310. Size of the SiO_2 particles in the transition zone is 3–4 μm, this being indicative of their partial dissolution. Monotonous growth of the concentration of chromium and nickel in transition from steel 40Kh to steel AISI310 (Figure 6) may be related to diffusion migration of these elements during a comparatively long stage of friction heating (t_h = = 30 s). Interlayers of an intermediate composition (Figures 5 and 6), having an increased hardness (Figure 7), can be seen in the transition zone on the side of steel 40Kh. Formation of this composition of interlayers may result from dilution of contact volumes of metal of the steels welded in the liquid or solid-liquid state at the initial stages of FW. These interlayers lead to deterioration of ductility and decrease in corrosion resistance of the joints [13, 14].

Deformed, radially elongated grains can be seen in the zone of the thermal-deformation effect on the side of steel AISI310 (see Figure 7), residual porosity of the base metal being conserved in this zone. Steel AISI310 has a fibrous structure with structural components up to 10 μm in size in the immediate proximity to the transition zone. No segregations of non-metallic SiO_2 inclusions and porosity were detected in this zone.

Annealing and repeated etching of the welded joints were carried out to reveal structure of the transition zone. As a result, the transition zone was found to have a lamellar structure and a composition intermediate between the steels welded (Figure 8, spectra 3–8).

In tensile tests, fracture of the welded joints occurred in the joining zone (see Figure 6, *b*). Chemical composition of metal on both sides of the fracture was close to that of steel AISI310. Fractography of the fractures revealed the presence of the two types of fracture within the limits of a section, i.e. tough and quasi-brittle (Figure 9). The increased niobium content was detected over the entire fracture surface and, particularly, in the circumferential region of the quasi-brittle fracture (see Figure 9, spectrum 2).

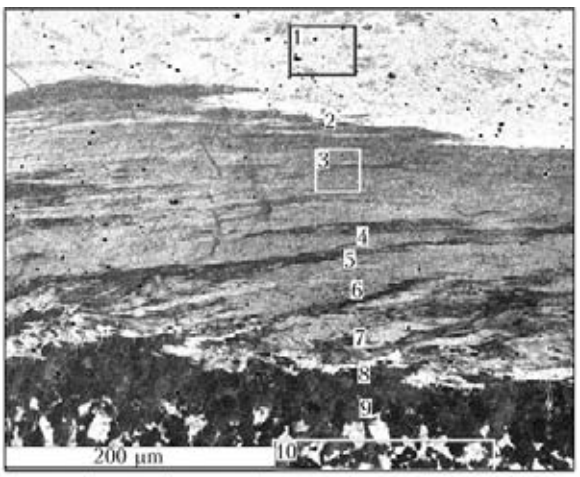

Spectrum	Si	Cr	Mn	Fe	Ni	Nb
1	1.77	21.93	0	51.76	22.20	2.33
2	0.85	16.51	0	57.09	25.55	0
3	0.82	12.77	1.52	72.14	11.05	1.70
4	0	10.65	0	80.97	8.38	0
5	0.62	11.38	1.33	73.68	13	0
6	0	10.05	1.55	74.22	12.86	1.32
7	0.49	10.83	1.45	71.76	15.47	0
8	0.67	8.62	0.97	81.25	8.49	0
9	0	0.78	1.18	98.04	0	0
10	0	1	0.99	98.01	0	0

Figure 8. Microstructure of the AISI310–40Kh steel joint made in mode 1 after annealing, and results of X-ray spectrum microanalysis of metal of the investigated regions (wt.%)

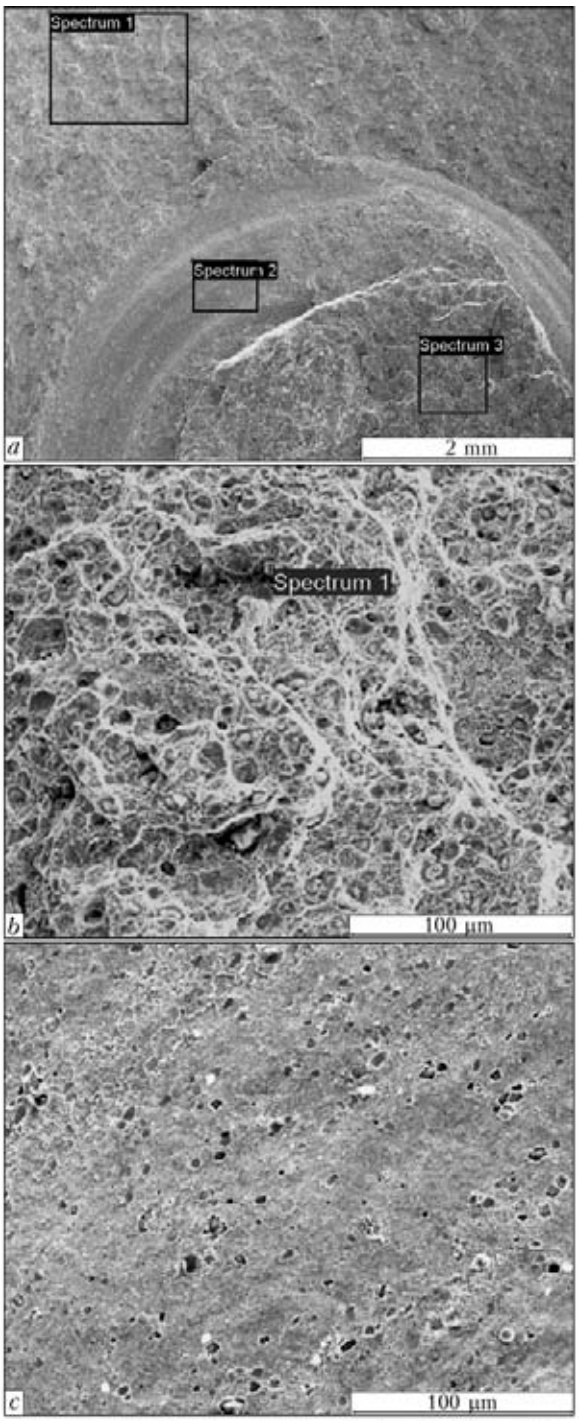

Spectrum	Si	Cr	Mn	Fe	Ni	Nb
1	2.91	22.20	0.42	51.57	16.74	6.16
2	1.64	25.11	0	40.17	16.88	16.20
3	3.16	25.03	2.66	44.15	20.24	4.75

Figure 9. Fracture surface of the AISI310–40Kh steel joint (mode 1) on the side of steel 40Kh (*a*), regions of tough (*b*) and quasi-brittle (*c*) fractures, and results of X-ray spectrum microanalysis of metal of the investigated regions (wt.%)

Results of the fractographic examinations show that fracture of the joints occurs between the transition zone and steel AISI310, and is localised in segregation clusters of the redundant phases with the increased niobium content.

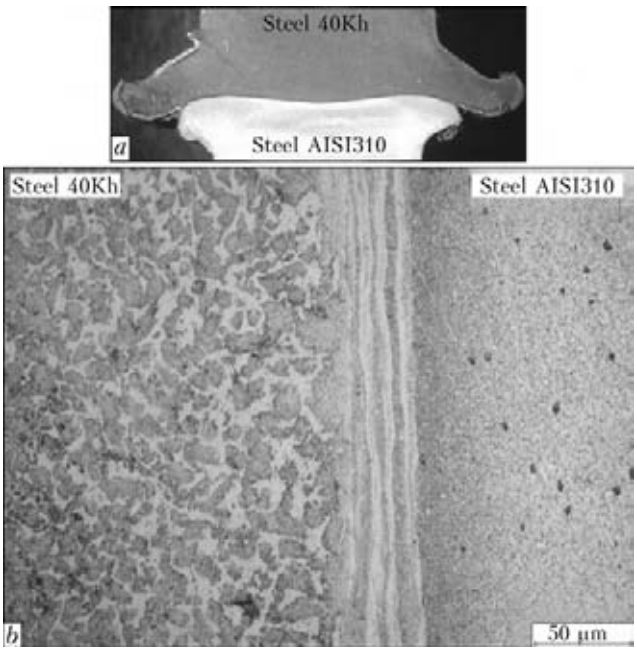

Figure 10. Macrosection (*a*) and microstructure (*b*) of the AISI310–40Kh steel joint (mode 2)

Therefore, the presence of an insignificant porosity and dispersed inclusions of SiO_2, having a high melting point (T_{melt} = 1713 °C), in the base metal of steel AISI310 does not exert any substantial effect on formation of the welded joints. At the same time, the presence of the segregations of niobium, which forms eutectic (T_{melt} = 1355 °C) with iron and leads to the «contact melting» phenomenon [15], in the base metal exerts a negative effect on the composition and mechanical properties of the joints in the «soft» mode of CFW.

Structure of the joint made in the «rigid» mode of CFW (mode 2, after annealing) is shown in Figure 10. The 40–60 μm wide transition zone, which is almost uniform across the section of the billets and consists of alternate layers with different etchability, was fixed in the joining zone. The character of variations in the concentrations of chromium and nickel (Figure 11) when passing from steel 40Kh to steel AISI310 cannot be caused by diffusion migration of these elements, but is a result of dilution of the steels welded.

Analysis of microstructure of the welded joints made at t_h = 0.5–1.5 s (initial stage of the FW process) showed that the lamellar structure of the joining zone was formed at the early stages of the FW process, and was determined by the character of contact interaction of the faying surfaces at the set level of the process parameters. At a low peripheral velocity and a high heating pressure the predominant mechanism of contact interaction at the initial stages of FW is the process of deep tearing out and dilution of contact

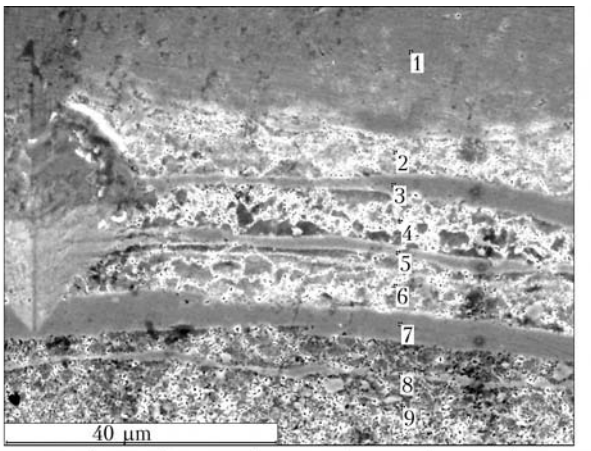

Spectrum	Si	Cr	Mn	Fe	Ni	Nb
1	0.47	0.62	0	98.60	0	0.31
2	0.83	5.49	1.35	73.78	18.54	0
3	0.84	4.28	1.01	90.03	3.84	0
4	1.78	5.01	0.39	63.81	27.04	1.97
5	0.23	8.10	1.86	71.49	18.32	0
6	0.59	8.45	1.03	67.30	22.14	1.49
7	0.61	6.40	0	87.76	5.23	0
8	1.56	13.55	1.46	63.58	19.53	0.32
9	1.33	11.46	0	54.60	25.37	7.24

Figure 11. Microstructure of the AISI310–40Kh steel joint (mode 2), results of SEM and X-ray spectrum microanalysis of metal of the investigated regions (wt.%)

volumes of the materials welded in the plasticised or solid-liquid state, going to a depth of several hundreds of microns [16, 17].

Therefore, the key feature of the joints made in the «rigid» mode of CFW is the presence of alternate constant-composition interlayers (Figure 11), including those corresponding to steels of the martensitic (see Figure 11, spectra 3 and 7) and austenitic grades (Figure 11, spectra 2, 4–6 and 8). It is commonly supposed [7, 8] that FW is a solid-state process of joining of materials. However, the presence of the lamellar structure consisting of alternate «alloys» of different compositions allows a conclusion that the local melting processes occurring in the contact interaction zone, at least at the initial stages of the FW process, play an important role in formation of the dissimilar joints.

No interlayers with the increased niobium content were fixed in the joint made in mode 2, despite the presence of local clusters of this element in the immediate proximity to the joining zone (see Figure 11, spectrum 9). The main difference between the «rigid» and «soft» modes of CFW consists in the burn-off rate during the friction heating process (v_b = 0.9 mm/s for mode 2, and 0.15 mm/s for mode 1). It is likely that a high burn-off rate and a short time of the heating stage (t_h = 6 s) in the «rigid» mode of CFW prevent formation of interlayers with the increased niobium content.

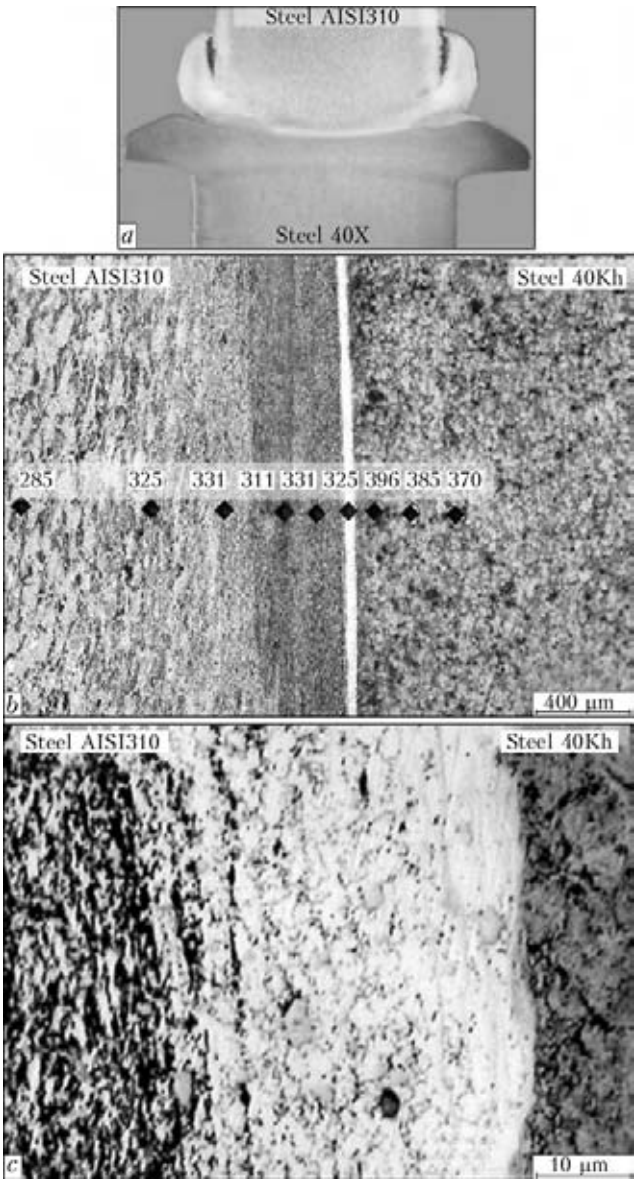

Figure 12. Macrosection (*a*) and microstructure (*b*) of the AISI310–40Kh steel joint, mode 3 (indentations *HV*3, MPa·10^{-1})

The joint made in mode 3 (combined FW with controlled deformation) was found to contain no increased-hardness interlayers. The up to 40 μm wide transition zone, being almost uniform across the section (Figure 12) and having a grain size of 5–6 μm, was fixed in this joint. The composition of metal of the transition zone across its width corresponded to that of steel of the austenitic grade (Figure 13, spectra 2, 3, 5–7), this preventing any decrease in corrosion resistance of the joints and eliminating the risk of cracking.

Of notice is the absence of local segregations of phases with the increased niobium content and the dramatic change in the concentrations of chromium and nickel in passing from steel 40Kh to steel AISI310, this being indicative of minimisation of dilution of the steels in the solid-liq-

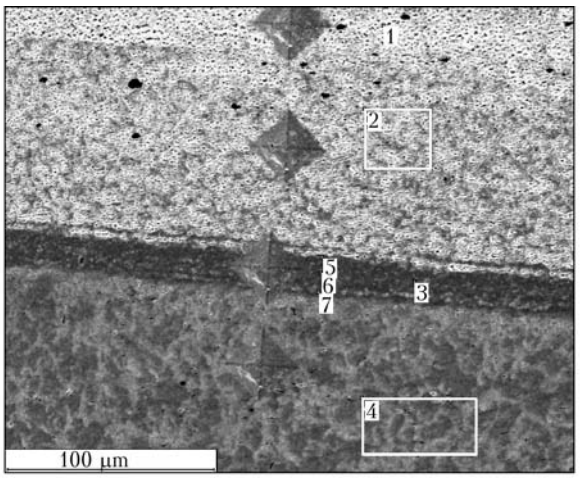

Spectrum	Si	Cr	Mn	Fe	Ni	Nb
1	1.71	26.15	1.25	47.44	21.09	2.37
2	0.56	23.31	1.47	53.88	20.39	0.40
3	1.22	22.67	0	54.03	20.62	1.46
4	0.55	1.26	1.61	96.58	0	0
5	0.67	23.40	0.47	56.23	18.88	0.36
6	0.22	19.37	2.45	60.92	17.04	0
7	0.53	18.20	0	58.59	22.68	0

Figure 13. Microstructure of the AISI310–40Kh steel joint (mode 3), results of SEM and X-ray spectrum microanalysis of metal of the investigated regions (wt.%)

uid state and insignificant development of the diffusion processes in the joining zone. The thermomechanically affected zone with fine-grained, dynamically recrystallised structure is immediately adjacent to the transition zone. No pores and non-metallic inclusions of SiO_2 were fixed in this zone, which was clearly shown by analysis of microstructure of the joint both in the as-welded state (see Figure 13) and after annealing (Figure 14). Disappearance of the SiO_2 particles from the joining zone may be related to their partial dissolution and the earlier established phenomenon of destruction of oxides by a flow of moving dislocations [18–21], including under the thermal-deformation conditions of inertia and combined FW.

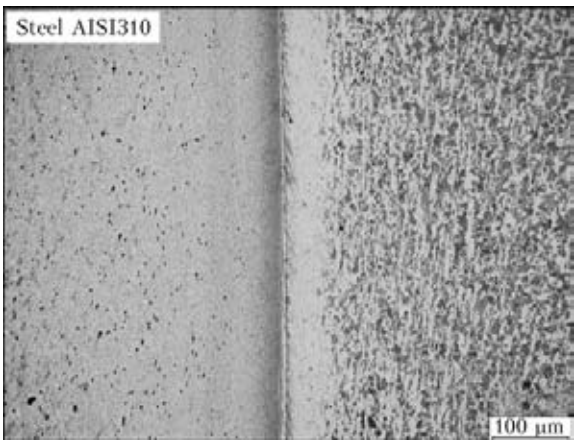

Figure 14. Microstructure of the AISI310–40Kh steel joint after annealing (mode 3)

Fracture of the joints in mechanical tests occurs in the base metal of steel AISI310 (Figure 15). The joints had tensile strength at a level of σ_t = 580–630 MPa. As shown by measurements of microhardness, metal of the joining zone with the fine-grained, dynamically recrystallised structure is characterised by the increased values of strength (see Figure 12), which is attributable to a substantial decrease (from 60 to 5–6 μm) in size of structural components.

Comparative analysis of structure and chemical composition of the zone of joints between PIM-steel AISI310 and steel 40Kh, made under different thermal-deformation cycles of FW suggests the following mechanism of formation of the transition zone in FW of the investigated materials combination.

At the initial stage of the FW process, because of a lower value of thermal conductivity of the austenitic steel, the surface of maximal shear deformations («friction plane») shifts towards austenitic steel AISI310. The «friction surface shift» phenomenon is known for other combinations of dissimilar materials as well [22–24]. The maximal values of the heating temperature are

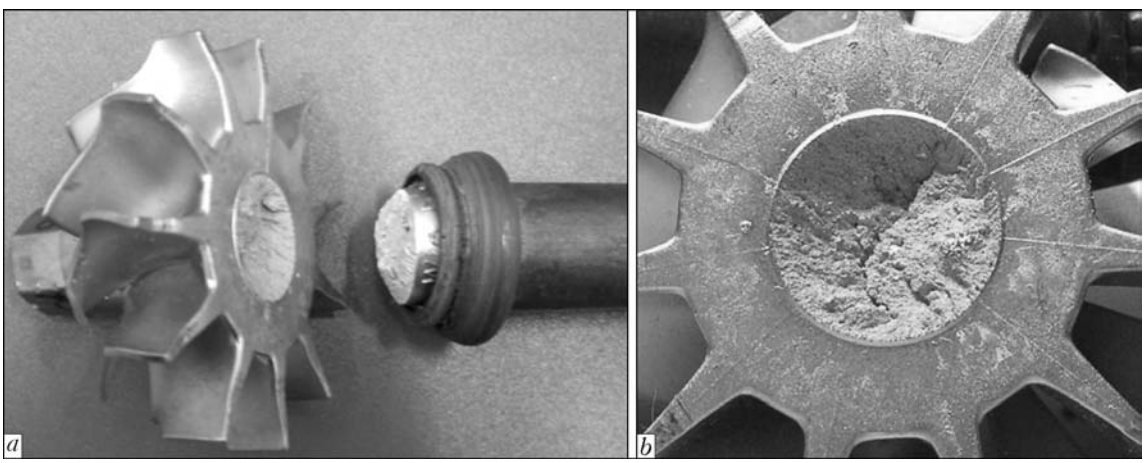

Figure 15. Welded TCR shaft after tensile tests (*a*), fracture surface in base metal of steel AISI310 made by the PIM-technology (*b*)

fixed in the friction plane. The transition zone, which in fact is an AISI310 steel based alloy «deposited» on steel 40Kh, forms between the friction plane and steel 40Kh. Burn-off of the billets and, therefore, displacement of the transition layer outside the section do not occur at the initial stage of the heating process.

As duration of the heating stage increases, width of the transition zone in peripheral parts of the section remains almost unchanged, whereas in the central part of the section it grows due to further displacement of the friction plane towards steel AISI310. This is proved by metallographic examinations of the joints made at different durations of the heating stage. As a result, the shape of the transition zone in the central part of the section becomes convex, directed to steel AISI310.

When CFW is performed in the «soft» mode, in the friction plane, where the heating temperature and tangential deformations are maximal, the rate of diffusion of alloying and impurity elements may be commensurable with that of the melts. As a result, clusters of low-melting point phases, in particular of the eutectic phases of iron with niobium, the redundant content of which was fixed in the base metal of steel AISI310, form in this zone.

The formed lamellar structure of the transition zone persists in passing to the quasi-stationary stage of heating, which is accompanied by burn-off of the billets. The process of burn-off of the billets occurs mainly due to steel 40Kh, the transition zone metal being partially displaced outside the section in the form of a thin layer deposited on the reinforcement surface of steel 40Kh. As the plane of maximal shear deformations is located in the austenitic steel, restoration of the «deposited» layer takes place simultaneously, i.e. there comes the state of equilibrium between the processes of formation and displacement of the transition zone metal.

The width and shape of the transition zone are determined by a difference in thermal-physical characteristics of the steels welded, and by the friction process parameters. «Soft» mode 1 is characterised by a low value of burn-off rate (about 0.15 mm/s). In this case the width of the transition zone is maximal, and the conditions for liquation of impurity elements and formation of low-melting point phases in the friction plane are most favourable. The applied force of forging performed on the non-rotating billets causes decrease in thickness of the transition zone, as well as partial displacement of the variable-composition interlayers and clusters of low-melting point phases from the joint, the remainder determining mechanical and service (corrosion, fatigue) properties of the welded joint.

As the peripheral rotation velocity is decreased and the heating pressure is increased («rigid» mode 2 of CFW), the deeper and deeper layers of metal of the billets welded are involved in the shear (tangential and radial) deformation process, burn-off rate substantially grows (up to 0.9 mm/s), and welding time is reduced. As a result of such a «rigid» thermal-deformation cycle of FW, the narrow (up to 60 μm) transition zone forms in the joint, consisting of alternate variable-composition interlayers, including those corresponding to steel of the martensitic grade. These interlayers forming at the initial stages of the FW process are not fully displaced from the contact zone at the subsequent stages of heating, and persist in the welded joint after forging.

As forging in CFW is performed after stopping of rotation of the billets, the effect on the transition zone metal is characterised by the presence of the radial deformation component. Burn-off occurs mainly due to deformation of metal in the heat-affected zone of steel 40Kh. Only decrease in thickness of the variable-composition interlayers takes place in this case.

The joints made by combined FW with controlled deformation (mode 3) are free from the above imperfections of structure. The fact that the transition zone contains no alternate interlayers corresponding in composition to martensitic and austenitic steels is caused by a peculiar quality of the initial stage of the FW process with controlled deformation. The process parameters (pressure, peripheral velocity) at this stage were set based on the requirement to minimise the processes of deep tearing out and dilution of contact volumes of the materials welded.

The absence of local segregations of low-melting point phases in the joint is caused by minimisation of duration of the quasi-stationary stage of heating, which is achieved by providing the preset rate of deformation (burn-off rate) of the billets at a certain combination of pressure and peripheral velocity values.

The forging stage plays the key role in formation of the joints. Programming of the duration of the rotation deceleration stage and application of increased forge pressure at this stage allow the burn-off rate and the intensity of deformation of contact volumes of the steels welded to be considerably increased. The fixed dramatic change in the concentrations of chromium and nickel

within the joining zone in mode 3 is indicative of minimisation of the processes of dilution of the steels welded and local melting in the contact zone. Substantial increase in the intensity of the thermal-deformation effect on the joining zone metal in combined FW is proved also by the absence in this zone of the SiO_2 particles, which are present in the base metal of steel AISI310 and transition zone of the joints made in the «soft» mode of CFW.

Therefore, the peculiarities of structure and composition of metal of the AISI310 to 40Kh steel joints made by CFW and combined FW are determined by the character and intensity of deformation in the contact zone at the initial, quasi-stationary and final stages of the process when using the above types of friction welding. The peculiar feature of the deformation effect in the contact zone at the final stage of formation of the joints in CFW is the presence of the radial component caused by applying the increased forge pressure to the non-rotating billets. Forging in this case provides an insignificant decrease in width of the transition zone and thickness of the brittle interlayers formed at the initial stages of the FW process.

Combined FW with controlled deformation creates conditions for minimisation of the processes of local melting and dilution of metal volumes in the solid-liquid state. The effect on the joining zone metal at the final stage of the FW process is characterised by the presence of both radial and tangential components under conditions of the temperature gradient growing during the rotation deceleration process. Localisation of deformation and a substantial increase in its intensity at the final stage of welding provide dispersion and destruction of oxide phases, as well as displacement of interlayers outside the section welded. The transition zone with a fine-grained, dynamically recrystallised structure and a dramatic change in the concentration of alloying elements is formed in the joint.

The data obtained served as a basis for the development of the technology for FW of the wheels of nickel superalloy Inconel 713C made by the PIM-technology to shanks of steel 40Kh.

CONCLUSIONS

1. Characteristic features of heat-resistant steel AISI310 produced by the powder injection moulding technology (feed stock — «Catamold») are the equiaxed crystalline structure with a grain size of about 60 μm, presence of austenite grains with a homogeneous and lamellar structure, insignificant residual porosity, as well as presence of uniformly distributed non-metallic inclusions of silicon dioxide, 2–10 μm in size, and segregations of phases with the increased niobium content.

2. In the «soft» mode of CFW of steel AISI310 to steel 40Kh, the 25 to 500 μm wide transition zone forms within the joining zone. This transition zone is non-uniform across the section, has a lamellar structure and is an AISI310 steel based «alloy» deposited on steel 40Kh. Constant-composition interlayers, including those corresponding to steel of the martensitic grade, are revealed in the transition zone on the side of steel 40Kh. Fracture of the joints in tensile tests occurs between the transition zone and steel AISI310. It is localised in segregation clusters of the redundant phases with the increased niobium content.

3. No segregations of low-melting point phases were revealed in the joints made in the «rigid» mode of CFW. However, alternate constant-composition interlayers corresponding to steels of the martensitic and austenitic grades were fixed. These interlayers form at the initial stages of the FW process. They are not fully displaced from the contact zone at the subsequent heating stages and in forging performed after stopping of rotation of the billets.

4. The presence of the lamellar structure consisting of alternate «alloys» of different compositions in the joints made by CFW is indicative of the dilution of the steels welded both in the plasticised and solid-liquid states occurring in the contact interaction zone at the initial stages of the FW process.

5. The technology was developed for combined FW with controlled deformation. With this technology the values of the process parameters are set based on the requirement to provide the certain deformation rate (burn-off rate) at the heating stage, while the forge pressure is applied at a stage of rotation deceleration that is controlled following the preset program.

6. The joints made by combined FW with controlled deformation have fine-grained, dynamically recrystallised structure with the up to 40 μm wide transition zone that is uniform across the section. The composition of metal of the transition zone across its width corresponds to steel of the austenitic grade. This metal contains no pores and no segregations of alloying elements and non-metallic inclusions. The transition zone–steel 40Kh interface is characterised by a dramatic change in the concentration of alloying

elements and absence of increased-hardness interlayers.

7. Parts of the materials made by the powder injection moulding technology can be applied to provide sound bimetal joints by using friction welding, subject to setting the appropriate values of the process parameters.

1. Dovydenkov, V.A., Krys, M.A., Fetisov, G.P. (2008) Production of metallic parts by moulding and sintering of metal-polymer compositions. *Tekhnologiya Metallov*, **6**, 28–31.
2. Heaney, D. (2004) Qualification method for powder injection molded components. *P/M Sci. & Technology Briefs*, 6(**3**), 21–27.
3. Graboj, I.E., Thom, A. (2005) Materials Catamold of BASF Company for pressure die casting of powders. Technology. Production. Application. In: *Proc. of Sci.-Pract. Seminar* (Joshkar-Ola, 20–21 June, 2005), 71–74.
4. Salk, N. (2011) Metal injection moulding of Inconel 713C for turbocharger applications. *PIM Int.*, 5(**3**), 61–64.
5. Froes, F.H. (2007) Advances in titanium metal injection molding. *Powder Metallurgy and Metal Ceramics*, 46(**56**), 303–310.
6. Hamill, J.A. (1993) What are the joining processes, materials and techniques for powder metal parts? *Welding J.*, Febr., 37–44.
7. Lebedev, V.K., Chernenko, I.A., Vill, V.I. (1987) *Friction welding*: Refer. Book. Leningrad: Mashinostroenie.
8. (2006) *Friction welding. Machine-building*: Encyclopedia. Vol. 1–4. Moscow: Mashinostroenie.
9. Kuchuk-Yatsenko, S.I., Zyakhor, I.V. *Method of friction welding and machine for its implementation*. Pat. 46460 Ukraine. Publ. 15.11.2004.
10. Son, C.-Y., Yoon, T.S., Lee, S. (2009) Correlation of microstructure with hardness, wear resistance and corrosion resistance of powder-injection-molded specimens of Fe-alloy powders. *Metallurg. and Mater. Transact. A*, 40(**5**), 1110–1117.
11. Heany, D.F., Mueller, T.J., Davies, P.A. (2003) Mechanical properties of metal injection moulded 316L stainless steel using both prealloy and master alloy techniques. *Powder Metallurgy*, **1**, 1–7.
12. Krug, S., Zachmann, S. (2009) Influence of sintering conditions and furnace technology on chemical and mechanical properties of injection moulded 316L: Tech. Pap. *PIM Int.*, 3(**4**), 66–70.
13. (1969) Transition joints for high temperature service. Discussion session 3. *Metal Construction and British Welding J.*, **12**, 134–142.
14. Gotalsky, Yu.N. (1981) *Welding of dissimilar steels*. Kiev: Tekhnika.
15. Zalkin, V.M. (1987) *Nature of eutectic alloys and effect of contact melting*. Moscow: Metallurgiya.
16. Kragelsky, I.V., Dobychin, M.N., Kombalov, V.S. (1977) *Principles of friction and wear calculations*. Moscow: Mashinostroenie.
17. Zyakhor, I.V. (2010) Formation of joints in friction welding of nickel superalloy JS3-DK to structural steel 40Kh. *Visnyk Chernigov. DTU*, **42**, 148–155.
18. Smiyan, O.D. (2002) Atomic mechanism of interaction between ambient material and wrought metal. *Fizyka ta Khimiya Tv. Tila*, **4**, 662–674.
19. Smiyan, O.D., Kruzhkov, A.G. (1972) About some peculiarities of motion of diffusion gas flow in metals. *Doklady AN SSSR*, 202(**6**), 1311–1313.
20. Smiyan, O.D., Kuchuk-Yatsenko, S.I., Kharchenko, G.K. et al. (2007) Distribution of interstitial impurities within the joining zone in friction welding. *The Paton Welding J.*, **9**, 2–5.
21. Smiyan, O.D., Zhyakhor, I.V., Nikolnikov, O.V. et al. (2008) Distribution and effect of hydrogen, oxygen and carbon in the joining zone of nickel superalloy in friction welding. *Visnyk Chernigov. DTU*, **34**, 138–143.
22. Voinov, V.P., Boldyrev, R.N., Mulyukov, K.I. et al. (1976) Pulse friction welding of alloy JS6-K to steel 40G. *Svarochn. Proizvodstvo*, **3**, 28–30.
23. Zyakhor, I.V. (2000) Peculiarities of friction welding of dissimilar metals and alloys. *The Paton Welding J.*, **5**, 36–44.
24. Kuchuk-Yatsenko, S.I., Zyakhor, I.V. (2002) Mechanism of bimetal joints formation in friction welding. *Ibid.*, **7**, 2–9.

PROBLEMS OF STIRRING AND MELTING IN EXPLOSION WELDING (ALUMINIUM–TANTALUM)

B.A. GRINBERG[1], **O.A. ELKINA**[1], **A.M. PATSELOV**[1], **A.V. INOZEMTSEV**[1], **A.V. PLOTNIKOV**[1], **A.Yu. VOLKOVA**[1], **M.A. IVANOV**[2], **V.V. RYBIN**[3] and **Yu.B. BESSHAPOSHNIKOV**[4]

[1]Institute of Metal Physics, Ural Division of the RAS, Ekaterinburg, RF
[2]G.V. Kurdyumov Institute for Metal Physics, NASU, Kiev, Ukraine
[3]St. Petersburg State Polytechnic University, St. Petersburg, RF
[4]OJSC «Uralkhimmash», Ekaterinburg, RF

The results of investigation of structure of transition zone of aluminium–tantalum joints, having different plane or wavy shape of the interfaces, are presented. Independently of the shape of boundaries, two types of fragmentation were revealed: one of them is similar to fragmentation in explosion, another one — at intensive plastic deformation. The same types of fragmentation were earlier observed also in joints of copper–tantalum having no mutual solubility unlike the aluminium–tantalum. Melting was observed in transition zone of joints being investigated. Structure of melted areas depends greatly on the availability of mutual solubility in metals being welded.

Keywords: *explosion welding, fragmentation, transition zone, local melting, mutual solubility, intermetallic*

Among the whole variety of materials and welding conditions the basic problem is stirring in the transition zone near the interface [1, 2]. It is the structure of transition zone that defines the possibility of adhesion of both materials. Stirring occurs as a result of strong external effect supposing large plastic deformation (including pressure, shear components, torque moments of stresses, deformation non-uniformity, etc.), friction of surfaces, influence of cumulative jet and other factors. However it is still unclear how stirring can occur at such a great external effect in a short time of welding procedure.

The explosion welding was carried out by CRSI of Structural Materials «Prometey» (St. Petersburg), Volgograd State Technical University, Ural Plant of Chemical Machine Building (Ekaterinburg). Depending on welding conditions different joints were produced having wavy or plane shape of interfaces.

Originally the welded joints of metal–intermetallic with normal mutual solubility were investigated [3–7]. In the capacity of metal the commercially pure titanium was selected, and as the intermetallic — orthorhombic aluminide of titanium (further named aluminide for briefness). Depending on welding conditions the different joints were produced which were called for convenience in different ways: A_w, A_p, B_w, B_p, where the low index designates the shape of an interface (plane, wavy). For joints A the orthorhombic alloy was used, containing 16 at.% Nb, for joints B — 23.5 at.% Nb. The molten areas of any of mentioned joints represent genuine solutions where stirring occurs at the atomic level.

To reveal the importance of mutual solubility of initial materials, the metals (copper–tantalum, iron–silver) were selected for explosion welding which have practically no mutual solubility both in solid and in liquid states, moreover they form non-mixed suspensions in liquid state. It was found that in joints C_p, C_w of copper–tantalum [8, 9] and D_p of iron–silver [10] the areas of local melting are filled with such colloid solutions.

Having used the obtained results the possible reasons for good quality of a copper–tantalum joint were revealed, due to which the explosion welding was successfully carried out on the large areas of plates [11] from which the chemical reactor was designed. The body of reactor was made of the carbon steel–copper–tantalum composite. The inner shell is composed of tantalum and on its corrosion resistance the whole structure is based. The colloid solutions have a risk of emulsion lamination [12]. However at the areas of local melting of joint C_w the lamination was not observed [9]. But the suspension, composed of tantalum particles in the copper matrix, on the contrary contributes to dispersion strengthening of the joint.

In the present work, which is the continuation of works [8, 9], the welded joints E_p and E_w of aluminium–tantalum with normal mutual solubility are investigated. The welding parameters (angle of collision γ, speed of contact point v_c) for these joints are given in Figure 1. With decrease of welding parameters of aluminium–tantalum ($\gamma = 7.5°$, $v_c = 1900$ m/s) the welding did not occur at all. The Figure shows also the welding parameters for the joints C_p, C_w of copper–tantalum. As is seen from Figure 1, the parameters for the joints E_p and C_p, having plane boundary surfaces, locate near the lower boundary of weldability. Comparing the joints E_w and C_w the welding parameters for the joint E_w are seen considerably higher. Basing on the comparison of results obtained for the mentioned joints, the authors tried to reveal the processes which are common both for the metals with mutual solubility as well as for the metals without it. Meantime the simultaneous use of both joints with different shape of an interface (plane, wavy) was successive for the same pair of metals.

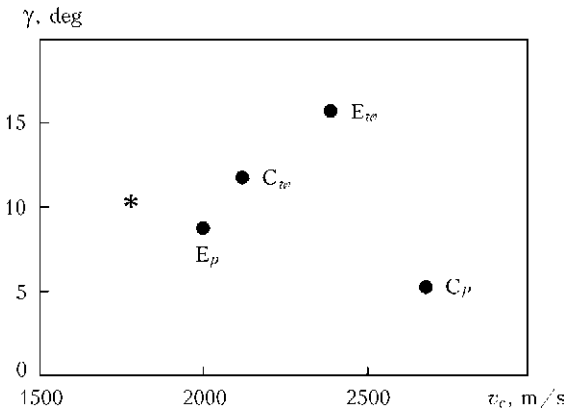

Figure 1. Welding parameters for joints being investigated (asterisk designates the mode accepted in the work [11])

The metallographic analysis was carried out using the optic microscope «Epiquant» equipped with the computational complex SIAMS. The microstructure was investigated using transmission electron microscopes JEM 200CX and CM-30 Super Twin and scanning electron microscope Quanta 200 3D. The X-ray shooting was performed in the diffractometer DRON-3M in monochromatic Co-K_α-radiation.

The images of interfaces, obtained using scanning electron microscopy (SEM), plane for the joint E_p (Figure 2, *a*) and wavy ones for E_w joint are given in Figure 2. For wavy interface the period is about 300 μm, the amplitude is 30 μm.

Fragmentation during explosion. The phenomenon of fragmentation as a process of splitting of solid body into parts (fragments) occurring at the intensive outer influence was known long ago. It came even into the name of weapon: fragmentation warhead, fragmentation shell, fragmentation bomb. The description of fragments separation is connected with the name of N. Mott [13]. He together with other authors (see for example [14]) showed that using methods of simple geometric fragmentation the dynamic fragmentation of cylindrical shell can be described.

We suppose that fragmentation during explosion investigated by Mott occurs also during explosion welding. In the titanium–aluminide joints A_w the separation of micron particles of aluminide has a striking resemblance to separation of fragments occurring during explosion but of other sizes [15]. Here it should be noted that during explosion the separation of fragments occurs in the open space, whereas in explosion welding the fragments are separated at closed space limited by the material of plates.

For fragmentation observed in explosion welding we used previously the notion «fragmentation of crushing type» (FCT). Though in both

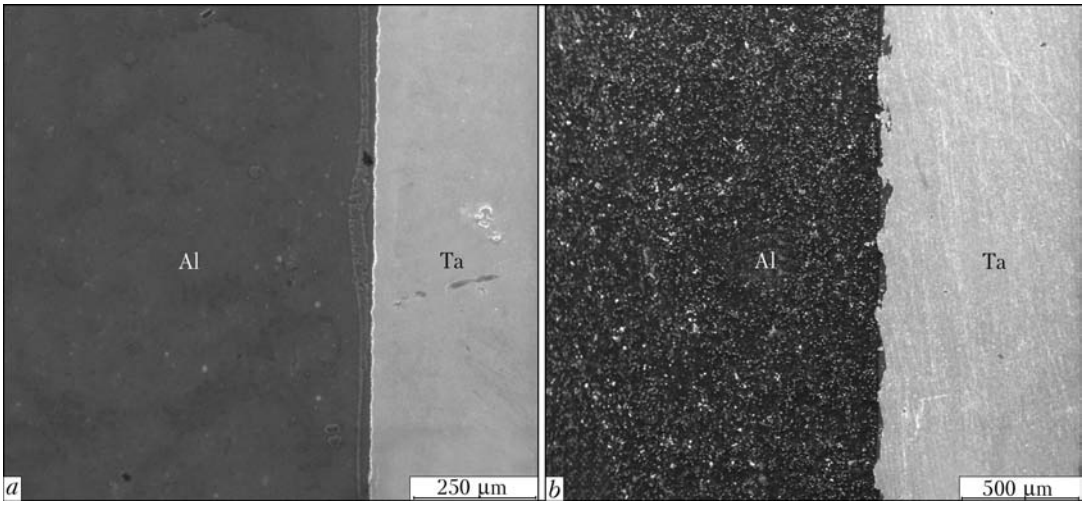

Figure 2. Interface (cross section) for the aluminium–tantalum joints: *a* — joint E_p; *b* — joint E_w

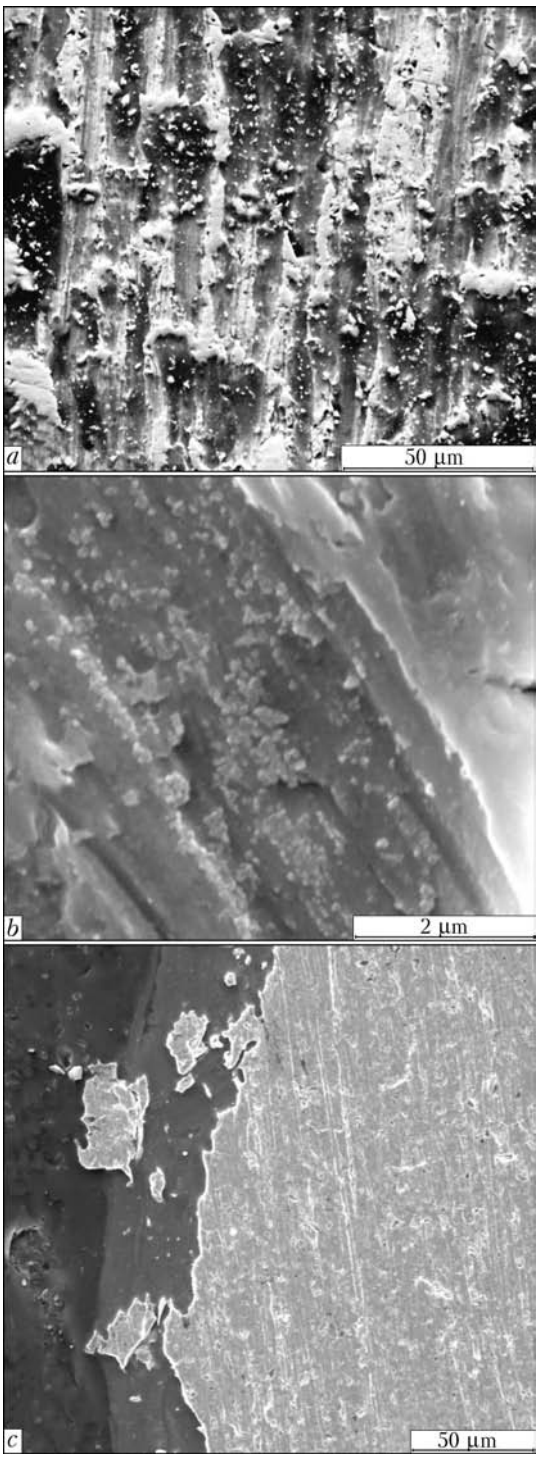

Figure 3. Microstructures of longitudinal section of transition zone (*a*, *b*) and cross section (*c*): *a* — joint E_p; *b* — joint E_p, aluminium is etched; *c* — joint E_w

cases the formation and separation of particles are observed, these types of fragmentation are not similar. FCT represents the process of splitting into particles which either separated or abutted each other. Similar to explosion fragmentation, FCT represents quick-running process which has time to occur during explosion.

Figure 3, *a* shows many particles of tantalum of arbitrary shape on the background of aluminium. We suppose that separation of tantalum particles observed in explosion welding as well as separation of aluminide particles mentioned above is similar to separation of fragments in explosion. In Figure 3, *b* after aluminium complete etching, the particles of tantalum were seen at the surface of tantalum, poured during aluminium removal. In Figure 3, *c* the coarse particles of tantalum are seen, reaching sizes of 20–40 μm which are much larger than those observed in the joint E_p. The possible reason for such difference is that joint E_w was obtained at more intensive outer influence than the joint E_p (see Figure 1).

The observation of particles separation in explosion welding proves the concept about fragmentation similar to fragmentation in explosion. FCT is observed both in the metal–metal joints, as well as in metal–intermetallic ones both at the normal solubility and also at the absence of mutual solubility of the metals being welded independently of the shape of interface. This is the evidence of dominating role of explosion in investigating welding method.

FCT provides a powerful channel for dissipation of induced energy, as the surface of separating particles has a large total area. FCT arises as a result of microfractures and is a process alternative to fracture. Instead of free surfaces, formation of which could result in fracture, the formation of surfaces due to microfractures is occurred, which either relate to separating particles or are «healed» at their consolidation. As a result, the FCT increases the «vitality» of material preventing its fracture even at such intensive outer influence as explosion welding.

Fragmentation at intensive deformation. In explosion welding the fragmentation of one more type is observed when the formation of new particles does not take place at all. It implies fragmentation [16], the existence of which is proved by many observations of material structure during strong deformation. Such, to the known extent, traditional fragmentation [15] includes pumping of dislocations (twins), formation of nodular, cellular and banded structures, and recrystallization.

In the present work for the joint E_p of aluminium–tantalum the TEM-images of strongly deformed structure of aluminium but not mixed with tantalum were given: regions with high dislocation density (Figure, 4, *a*) and recrystallized regions (Figure 4, *b*, *c*). Thus, in Figure 4, *b* the formation of triple butt is seen. The images of strongly deformed structure of tantalum are simi-

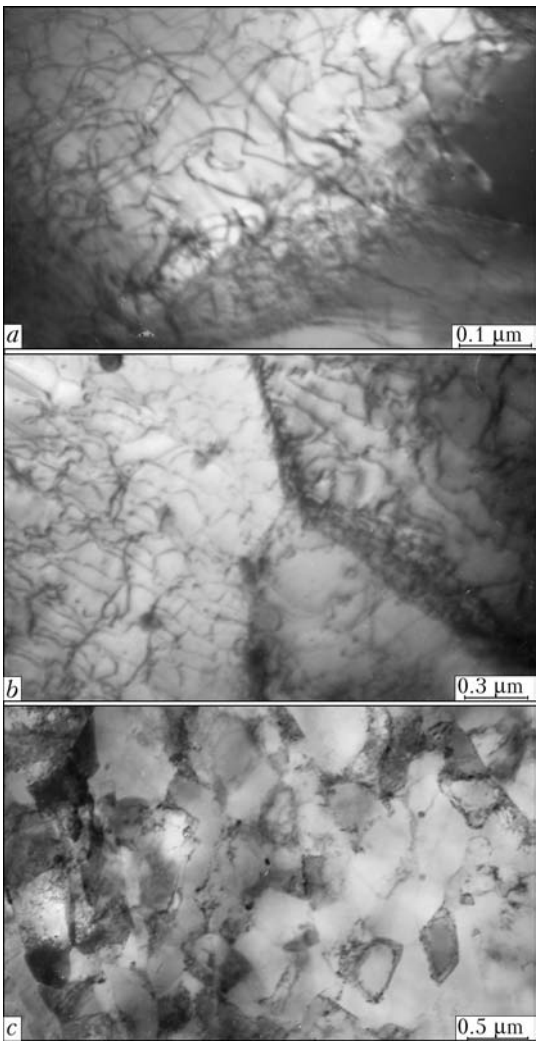

Figure 4. TEM-image of structure of strongly deformed aluminium: *a* — cold working; *b*, *c* — recrystallized areas

lar to those observed for the copper–tantalum joint C_p [15]. If to compare the images of deformed structure of aluminium and copper [15] it is seen that recrystallization of aluminium occurs more completely as compared to recrystallization of copper. It is connected with the fact, that, firstly, aluminium is fusible and, secondly, it has higher energy of packing defect.

Though the temperature in the contact zone in explosion welding can be extremely high, however at quick-running explosion effect the proceeding of thermally-active processes, defining the movement and restructuring of dislocations, is complicated and is hardly possible. It can be assumed that these processes the same as diffusion become possible only at residual temperatures and stresses. These are the processes that define the traditional fragmentation. As compared to the traditional fragmentation, the FCT occurs only in narrow area near the interface where outer influence is the most intensive. However the traditional fragmentation is observed somewhat farther from the boundary surface. Respectively, the FCT is, by all means, the more rapid process than traditional fragmentation. The characteristic periods can be evaluated approximately as microsecond for FCT and 10^8–10^9 μs (time of structural relaxation) for traditional fragmentation.

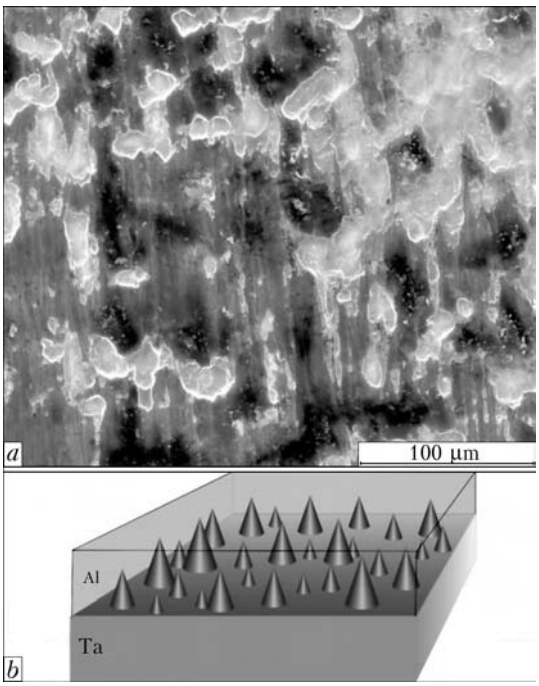

Figure 5. Transition zone for joint E_p: *a* — microstructure from the area of tantalum, aluminium and zone of local melting (longitudinal section); *b* — schematic image of projections (cones) at plane interface

Heterogeneities of interface surface: projections, zones of local melting. In Figure 5, *a* the image is composed of spots of three colors: white, black and grey. Respectively, the transition zone is composed of areas of three types which is the result of formation of projections at the interface surface. At the first time, the projections were revealed in the titanium–aluminide joints [5]. The data on chemical composition of mentioned areas forming the transition zone were obtained using SEM from repeated measurements. It was shown that area of tantalum corresponds to white color, aluminum area — to black, mixture of initial metals — to grey one.

The projections are formed most probably as a result of diffusion-free (due to quick run of welding) outburst of one metal into another (Figure 5, *b*). Actually, they certainly do not have perfect conic shape: the peaks are rounded and surfaces are not so smooth. Only by formation of projections it is possible to explain the pattern of transition zone for joint E_p in Figure 5, *a*. As a result, the surface represents chaotic relief with a large number of projections of one material into another one, similarly to that observed in work [8].

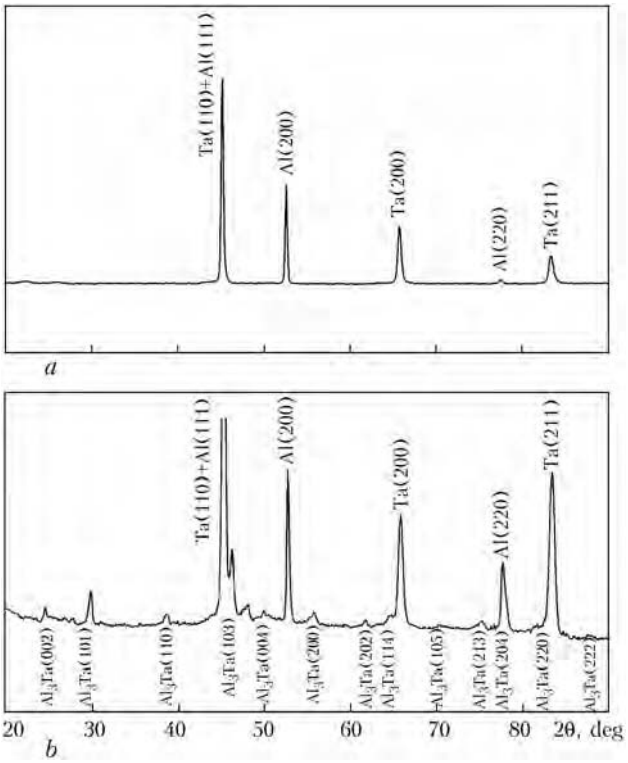

Figure 6. Diffractogram of transition zone (longitudinal surface of section): *a* — joint E_p; *b* — joint E_w

In the both joints E_p and C_p the drawing up of projections along some marked direction is clearly seen. It can be assumed that there is a connection between self-organization of projections and wave-formation, however it requires special investigations.

If the interface was smooth, then the problems with adhesion could arise and either reconstruction of metallic links or transportation of spot defects would be required. However presence of projections solves this problem: here the projections play role of «wedges», linking the contacting materials with each other. The friction on the surface of projection, strengthened due to the fact that the projection itself is not smooth, contributes to adhesion of surfaces.

There is a point of view [17] that strength of bimetal produced by explosion welding can be increased due to preliminary profiling of surfaces of a fixed plate, which can be performed, for example, due to longitudinal cavities and projections oriented approximately parallel to the direction of detonation spreading. A.Z. Bogunov et al. [17] consider that at the presence of projections it can be spoken about explosion riveting, which in case of profiling accompanies the explosion welding.

We suppose that the similar situation occurs in explosion welding due to projections forming in natural way, though their sizes are less than in preliminary profiling. In our investigated cases the sizes of projections are changed from micrometer to hundreds of micrometers, whereas after profiling the sizes of projections varied in the limits from several millimeters to dozens of millimeters [17].

Moreover, it can be assumed that existence of lower limit of weldability is connected indeed with impossibility to form projections on the plane interface. Below the indicated limit the projections either are not formed at all or appear to be rather small. There is obviously some critical height of projections when they provide adhesion of surfaces. With increase in external effect the projections are growing and lining up. Further, the wavy formation begins.

The X-ray diffractogram of transition zone (Figure 6, *a*) contains lines of tantalum and aluminium, and does not contain lines of other phases. The results of spot measurements of chemical composition of grey zone obtained using SEM showed that concentration of tantalum does not exceed 5 at.% here, therefore grey zone represents a zone of local melting of aluminium alloyed with tantalum. However it requires melting of narrow edge of tantalum.

It is grey zone, being the zone of mixing, that is sensitive to the fact whether materials being welded have mutual solubility or not. At normal solubility they form natural solutions. At the absence of mutual solubility the colloid solutions arise as in case of copper–tantalum [8].

Melting along the interface. Near the wavy interface, in contrast to plane one, the interface is corrugated, therefore, its longitudinal section represents a set of alternating bands of both materials with almost parallel boundaries. The longitudinal section of transition zone near the aluminium–tantalum joints E_w, given in Figure 7, *a*, represents really a slightly inclined section due to small amplitude of wavy surface. At the longitudinal section of transition zone at the same joint after the aluminium was etched (Figure 7, *b*) the bands of tantalum are seen and also particles which poured after aluminium dissolution.

For comparison, Figure 8, *a* shows the longitudinal section of transition zone for the copper–tantalum joint C_w. The system of bands in Figures 7, *a* and 8, *a* is not regular. If we restore the interface according to given images, then in both cases it will be not perfect. In Figure 8, *a* the numerous zones of local melting are clearly seen having the vortex structure. As is seen from Figure 8, *b*, for the both joints C_p and C_w of copper–tantalum the zone of local melting is

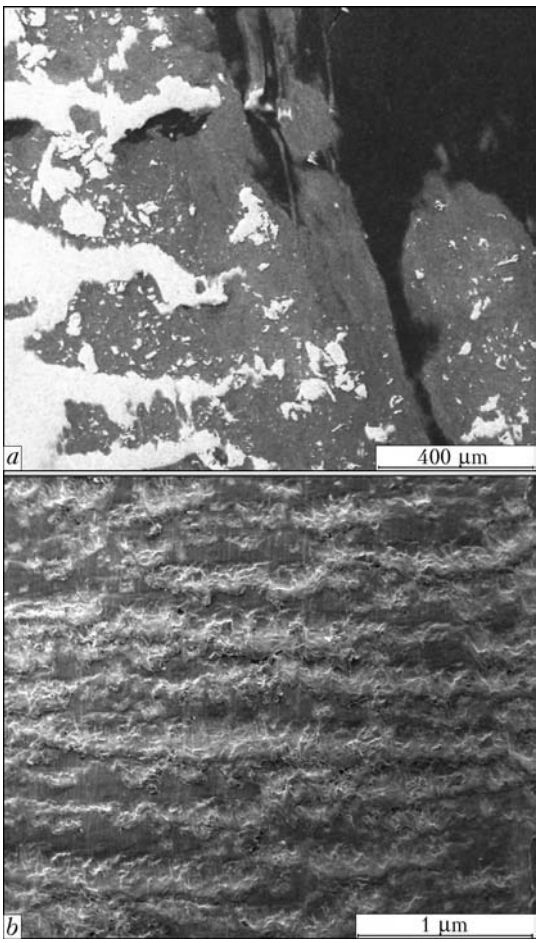

Figure 7. Microstructures of transition zone for joint E_w (longitudinal section): *a* — bands of aluminium and tantalum; *b* — aluminium is completely etched

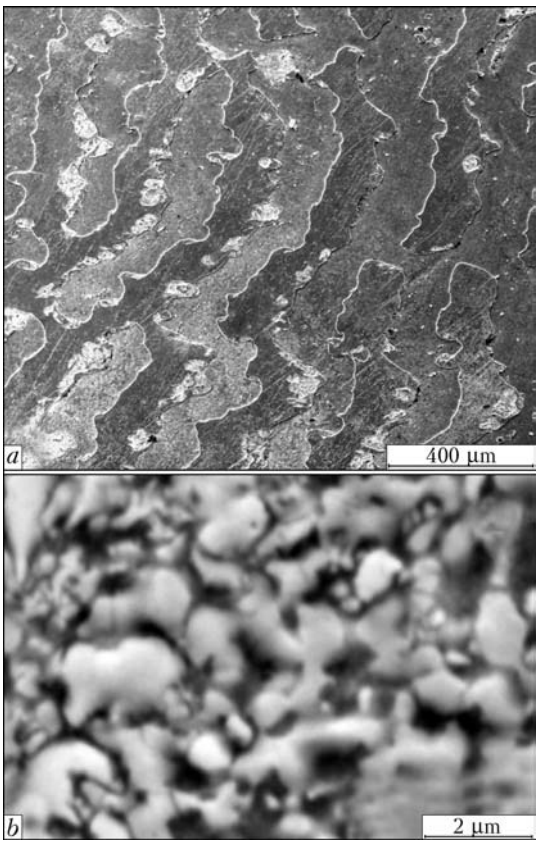

Figure 8. Microstructures of longitudinal section of the interface for joint C_w: *a* — bands of copper and tantalum; numerous zones of local melting are seen; *b* — zone of local melting

filled with colloid solution, independently of the interface shape.

In Figure 8, *a* many projections of different sizes from several micrometers to 100–150 μm are seen. Some of them begin in one band, intersect another one and form adhesion between the bands. The role of projections, promoting the formation of joints was mentioned above during analysis of the joint E_p.

As is seen from Figures 7 and 9, in the joint E_w, in contrast to C_w, the zone of local melting, i.e. isolated melted areas, are not observed. Instead of them, in Figure 9 while moving from the solid phase of aluminium the layers of molten aluminium are seen, first not containing and then containing particles of other phase (with small and then large density of particles). The sizes of particles are changed within wide range: from 50 to 500 nm. Quite sharp cut of particles is particularly noticeable. Further the edge of tantalum is followed, observed in Figure 9, *a*, *b* as illuminating line. Such illuminating boundary («braid»), which represents a molten film, was observed by the authors before in the titanium–aluminide joints A_p [5].

The diffractogram taken from the longitudinal surface of the section (see Figure 6, *b*) shows clearly how X-ray peaks are recorded not only from tantalum and aluminium, but also from intermetallic phase Al_3Ta. Compound Al_3Ta has tetragonal crystal lattice, spatial group $14/mm$, structural type — Al_3Ti. Namely the particles Al_3Ta are seen in Figure 9, *b*. It is obvious that melting of tantalum is required for running of intermetallic reaction. In fact in Figure 9, *c* the spherolites are seen which are the evidence of tantalum melting. The above-mentioned molten film for the titanium–aluminide joint A_p has a similar structure, where the spherolites were also observed (see Figure 5, *e* in work [5]).

In Figure 9, *d* the structure of layer is given containing intermetallic inclusions after annealing at 500 °C for 1 h. It is seen that the structure is heterogeneous but in general the coarsening of particles occurred as compared to those observed in Figure 9, *b*.

In the joint E_w the film includes edge of tantalum of 2.0–2.5 μm width and above-mentioned molten layer of about 40 μm width (30 μm with particles, 10 μm — without). The observed structure of transition zone is formed in the following

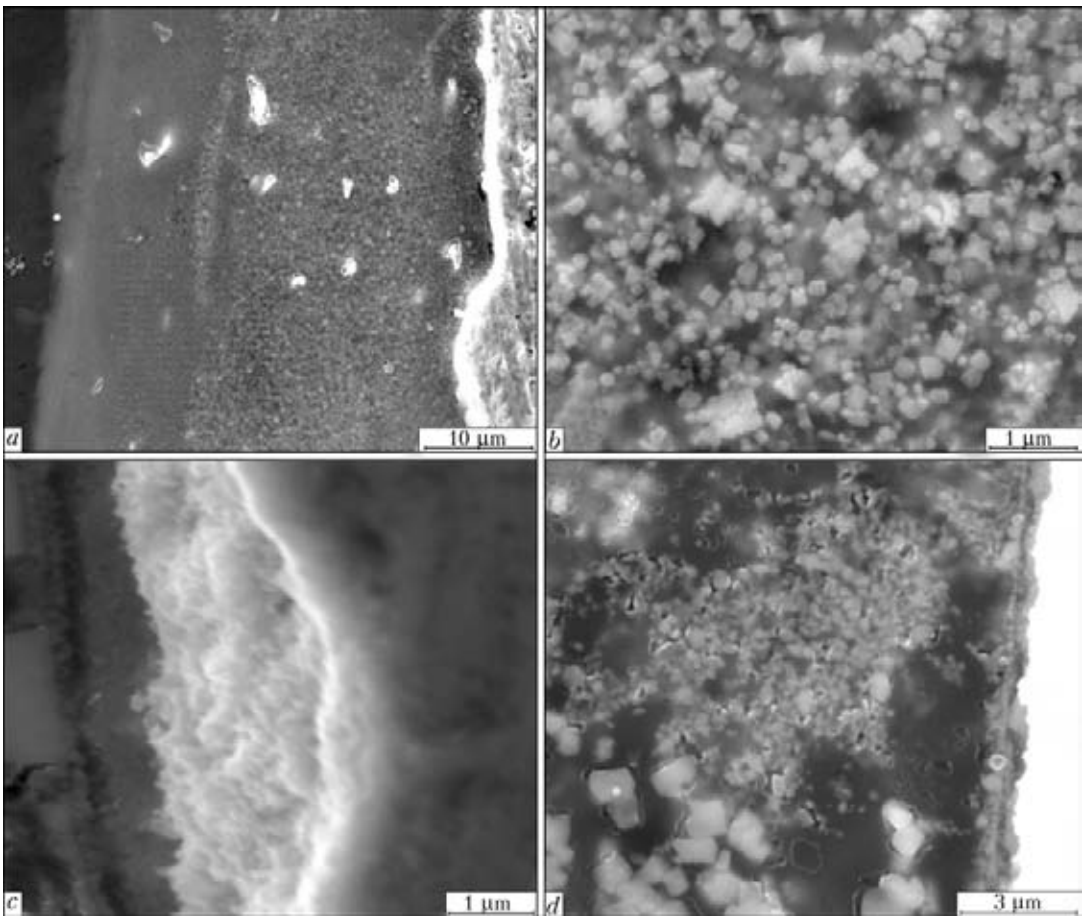

Figure 9. Microstructures of the transition zone cross section for joint E_w: *a* — layers of melted aluminium without and with particles; *b* — particles of intermetallic Al_3Ta in the melt of aluminium; *c* — spherolites; *d* — after annealing

way: at first, the melting of aluminium as more fusible one is occurred, then followed the partial melting of tantalum surface, formation of solid solution based on aluminium, and formation of intermetallic phase at achieving the certain concentrations. The mentioned particles are retained during dissolution of aluminium and observed together with tantalum particles (see Figure 7, *b*).

However, before melting begins in accordance with the scenario offered above, the most quick-running process takes place: separation of solid particles of tantalum which are seen in Figures 3, *c*; 7, *a*; 9, *a*.

The fact is that the molten zone in the joint E_w represents a film at the interface, while in the joint E_p the isolated zones are coordinated with intensification of welding condition used to produce joint E_w as compared to the joint E_p (see Figure 1). Here the observation of intermetallic inclusions in the joints E_w and their absence in the joint E_p is also related to this.

Melting and adhesion. Strong explosion effect during producing of the joint E_w evidence of approaching to the upper limit of weldability. In this case the melting becomes dangerous for integrity of the joint. However, as authors suppose, in favorable case (at not very high values of parameters of explosion effect) the melting, on the contrary, facilitates the formation of joint due to adhesion of surfaces. In this relation, microphotography is very convincing (see Figure 9, *a*), demonstrating transition from aluminium to tantalum, occurring due to melted aluminium, aluminium with particles, and melted tantalum. It is obvious that such a transition facilitates the adhesion of aluminium and tantalum comparing with abrupt solid-phase transition.

For other materials, namely polymers, the best adhesive substance is solution or melt of the given polymer [18]. It gives a certain prove to the possibility of adhesion also the investigated materials due to their melting in explosion welding, as far as during melting the problems of wetting, adhesion and protection from contact corrosion are instantly solved. Let us pay attention to the following fact. Aluminium is one among few metals, the adhesion of which is impossible without preliminary chemical treatment of surface [19]. Only mechanical treatment turned to be not sufficient. However aluminium plate was not subjected to chemical treatment

before welding. Nevertheless welded joint with tantalum was produced. Here, most obviously, the remarkable feature of explosion welding was manifested, i.e. self-cleaning of surfaces to be welded due to cumulative effect [1, 20].

It is known that a film of adhesive substance should not exceed the specified value for thickness [18]. As applied to welded joints it can mean the restriction for thickness of melted area. During intensification of welding condition and approach to the upper limit of weldability the critical thickness of melted area will be reached, at which the adhesion becomes impossible.

Thus, explosion welding comprises to a definite extent also another method of joining materials, namely their adhesion by formation of melted areas.

The electron-microscopic investigations were carried out in the Center of collective use of electron microscopy of Ural Division of the RAS.

The work was carried out at financial support of RFFI grant No. 10-02-00354, project of Presidium of the RAS No. 12-P-2-1053, projects of the RAS UrD Nos. 12-U-2-1011 and 12-2-006-UT and State Purposeful Program of Ukraine «Nanotechnologies and nanomaterials» No. 1.1.1.3-4/10-D.

1. Deribas, A.A. (1980) *Physics of strengthening and explosion welding*. Novosibirsk: Nauka.
2. Lysak, V.I., Kuzmin, S.V. (2012) Lower boundary in metal explosive welding. Evolution of ideas. *J. Mat. Proc. Technol.*, **212**, 150–156.
3. Rybin, V.V., Semenov, V.A., Sidorov, I.I. et al. (2009) Bimetallic joint of orthorhombic titanium aluminide with titanium alloy (diffusion bonding, explosion welding). *Voprosy Materialovedeniya*, 59(**3**), 17–31.
4. Rybin, V.V., Grinberg, B.A., Antonova, O.V. et al. (2009) Formation of vortexes in explosion welding (titanium–orthorhombic titanium aluminide). *Fizika Met. i Metallovedenie*, 108(**4**), 371–384.
5. Rybin, V.V., Grinberg, B.A., Ivanov, M.A. et al. (2010) Structure of zone of titanium joint with orthorhombic titanium aluminide in explosion welding. *Deformatsiya i Razrush. Materialov*, **11**, 27–33.
6. Grinberg, B.A., Ivanov, M.A., Rybin, V.V. et al. (2010) Structure of zone of titanium joint with orthorhombic titanium aluminide in expolsion welding. II. Localized vortex melted zones. *Ibid.*, **12**, 26–34.
7. Rybin, V.V., Greenberg, B.A., Ivanov, M.A. et al. (2011) Nanostructure of vortex during explosion welding. *J. Nanosci. and Nanotechnol.*, 11(**10**), 8885–8895.
8. Grinberg, B.A., Elkina, O.A., Antonova, O.V. et al. (2011) Peculiarities of formation of structure in the transition zone of the Cu–Ta joint made by explosion welding. *The Paton Welding J.*, **7**, 20–25.
9. Grinberg, B.A., Ivanov, M.A., Rybin, V.V. et al. (2012) Nonuniformities of interface in explosion welding. *Fizika Met. i Metallovedenie*, 113(**2**), 187–200.
10. Grinberg, B.A., Ivanov, M.A., Rybin, V.V. et al. (2012) Explosion welding: Stir processes of metals without mutual solubility (iron–silver). *Ibid.*, 113(**11**) (in publ.).
11. Frey, D., Banker, J. (2003) Recent successes in tantalum clad pressure vessel manufacture: A new generation of tantalum clad vessels. In: *Proc. of Corrosion Solutions Conf.* (2003, USA), 163–169.
12. Gelfman, M.I., Kovalevich, O.V., Yustratov, V.P. et al. (2004) *Colloid chemistry*. St.-Petersburg: Lan.
13. Mott, N.F. (1947) Fragmentation of shell cases. *Proc. Royal Soc. A*, 189, Jan., 300–308.
14. Grady, D. (2006) *Fragmentation of rings and shells*. The legacy of N.F. Mott. Berlin, Heidelberg: Springer.
15. Grinberg, B.A., Ivanov, M.A., Rybin, V.V. et al. (2012) Fragmentation processes in explosion welding. *Deformatsiya i Razrush. Materialov*, **8**, 2–13.
16. Rybin, V.V. (1986) *High plastic deformations and fracture of metals*. Moscow: Metallurgiya.
17. Bogunov, A.Z., Kuzovnikov, A.A. (2009) Production of aluminum–steel bimetal with profiled interface. *The Paton Welding J.*, **11**, 65–68.
18. Frejdin, A.S., Turusov, R.A. (1990) *Properties and design of adhesive bonds*. Moscow: Khimiya.
19. Kapelyushnik, I.I., Mikhalev, I.I., Ejdelman, B.D. (1972) *Technology of gluing of parts in aircraft construction*. Moscow: Mashinostroenie.
20. Zakharenko, I.D. (1990) *Explosion welding of metals*. Minsk: Navuka i Tekhnika.

EFFECT OF PALLADIUM ON STRUCTURE AND TECHNOLOGICAL PROPERTIES OF Ag–Cu–Zn–Ni–Mn SYSTEM BRAZING FILLER ALLOYS

V.F. KHORUNOV, S.V. MAKSYMOVA and **B.V. STEFANIV**
E.O. Paton Electric Welding Institute, NASU, Kiev, Ukraine

The effect of palladium on structure, melting ranges and technological properties of alloys of the Ag–Cu–Zn–Ni–Mn system was investigated. It was established that alloying with palladium allows improving strength properties of the brazed joints at an insignificant decrease of the contact angle.

Keywords: *brazing, diamond-hard alloy tool, cadmium-free filler alloys, structure, melting range, contact angle, induction heating, phase transformation temperature, palladium, silver filler alloy, strength of joints*

Silver-base cadmium-containing filler alloys are widely applied for brazing of various materials. Considering the negative effect of cadmium on human health, investigations were carried out to determine the possibility of producing cadmium-free filler alloys with the same or similar wetting characteristics and melting temperatures [1–3].

As proved by analysis of literature data, cadmium-free filler alloys of the Ag–Cu–Zn–Ni–Mn system proved well for brazing of diamond-hard alloy tools. Their typical representative is American filler alloy BAg-22. This filler alloy has the following chemical composition, wt.%: 48–50 Ag, 15–17 Cu, 21–25 Zn, 4–5 Ni, 7–8 Mn; T_S = = 680 °C, T_L = 699 °C, and T_{br} = 699–830 °C.

The purpose of this study was to investigate technological properties of a standard filler alloy in brazing of hard alloy plates, determine strength characteristics of the brazed joints and evaluate the possibility of improving the latter due to additional alloying.

Induction heating by using a high-frequency generator of the VChI4-10U4 type with a double-coil inductor was employed to melt experimental alloys of the Ag–Cu–Zn–Ni–Mn and Ag–Cu–Zn–Ni–Mn–Pd systems under laboratory conditions. The filler alloys were melted in alundum crucibles, the latter being placed in graphite crucibles. That is, practically it was radiation heating. First the PV-200 flux was poured into a crucible, then the Ag–Cu–Ni–Mn(Pd) charge placed into a nickel foil was loaded, and after that the flux was poured again. The charge was heated up to its complete melting and formation of the liquid pool. The ingot thus formed was placed into a new crucible, the PV-209 flux was poured, and the alloy was heated up to formation of the liquid pool. Zinc was added in the process of cooling the pool to a temperature of 400–500 °C. This was followed by a short-time heating performed several times to complete melting and achieving the homogeneous melt due to induction and mechanical stirring.

The temperature range of melting of the alloys was determined by differential thermal analysis using the VDTA-8M unit in crucibles made from zirconium oxide. Heating and cooling were performed in the helium atmosphere at a rate of 80 °C/min. Weight of a specimen investigated was 1.25±0.05 g. The specimens were heated twice to provide a good fit of the charge to the crucible bottom and generate reliable data on thermal effects. The thermal effects were fixed from the second heating curve. Solidus and liquidus of the alloy were determined from the heating curve (in cooling of the alloy the substantial effect is exerted by overcooling prior to solidification). At the same time, values of the thermal effects are best seen from the cooling curve of the alloys.

Analysis of the obtained data shows that alloying with palladium exerts a significant effect on the phase transformation temperature and melting range (Table 1; Figure 1, *a*). For instance, only one phase (Figure 1, *b*) was fixed in the Ag–Cu–Zn–Ni–Mn system alloy. The solidus temperature was 670 °C, and the liquidus temperature was 710 °C. In alloy with the 2 % Pd the content the second phase in heating had a non-pronounced thermal effect, but in cooling this effect showed up very clearly (Figure 1, *c*). The solidus temperature was 660 °C and the liquidus temperature was 720 °C, i.e. the solidification range became somewhat wider. Alloy with the 5 % Pd content was also the two-phase one (Figure 1, *d*; Table 2).

Table 1. Melting ranges of commercial filler alloy (1) and alloys under investigation (2–4)

Alloy number	Alloy composition	T_S, °C	T_L, °C
1	40Ag–17Cu–17Zn–26Cd	590	610
2	49Ag–16Cu–23Zn–4.5Ni–7.5Mn	670	710
3	49Ag–16Cu–23Zn–4.5Ni–7.5Mn–2Pd	660	720
4	49Ag–16Cu–23Zn–4.5Ni–7.5Mn–5Pd	670	740

Increase in the palladium concentration led to increase in the solidus and liquidus temperatures (Figure 2).

Metallographic examinations and X-ray spectrum microanalysis of the alloys were conducted on specimens after determination of the melting temperature range. For this all the alloys were cooled down to room temperature at the same cooling rate.

Alloy of the Ag–Cu–Zn–Ni–Mn system had three clearly defined phases (Figure 3, *a*). All of them solidified in close temperature ranges. That is why they had no effect on the thermal curve. It is significant that the solid solution-based primary dendrites contained approximately equal amounts of copper, nickel and zinc, approximately 15 % Mn, but a low amount of silver (Table 2). The silver-based (74.4 %) solid solution solidified in a close temperature range. This phase contained no nickel, the contents of copper and manganese was several times lower, and that of zinc was twice as low. These two phases participated in the process of solidification of the eutectic, the typical structure of which could be seen in some regions (Table 2; Figure 3, *a*).

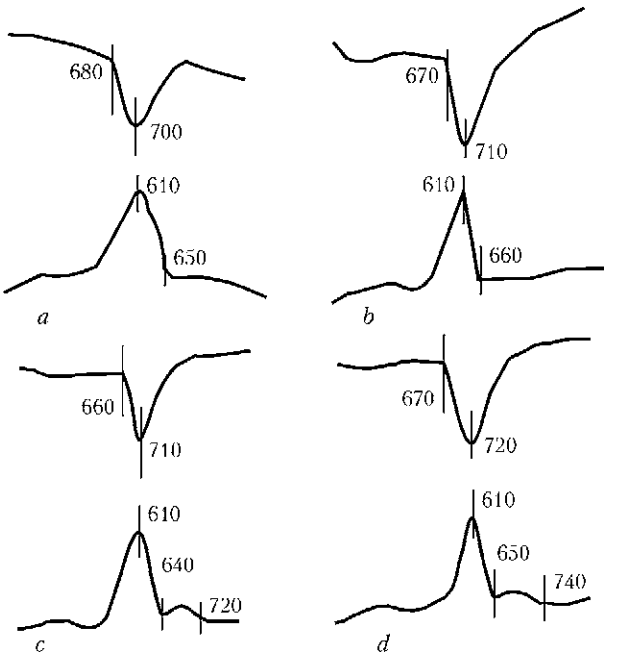

Figure 1. Data of differential thermal analysis of the alloys: *a* — Ag–Cu–Zn–Ni–Mn (amorphous foil); *b* — Ag–Cu–Zn–Ni–Mn (cast); *c* — Ag–Cu–Zn–Mn–2Pd; *d* — Ag–Cu–Zn–Ni–Mn–5Pd

The described solidification mechanism became more pronounced in alloying this composition with palladium. No development of solidification of the primary dendrites (copper-based dark crystals; Figure 3, *b*; Table 2) was detected, as the second phase (silver-based) immediately started solidifying around them. Separate solidification of the phases making up the eutectic took

Table 2. Chemical heterogeneity of the Ag–Cu–Zn–Ni–Mn(Pd) system alloys

Investigated region (phase)	Ag	Cu	Zn	Ni	Mn
49Ag–16Cu–23Zn–4.5Ni–7.5Mn					
Total	49.885	16.894	21.024	6.592	5.607
Dendrite (dark)	4.591	28.938	27.285	24.802	14.987
Grain (light matrix)	74.483	6.692	16.068	0	2.761
Eutectic	58.706	15.784	21.284	1.088	3.139
49Ag–16Cu–23Zn–4.5Ni–7.5Mn–2Pd					
Total	64.541	11.082	16.919	1.044	3.430+(2.995Pd)
Dendrite (dark)	13.696; 11.471	43.421; 34.875	14.573; 25.190	10.905; 14.031	5.274+(12.123Pd)–7.258+(6.162Pd)
Grain (light matrix)	74.810	6.214	16.959	0	2.021+(0Pd)
Eutectic (banded)	67.617; 52.748	9.727; 20.488	15.417; 21.156	1.291; 0.335	2.564–2.219+2.850–3.057Pd
49Ag–16Cu–23Zn–4.5Ni–7.5Mn–5Pd					
Total	63.603	11.371	16.723	1.932	3.239+(3.143Pd)
Dendrite (dark)	8.122	22.072	27.821	13.127	9.753+(19.038Pd)
Grain (light matrix)	70.685	7.437	15.380	0.905	2.676+(2.919Pd)
Eutectic (banded)	60.781; 59.666	13.038; 12.086	17.836; 14.758	1.105; 2.363	2.153+(5.093Pd)–2.963+(8.166Pd)

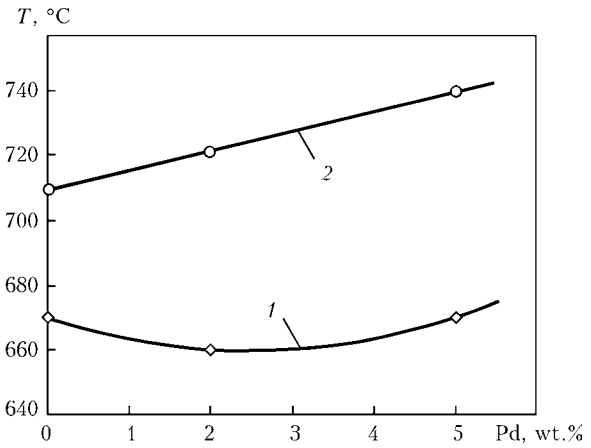

Figure 2. Solidus (*1*) and liquidus (*2*) temperatures of the alloys depending on the palladium content

place first. It was followed by solidification of the normal eutectic occupying the major part of the section. This mechanism was assumed to take place in the study by A.A. Bochvar [4]. However, it is more characteristic of organic materials, and rarely occurs in metal alloys [5]. Note that nickel and palladium were concentrated in dendrites (of a dark colour), and were absent in the light phase (silver-based) (see Figure 3).

Increase in the palladium content of an alloy caused increase in the quantity of the primary crystals. However, they did not grow much, as the silver-based phase started solidifying. The regions of separate solidification of the eutectic occupied the major part of the section. And regions of the normal eutectic occurred much more rarely (Figure 3, *c*). Note that in this alloy the

Table 3. Area of spreading and shear strength of brazed specimens of steel 12Kh18N10T

Filler alloy number	Alloy system	Spreading area S_{spr}, mm^2	Average values of shear strength τ_{sh}, MPa
1	Ag–Cu–Zn–Cd	–	263.3 [6]
2	Ag–Cu–Zn–Ni–Mn	704.7	342.3
3	Ag–Cu–Zn–Ni–Mn–2Pd	573.0	321.3
4	Ag–Cu–Zn–Ni–Mn–5Pd	971.0	359.1

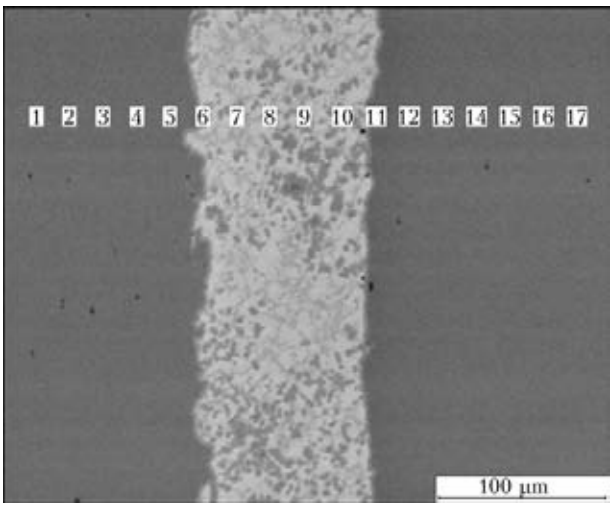

Figure 4. Location of X-ray spectrum analysis points in the brazed seam and base metal

copper-based grains contained a low amount of nickel and palladium.

Experiments on determination of the spreading area over stainless steel and hard-alloy material VK8, as well as strength of the brazed joints produced by joining these materials were carried out by using the investigated brazing filler alloys. The experiments were conducted on stainless steel according to GOST 23904–79 and GOST 23047–75, respectively. The results obtained are given in Table 3.

Structure and chemical heterogeneity of the stainless steel joints produced by using the Ag–Cu–Zn–Ni–Mn system filler alloy were investigated. Structure of the brazed seam turned out to be identical to that of the pure filler alloy: solid solution-based primary dendrites were clearly revealed with the second phase and normal eutectic regions solidifying around them, i.e. there was no intensive development of diffusion exchange at interfaces of the joints. This was proved both by the data of X-ray spectrum microanalysis at separate points (Figure 4; Table 4) and by the diagrams of distribution of elements in cross sections of the seams (Figure 5).

As follows from the data of Table 4, iron and chromium, which are the main elements of the

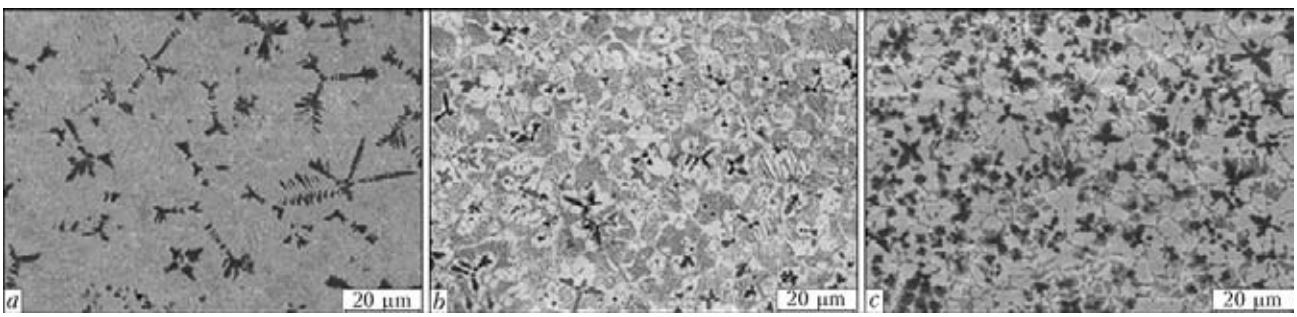

Figure 3. Microstructures of the experimental alloys: *a* — 49Ag–16Cu–23Zn–4.5Ni–7.5Mn; *b* — 49Ag–16Cu–23Zn–4.5Ni–7.5Mn–2Pd; *c* — 49Ag–16Cu–23Zn–4.5Ni–7.5Mn–5Pd

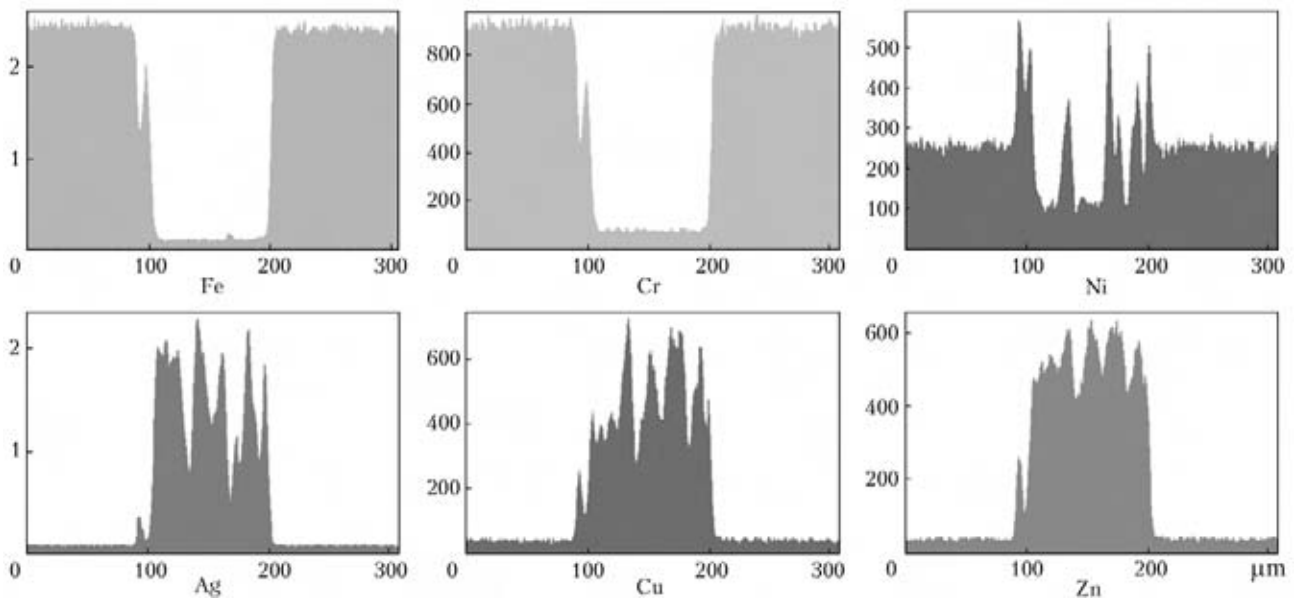

Figure 5. Diagrams of qualitative distribution of elements in the brazed seam metal produced by using the Ag–Cu–Zn–Ni–Mn system filler alloy

brazed metal, were absent in the seam, the transition zone was absent either. The weight content of iron in the base metal near the interface of the joint was 60–70 %, whereas that on the seam side was 0.30–0.75 %. The situation with chromium was similar: near the fusion boundary on the side of the base metal its concentration was 13.5–16.5 %, and on the side of the filler alloy it was 0.18–0.40 %. The seam contained no titanium and silicon at all.

Elements of the filler alloy were present in the seam, and were hardly revealed in the base metal (Table 4). For example, the weight content of silver near the interface of the joint on the seam side was within 65.0–69.5 %, and on the base metal side — within 0–0.97 %. The similar situation was characteristic also of copper and zinc.

The experiments on spreading were carried out by using the 13.5 mm diameter and 4.5 mm

Table 4. Content of elements (wt.%) at separate points of the brazed joint

Spectrum number	Si	Ti	Cr	Mn	Fe	Ni	Cu	Zn	Ag
1	0.6	0.43	17.08	1.8	70.51	9.58	0	0	0
2	0.5	0.38	17.06	1.89	70.62	9.54	0	0	0
3	0.57	0.77	17.6	1.84	69.54	9.68	0	0	0
4	0.7	0.3	16.7	1.33	69.9	11.08	0	0	0
5	0.66	0.52	17.04	2.02	69.45	9.62	0.7	0	0
6	0.26	0.35	13.57	3.4	59.74	17.34	2.51	2.84	0
7	0	0	0.4	0.71	0.3	3.12	13.34	17.13	64.99
8	0	0	0.24	0.67	0.65	2.13	11.33	15.52	69.46
9	0	0	0	0.37	0.23	0.74	8.9	13.4	76.37
10	0.11	0	0	0.95	0.76	4.25	11.59	15.34	67
11	0	0	0.18	0.79	0.75	3.24	11.65	13.79	69.6
12	0.36	0.44	16.56	2.21	70.02	9.43	0	0	0.97
13	0.26	0.71	16.95	2.09	70.91	9.06	0	0	0
14	0.5	0.41	16.99	1.44	70.71	9.95	0	0	0
15	0.6	0.59	17.33	1.71	68.7	9.81	0	0	1.26
16	0.53	0.27	17.18	1.92	70.44	9.67	0	0	0
17	0.34	0.5	17.7	1.62	69.45	9.34	0	0	1.06

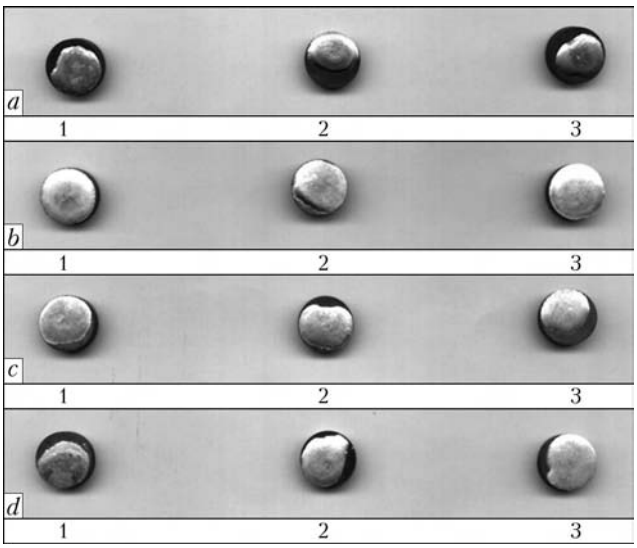

Figure 6. Appearances of specimens 1–3 for investigation of spreading of filler alloys 1–4 (*a–d*) over hard alloy material VK8

thick plates of hard alloy material VK8 and filler alloys in the form of cubes measuring 4 × 4 × × 4 mm.

Prior to brazing the specimens were degreased with acetone (alcohol), then the filler alloy being studied was placed at the specimen centre, and flux of the PV-209 grade having the reactivity temperature range equal to 600–850 °C was deposited on the top over the entire perimeter of a specimen [7]. Heating of the specimens was performed by using high-frequency generator VChI4-10U4 with a frequency of 440 kHz and power of 10 kW. The double-coil inductor was employed for these studies. A rack of heat-resistant ceramics with a channel to attach a thermocouple for measuring the temperature of heating of a specimen up to complete spreading of the filler alloy was installed inside the inductor. Holding for three seconds was performed after melting of the filler alloy. After that heating was stopped. The degree of wetting of a solid substrate with the filler alloys was determined by evaluating the area of spreading of a molten filler alloy (three specimens for each filler alloy) and contact angle between the substrate and a spread droplet of the filler alloy metal (Figure 6). The contact angle was determined on the sections cut out from the specimens normal to the wetting plane (Figure 7). The data were obtained by using the AutoCad software.

Table 5. Results of tests of the VK8 joints brazed with filler alloys of different systems

Filler alloy number	Filler alloy system	Spreading area S_{spr},* mm^2	Contact angle θ, deg	Shear strength τ_{sh}, MPa
1	Ag–Cu–Zn–Cd	95.30	17	245
2	Ag–Cu–Zn–Ni–Mn	136.32	10	225
3	Ag–Cu–Zn–Ni–Mn–2Pd	111.06	16	250
4	Ag–Cu–Zn–Ni–Mn–5Pd	112.01	13	315

*Spreading area was determined by using high-frequency heating following a non-standard procedure

Specimens for mechanical tests were brazed in air by using high-frequency heating. Flux in the form of a paste mixed up with water was preliminarily deposited on the hard alloy plates (VK8+VK8, VK15+VK15 etc.). Then a filler alloy charge was placed between the hard alloy plates, and heating was performed up to complete melting of the flux and filler alloy, as well as up to formation of the joint.

Shear strength was determined by the V.N. Bakul Institute for Superhard Materials of the NAS of Ukraine by using a special attachment (to the tensile testing machine P-05). As seen

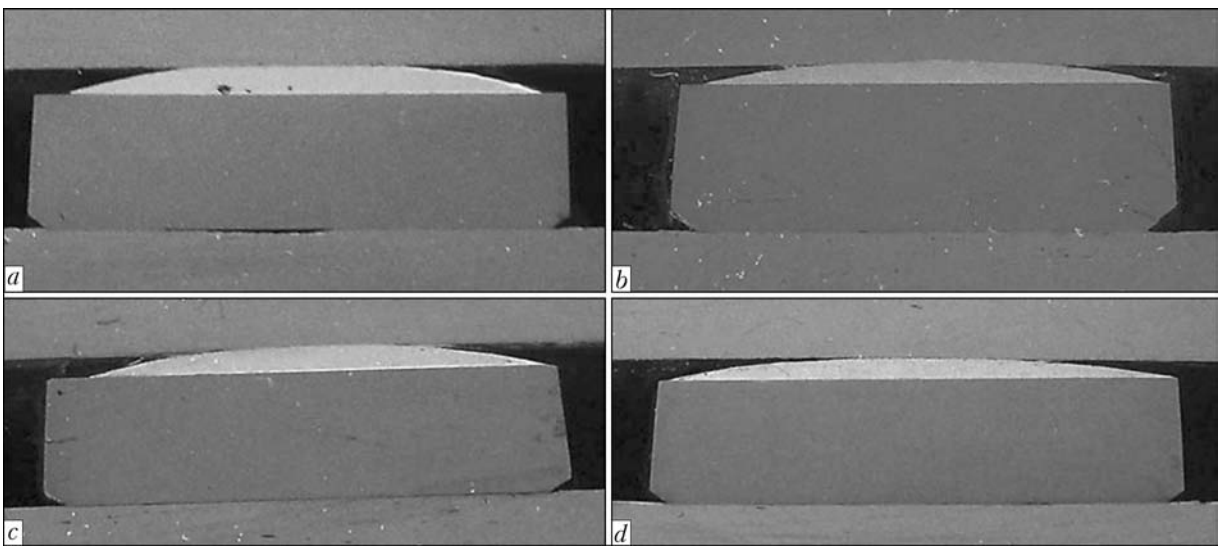

Figure 7. Cross section of specimens after spreading tests using filler alloys 1–4 (*a–d*) (see Table 5)

from the data given in Table 5, alloying of the experimental filler alloy with palladium substantially increased strength of the joints.

Filler alloys of the investigated systems were employed to manufacture a batch of bits for drilling the wells to produce dispersed methane, which increased several times the length of deepening of the wells [8].

Therefore, application of the environmentally clean filler alloys of the Ag–Cu–Zn–Ni–Mn and Ag–Cu–Zn–Ni–Mn–Pd systems instead of filler alloys of the Ag–Cu–Zn–Cd system for brazing of rock and metal cutting tools makes it possible not only to avoid the harmful effect of cadmium on human organism, but also to provide the increased-strength brazed joints.

1. Roberts, P.M. (1978) Recent developments in cadmium-free silver brazing alloys. *Welding J.*, **10**, 23–30.
2. Timmins, P.F. (1994) The development of Ag-based brazing alloys. *Ibid.*, **10**, 31–33.
3. Khorunov, V.F., Maksymova, S.V., Stefaniv, B.V. (2010) Effect of tin additions on structure and technological properties of brazing filler metals of the Ag–Cu–Zn system. *The Paton Welding J.*, **7**, 16–21.
4. Bochvar, A.A. (1956) *Metals science*. Moscow: Metallurgizdat.
5. Taran, Yu.N., Mazur, V.I. (1978) *Structure of eutectic alloys*. Moscow: Metallurgiya.
6. Petrunin, I.E., Lotsmanov, S.N., Nikolaev, G.F. (1973) *Brazing of metals*. Moscow: Metallurgiya.
7. Klochko, N.A. (1981) *Fundamentals of the technology for brazing and heat treatment of hardalloy tool*. Moscow: Metallurgiya.
8. Khorunov, V.F., Maksymova, S.V., Stefaniv, B.V. (2010) Manufacture of drill bits for production of dispersed methane in mine working. *The Paton Welding J.*, **6**, 41–43.

RESEARCH AND DEVELOPMENT OF THE TECHNOLOGY FOR WELDING OF DISSIMILAR HEAT-RESISTANT CHROMIUM AND HIGH-TEMPERATURE STEELS FOR MODERN POWER PLANTS

The research work on the above subject was completed in 2011 by the E.O. Paton Electric Welding Institute (supervisor – Dr. A.K. Tsaryuk)

The object of the research was heat-resistant and high-temperature steels with improved service properties, as well as their welded joints.

The purpose of the research was to identify physical-metallurgical factors that determine formation of structure and mechanical properties of the joints between heat-resistant chromium martensitic steels and high-temperature austenitic steels, and develop the technology for welding these steels.

The research methods included spectral analysis, X-ray spectral microanalysis, metallographic analysis, measurement of hardness and microhardness, and testing of mechanical properties according to GOST 6996–66.

The research showed that welding of martensitic chromium steel of the 10Kh9NMFB type to chrome-nickel steel of the 18-10 type by using austenitic consumables results in structural and chemical heterogeneities taking place in the fusion zone and showing up in formation of soft decarbonised interlayers of structurally free ferrite in HAZ of steel 10Kh9NMFB. Size of this zone decreases with decrease in welding heat input. However, it is impossible to fully avoid it even in welding at minimal heat inputs.

Formation of the ferrite interlayer in HAZ of steel 10Kh9NMFB can be prevented owing to deposition of a purely nickel metal. However, in this case it is impossible to ensure the required service properties of the welded joints. It was established that the ferrite interlayer will not form if steel 10Kh9NMFB is preliminarily coated with martensitic deposited metal.

Lately, along with the traditional technology for welding of dissimilar joints using austenitic-grade consumables, an increasingly wider acceptance is gained by a process that provides for the use of low-carbon chromium filler metal alloyed with nickel, molybdenum, etc.

To ensure strength of the fusion zone at a level of that of steel 08Kh18N10T, it is recommended to preliminarily coat the base metal with materials that provide deposited metal of the 05Kh6M type, while the main volume of the weld can be filled up with both martensitic and austenitic materials.

A new slag system of the fluoride-magnesium type was developed. It provides decrease in the content of carbon in the deposited metal to 0.04 % at a sufficiently low content of diffusible hydrogen. Electrodes developed on the base of this system have good welding-technological properties and provide the deposited metal with optimal chemical composition and mechanical characteristics.

SUBSTANTIATION OF «LEAK-BEFORE-BREAK» CRITERION FOR VERTICAL CYLINDRICAL TANKS FOR OIL STORAGE

V.V. KNYSH, A.Yu. BARVINKO, Yu.P. BARVINKO and **A.N. YASHNIK**
E.O. Paton Electric Welding Institute, NASU, Kiev, Ukraine

The paper gives the results of experimental studies of cyclic crack resistance of samples of butt-welded joints on 06GB-390 steel in the case of oil storage tanks at stable development of a through-thickness fatigue crack, initiating from the notch surface along the fusion line, from the moment of its initiation up to reaching the length of about 30 mm. Large-scale samples of welded joints of 650 × 160 × 20 mm dimensions were tested at harmonic alternating zero-to-tension stress cycle with $\sigma_{max} = 2/3\sigma_y$. It is shown that application of rolled sheets of the above-mentioned steel for design rings of tank wall allows, at application of «leak-before-break» criterion, eliminating extended fractures in the wall welded joints.

Keywords: *fatigue crack, development of through-thickness fatigue crack, «leak-before-break» criterion, cyclic loading*

Over the recent decades, because of instability of oil price in the world oil market, many countries are building tanks of 50,000–100,000 m^3 and greater capacity to create the required stock of this product. Requirements to ecological safety of such constructions are becoming more stringent with every year, accordingly. Normative requirements as to steel mechanical properties, in particular in *Z*-direction, for rolled sheets of tank walls and their welded joints have grown significantly. However, in view of various peculiarities, defects in the wall welded joints cannot be eliminated completely, which at wall operation under cyclic loading conditions can become the source of initiation and development of tough fatigue fractures. Under such conditions, the problem of establishing the fatigue life of the stage of stable subcritical propagation of through-thickness fatigue crack in design rings of tank wall is becoming particularly urgent. Appearance of a dark spot on the white wall from seeping oil from the formed through-thickness crack, can be a reliable criterion of crack detection in those cases when the time of its growing up to critical size will allow guaranteed detection of the crack under the conditions of technical examination of tanks according to the applied procedures. Such a criterion of crack detection in pressure vessels was called «leak-before-break» [1].

The purpose of the proposed work was experimental substantiation of the possibility of application of «leak-before-break» criterion to vertical tanks for oil storage, in which the lower rings are made of a new class of high-quality steel 06GB-390.

Application of new generation niobium-containing steels 06GB-390, 06G2B-440 [2] with impact toughness values $KCV_{-40} \geq 120$ J/cm^2 8 to 40 mm thick (furtheron strength classes will be omitted in the work) and with fine-grained isotropic structure for design lower rings of the walls essentially improved their crack resistance. In this respect study [3] is of interest, which shows that stabilization of critical crack opening displacement within $\delta_{cr} = 0.18–0.20$ mm is observed for a number of tested steels with $KCV_{-20} \geq 80$ J/cm^2. In view of that, it is logical to expect that at application of 06GB steel for lower rings of tank wall and possible formation of a fatigue crack in it, its growth rate will give enough time for detection of the above crack at subcritical stage of its development.

As was noted above, at application of «leak-before-break» criterion under the conditions of tank operation, it is important that the duration of the stage of stable crack growth in the linear (second) section of fatigue fracture diagram [4], expressed by the number of tank filling–emptying cycles, allowed enough time to enable detection of a through-thickness crack after oil outflowing from it, and taking the required safety measures. In this work flat samples with a transverse butt weld were tested to substantiate the criterion «leak-before-break» for a wall of oil storage tank (Figure 1). In samples made from rolled sheets of 06GB steel, cross-section with removed weld reinforcement was equal to 160 × 19.5 mm, and length was 650 mm. Maximum stress of harmonic loading cycle was taken, allowing for maximum

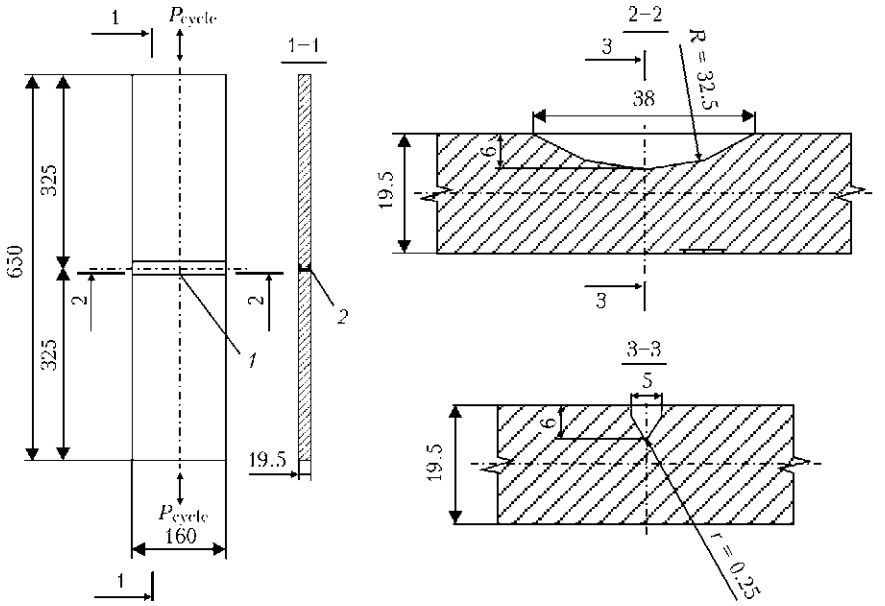

Figure 1. Schematic and dimensions of samples for testing welded joints of 06GB steel for cyclic crack resistance: *1* — notch in the fusion zone; *2* — weld reinforcement was removed from two sides

value of calculated hoop stresses in the tank wall [5] found from the following condition:

$$\sigma_h \le R_y \gamma_w / \gamma_n,$$

where R_y = 350 MPa is the calculated resistance; γ_w = 0.8 is the coefficient of operating conditions of wall rings; γ_n = 1.1 is the fitness-for-purpose factor.

In view of the above, maximum stress of alternating loading cycle was taken as σ_{max} = = 260 MPa. Such a level of hoop stresses allows for tolerances [5] for deviation of the geometrical shape of new tank wall from the design value. Considering that the tank wall is a thin-walled shell of up to 60 m diameter and up to 20 m height, after 15–20 years of service the norms [6] allow exceeding the initial geometrical deviations (foundation sagging under the wall, appearance of dents, etc.) 2 times. It is natural that under these conditions, in individual regions of the wall hoop stresses will be significantly higher than the initial values, that was allowed for by coefficient γ_w = 0.8, but these stresses should not exceed the calculated values for this steel considering the periods of technical examination of tanks. Growing of the initial surface notch in the sample at the first stage up to formation of a through-thickness crack, and then growth of this crack leads to reduction of sample net section area and increase of stresses in the sample that to a certain extent simulates the noted local increase of hoop stresses in the actual tank wall.

Initial crack-like surface notch was made in sample center at a distance from the weld fusion line with specially ground cutter. Length of semielliptical notch 2a was 38 mm, and its depth was 6 mm at notch rounding-off radius of 25 mm. All the samples were tested in hydro-pulsator TsDM 200pu at uniaxial zero-to-tension alternating stretching with 5 Hz frequency. Duration of the stage of surface crack initiation from the notch and its growing through sample thickness up to appearance of through-thickness crack is given in [7].

Fatigue testing of samples was conducted at room temperature; however, considering that rolled sheets of 06GB steel of 8–50 mm thickness maintain their high plastic properties in the temperature range T = +20 – –40 °C [2], it can be assumed that the obtained test results are correct up to temperature T = –40 °C. During testing the initial length of the formed through-thickness crack was measured on sample side opposite to the notch and number of cycles, at which it formed, was measured. Furtheron cycle number was recorded at its elongation by each 3–6 mm. At crack length 2a ≈ 40 mm its tip developed plastic contractions and testing was stopped. Results of fatigue testing of the samples are given in the Table. Figure 2 gives the dependence of fatigue crack length on number of alternating loading cycles.

Table data show that at crack length 2a ≤ ≤ 30 mm in sample net section stresses did not exceed the calculated resistance of 06GB steel (R_y = 350 MPa). After the crack has grown to the length of 2a > 40 mm in sample net section, maximum stresses reached values close to steel yield point, i.e. appearance of observed plastic contractions at such a crack length is not related

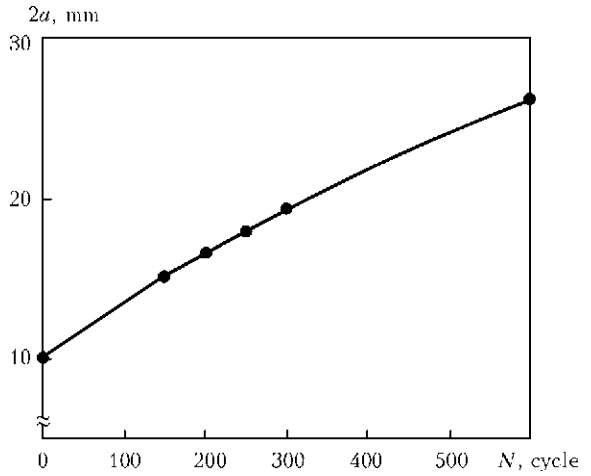

Figure 2. Dependence of length $2a$ of through-thickness crack in the fusion zone on the number of loading cycles N of samples of butt welded joints of 06GB steel (value of crack length $2a$ in each point is given as an average from testing 6 samples)

to limit state of cyclic crack resistance, but is due to limited dimensions of the sample. Such high stresses will not develop in the rings of actual tank wall at specified crack length, because of many times smaller weakening of the wall by the considered defect.

Application of empirical dependence between K_{1C} and KCV specified in the norms allows determination of critical crack length $2a_{cr}$ for the given welded joint at minimum temperature of tank service $T = -40$ °C. In keeping with [8] $K_{1C} = 0.1\sqrt{0.1\dfrac{E}{1-\mu^2}KCV_{-40}}$, MPa·$\sqrt{\text{m}}$. At $KCV_{-40} = 246$ J/cm^2 we get $K_{1C} = 236$ MPa·$\sqrt{\text{m}}$ for the weld. At possible increased hoop stresses in the wall $\sigma_h = R_y = 350$ MPa, proceeding from the known relationship for through-thickness crack of critical length $2a_{cr}$, $K_{1C} = \sigma_h\sqrt{\pi a_{cr}}$, we get value $a_{cr} = 145$ mm for the given σ_h and $2a_{cr} = 290$ mm, respectively. For new tanks of 50,000 m^3 capacity in keeping with the norms [5], hoop stresses in the wall are taken to be equal to 260 MPa. At such stresses the calculated value of critical crack length reaches $2a_{cr} = 520$ mm.

Considering that KCV_{-40} values for base metal and weld are actually the same, obtained values of critical crack length can be extended also to the wall base metal.

Conservative value of critical length of through-thickness crack of about 30 mm taken at fatigue testing of welded joint samples, which allows reliably fixing the dark oil spot on the wall surface, gives a ten-fold margin for actual critical length of the tank crack of approximately 300 mm.

From Figure 2 it is seen that at steady stable development of a through-thickness fatigue crack in the samples, dependence of its length on the number of loading cycles is close to the linear one. Its stable propagation up to the length of 20 mm is observed during the first 300 loading cycles. At subsequent 300 cycles crack length increases by just 6 mm. Crack length, corresponding to 300 loading cycles, is of important practical value, as this number of loading cycles (oil discharge–filling) corresponds to one year of tank service in some oil tank farms [9]. In regular oil tank farms this value is not higher than 100–120 per year.

For tanks in service results obtained at sample testing should be corrected by the safety factor by the number of loading cycles. This correction is required to allow for the scale factor as to the possible presence of unrevealed defects in real tanks. In [10] proceeding from generalization of investigation results of a broad experimental program of full-scale fatigue testing of pressure vessels, it is proposed to take the safety factor by cycle number equal to 20. In our case it means that in reality the time for detection of outflowing oil spot on the tank wall equal to fulfillment of fifteen (330:20) cycles of oil discharge–filling

Growth of through-thickness crack length $2a$ on the surface opposite to the notch and stresses in the sample net section depending on the number of loading cycles N

#	Number of loading cycles N	Length of through-thickness crack* $2a$, mm	Sample weakening area, cm^2	Net sample area, cm^2	Maximum stresses across net section**, MPa
1	0	10.1	6.2	25.0	332.0
2	150	15.2	6.7	24.5	338.8
3	200	16.7	6.9	24.3	341.5
4	250	18.0	7.0	24.2	343.0
5	300	19.4	7.2	24.0	345.0
6	600	26.2	8.0	23.4	354.2
7	1400	40.0	9.5	21.7	373.0

*Crack length, cross-sectional area and stresses are given as average value by the results of testing 6 samples. **Maximum cycling force of 8300 kg; through-thickness crack of $2a$ length is located along the fusion line of butt welded joint of 06GB steel.

will be guaranteed. For oil tank farms with regular operation mode this is equal to one month, and at more intensive mode — to not less than two weeks of service. In case of compulsory everyday visual examination of tank wall surfaces in keeping with the rules of tank operation, this time is quite sufficient for guaranteed detection of the formed defect by «leak-before-break» criterion, and for taking measures to repair it. Period of stable crack growth at subsequent loading cycles from 300 up to 600 can be regarded as a guarantee of safe crack detection under force-major circumstances.

Guaranteed detection of fatigue cracks at the stage of their stable development prevents the possibility of fracture of tank design rings either in base metal or in welded joints. Therefore, in tank design it is necessary to first of all provide the conditions for elimination of local fractures of the main wall, bottom, r-bars and branchpipe assemblies. Ensuring the static strength of the main tank wall becomes the main objective for its design. Elimination of extended fracture formation on its surface will be ensured by application of the criterion of «leak-before-break», provided steels with Z 35 group of lamellar fracture resistance and impact toughness $KCV \geq$ ≥ 80 J/cm^2 at minimum service temperature of the tanks are used for the wall. Such requirements are met, in particular, by 06GB steel. In the presence of the main wall with application of this steel, the protective wall will just contain the possible oil spill within its limits, while taking the static load.

The proposed approach eliminates the need for construction on the main wall of additional structural elements in the form of bands or other solutions, as a tool for arresting extended fractures, or construction of special stiffener rings on the protective tank wall for preservation of the wall geometrical shape.

Prevention of extended fractures on the tank wall by application of rolled sheets of the new steels with the above mechanical properties and substantiated application of «leak-before-break» criterion does not eliminate the requirements of the high quality of rolled sheets and their welded joints. Producing welded joints on the new steels with mechanical properties not inferior to those of base metal and elimination of cold crack formation in them, requires application of special welding technologies and increased scope of their quality testing compared to the norms for tanks [11].

Results of experimental investigations, given in this publication and in work [12], have been successfully implemented at design and construction of two tanks with the protective wall, each of 50,000 m^3 capacity at oil-pumping station «Mozyr» (Belarus Republic). Erection and welding operations at construction of these tanks were performed with field supervision of PWI specialists.

CONCLUSIONS

1. It is shown that the fatigue life of the stage of stable subcritical development of the formed through-thickness fatigue crack exceeds 300 loading cycles. Considering the safety factor by cycle number equal to 20, which is taken for pressure vessels, the above fatigue life provides minimum two weeks of safe operation of oil storage tank. At performance of compulsory daily visual inspection of the tank wall surface in keeping with tank service rules, this time is sufficient for guaranteed detection of the formed defect by «leak-before-break» criterion and taking measures for its repair.

2. Making design rings of tank wall of 06GB steel up to 30 mm thick using the criterion of «leak-before-break» allows eliminating extended fractures in the wall welded joints and preventing the possibility of appearance of oil outflow with a high kinetic energy. In this connection there is no need to envisage additional structural elements in the form of bands on the tank main wall, or special reinforcing rings for preservation of the wall geometrical shape.

1. Broek, D. (1980) *Elementary engineering fracture mechanics*. Moscow: Vysshaya Shkola.
2. *TU U 27.1-05416923-085:2006*: Rolled sheets welded from quality steel of strength grades 355–590 for machine-building. Introd. 02.04.2007.
3. Paton, B.E., Trufyakov, V.I., Kirian, V.I. (1982) Requirements to toughness of steel for main gas pipelines at mounting of extended fracture arresters in them. *Avtomatich. Svarka*, **12**, 5–9.
4. Karzov, G.P., Leonov, V.P., Timofeev, B.T. (1975) *Welded high-pressure vessels*. Leningrad: Mashinostroenie.
5. *PB 03-605–03*: Rules of design of vertical cylindrical steel tanks for petroleum and petroleum products. Moscow.
6. (2003) *Instructions on technical supervision, methods of inspection and rejection of pipe furnaces, tanks for petroleum and petroleum products*. Moscow.
7. Barvinko, A.Yu., Knysh, V.V., Barvinko, Yu.P. et al. (2012) Development of surface crack-like defect in welded joints of 06GB-390 steel at cyclic loading. *The Paton Welding J.*, **5**, 40–42.
8. *VBN V.2.3-00018201.04–2000*: Strength analysis of operating main pipelines with defects. Kiev.
9. *RD 16.01-60.3000-KTN-026-1–04*: Codes of design of steel vertical tanks of 1000–50000 m^3 volume for petroleum storage. Moscow: AC Transneft.
10. Nichols, R. (1975) *Pressure vessel engineering technology*. Moscow: Mashinostroenie.
11. *GOST 31385–2008*: Vertical cylindrical steel tanks for petroleum and petroleum products. General technical requirements. Moscow.
12. Poznyakov, V.D., Barvinko, A.Yu., Barvinko, Yu.P. et al. (2012) Cold resistance and lamellar fracture resistance of welded joints on steel 06GB-390. *The Paton Welding J.*, **3**, 35–39.

TRANSISTOR POWER SOURCES FOR ELECTRIC ARC WELDING (Review)

A.V. LEBEDEV
E.O. Paton Electric Welding Institute, NASU, Kiev, Ukraine

The paper describes the most widely accepted circuits of electric arc transistor power sources. Features of parallel operation of transistors, methods of overvoltage protection and switching path formation, modern drivers, design of high-frequency transformers, power correctors, systems of control of electrode metal melting and transfer are considered.

Keywords: *electric arc welding, power source, transistor, transformer, control system, metal melting and transfer*

Leading manufacturers of welding equipment are mainly producing transistor-type power sources for electric arc welding. Thyristor rectifiers and rectifiers with step voltage switching are manufactured in small quantities. Transistor sources have small weight and overall dimensions, high accuracy of adjustment and fast response. The simplest transistor source is the one based on pulse controller (chopper) (Figure 1). Compared to inverter sources, transistors operate at significantly lower voltages without any through currents, their control circuit is much simpler, and there is no high-frequency transformer. Chopper sources generate relatively low interference and only slightly distort the mains voltage, and their power factor is close to 1. Their large weight is a disadvantage. Chopper source Origo Mig 4002c (ESAB) for 400 A has the weight of 139 kg. Weight of inverter power source Origo Mig 4001i for the same current is equal to 43.5 kg.

One of the first transistor sources, manufactured in Ukraine in 1972 at the Institute of Electrodynamics by the order of the E.O. Paton Electric Welding Institute, was designed for consumable-electrode welding in space. Maximum current was equal to 300 A, at 27 V power supply from the spaceship on-board mains. In 1980s the Institute of Electrodynamics developed chopper sources for 500 A for multi-station semi-automatic welding in shipbuilding [1]. A source for 1000 A was manufactured for investigation of metal transfer in consumable-electrode welding, which lowered metal losses for spattering to 0.5 % in CO_2 welding [2, 3].

Application of two transistors and high-frequency transformer in the chopper enables eliminating the mains transformer (Figure 2). Other names of such a circuit are single-step converter, asymmetrical bridge, and «skew» bridge [4–6]. Application of such a circuit allows eliminating the causes for appearance of through currents and asymmetrical magnetization of high-frequency transformer. Therefore, at the initial period of development of inverter sources «skew» bridges were very popular. Now a considerable portion of the sources are made by this circuit.

Lowering of output voltage ripple and power increase are achieved at operation of two «skew» bridges for one load (Figure 3). The disadvantage of the «skew» bridge — doubled weight of the high-frequency transformer — is eliminated by semi-bridge circuit (Figure 4). Such a circuit is the most often used in sources of several kilowatt power and mains voltage of 220 V. There is, however, a possibility of through current flowing through transistors in it that may lead to inverter malfunction. Another disadvantage is a two-times increased current load on the transistors

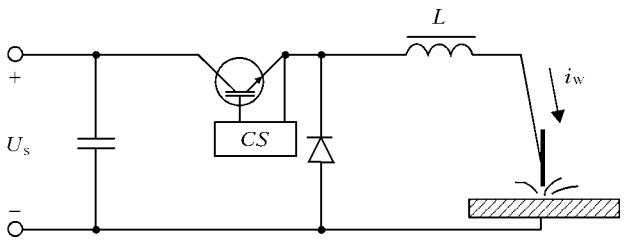

Figure 1. Circuit of reducing pulse controller (chopper)

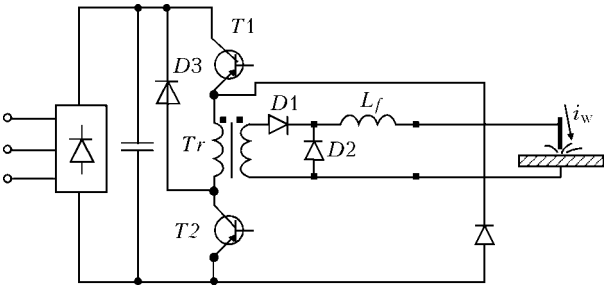

Figure 2. Circuit of asymmetrical («skew») bridge

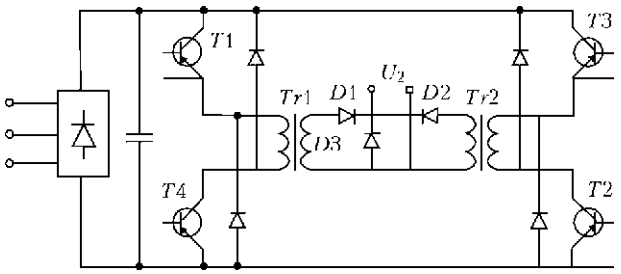

Figure 3. Circuit of power source consisting of two asymmetrical bridges

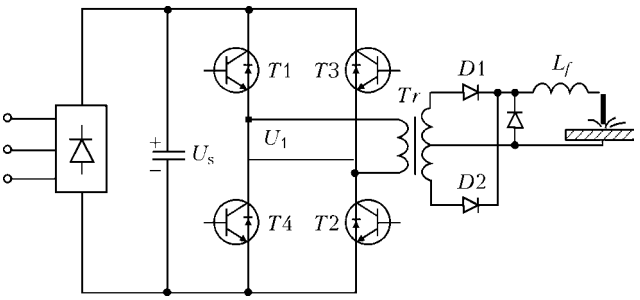

Figure 5. Circuit of bridge inverter

compared to bridge circuit (Figure 5). A pilot sample of bridge welding inverter with power supply from 380 V mains was manufactured in 1982 at the Institute of Electrodynamics. Absence of reliably operating transistors for more than 600 V voltage at that time did not allow introducing it into batch production. This problem is not completely solved even now.

Maximum admissible current of the most popular IGBT transistors at case temperature of 25 °C is 50 A. With temperature increase up to 100 °C, current drops markedly. For reliable operation of the transistors, they should be loaded by not more than 30–50 % of the maximum admissible current. Therefore, parallel connection of transistors, which began to be applied already in 1950s [7], is often used even in sources with power supply from 220 V voltage and welding current of 120 A. Reliability of such a connection can be smaller than that of one transistor, as the quantity of semi-conductor crystals and brazed joints is increased.

In order to improve the reliability of parallel connection rather than lowering it, the Institute of Electrodynamics proposed deep redundancy method. At the start of 1960s this method was used to manufacture a transistor switch for 100 A [8]. One thousand (!) germanium transistors were connected in parallel, each of which with maximum admissible current of 0.4 A. Transistors were first sorted by voltage drop. Transistors with the same voltage drop were connected in parallel that reduced current scatter between the transistors. In addition, fuses were connected into the emitter and base circuit of each transistor. Transistor failure led to fuse blowing and its switching off. Current switched by the failing transistor was redistributed between the remaining transistors. As all the transistors operated at significant underloading even in the case of maximum current switching, current increase by 1/1000 did not lower operation reliability. Theoretical investigations and experiments confirmed the high reliability of such connection. In modern power sources deep redundancy method is not used, so that failure of one transistor can lead to malfunction of the source.

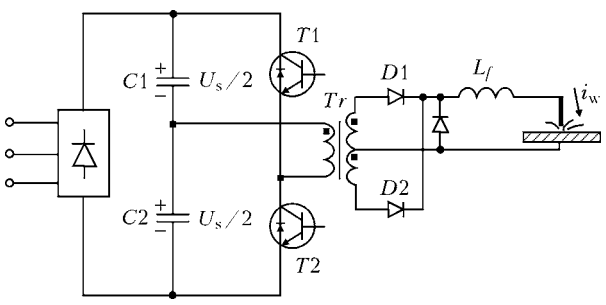

Figure 4. Circuit of semi-bridge inverter

At design of high-frequency power transformers two main problems have to be solved: achievement of minimum leakage inductance, and taking measures for elimination of the influence of surface effect in conductors. Leakage inductance causes pauses in rectified voltage, which lower the source effectiveness [9].

The simplest method to suppress leakage inductance is to use it as inductance in the resonance power source. In the other cases, inductance should be lowered by minimizing the distance between the windings and their sectionalization. Frequency from 20 up to 80 kHz is used in modern sources. Transformer magnet cores are made of ferrite. Depth of current penetration into the conductor at such frequencies is from 0.50 up to 0.34 mm. Therefore, it is rational to use wires with not more than 1–2 mm cross-sectional dimensions. In sources of several kilowatt power currents are relatively low, so that primary winding is wound from wire of round section. Parallel connection of wires of round or rectangular section is used in the secondary winding [6, 10, 11].

Another variant of reducing the surface effect is application of RF cable as the conductors, which can be replaced by simultaneous winding with parallel conductors. In high power transformers the primary winding is wound with wire of rectangular cross-section. Secondary winding can be made of insulated copper strip equal to doubled depth of current penetration and width covering the entire primary winding. Shell-core transformer of such a design of 15 kW power

(100 % duty cycle) and 1 kg weight was manufactured in 1982 for inverter power source.

Modern power sources mainly use shell-type transformers as the most manufacturable ones, rather than core-type or ring transformers, although they lower the leakage inductance and improve the cooling conditions. The most manufacturable cable transformers are used even more seldom. For 3 kW source cable transformer magnet core consists of several ferrite rings with cross-sectional area of 8 cm^2, and windings with w_1 = 12 and w_2 = 2 turns [12, 13].

In modern power sources IGBT transistors are mainly used. Field-effect transistors are applied much more seldom. At parallel connection of IGBT transistors the transistor with the lowest saturation voltage, transmits greater current and is heated more [14, 15]. The sign of the temperature coefficient of saturation voltage (TCSV) has the greatest influence on connection reliability. If TCSV has a positive value, then temperature rises and voltage drop becomes greater in the transistor with greater current, thus leading to current decrease. If TCSV value is negative, transistor with higher current is heated more, voltage drop in it decreases, thus leading to an even greater load by current and further heating. In IGBT transistors TCSV sign depends on current. For instance, for transistors of GA100TS60SQ type TCSV is negative at small currents, and positive at high currents [15].

There are several factors promoting equalizing of current between transistors connected in parallel [16]. The first factor is that transistors should have the same temperature that is achieved by mounting them on one radiator. In this case crystal temperatures differ only slightly, that promotes lowering of current disbalance. Line current increase (second factor) leads to greater voltage drop on all the transistors, thus promoting an even more uniform distribution [15]. The third factor is connection of pre-selected transistors with similar voltage drops. This enables achieving a current difference of less than 5 % [17, 18]. If transistors are not selected, then the non-uniformity of current distribution is increased with increase of their number that eventually will lead to failure of one of them. Welding current rectifier diodes are also connected in parallel in power sources. Diodes with the same voltage drop should be used to reduce currents disbalance [18].

In addition to non-uniform current distribution in statics, there exists non-uniform current distribution in dynamics. This is caused by different times of transistor switching on and off and threshold voltages of transistor activation. Selection of transistors with similar dynamic characteristics is practically not used. Therefore, to reduce current disbalance in dynamics, it is rational to connect a resistor into control circuit of each transistor [18]. Non-uniformity of current distribution at transistor switching is caused by inductances of connecting conductors [19]. Application of IGBT modules eliminates the problem of reducing the non-uniform distribution of current between discrete transistors and diodes for the developer [20].

Power source output voltage can be controlled by several methods. The first is variation of inverter supply voltage, for instance, using a chopper. The second method consists in application of controllable welding rectifier of output voltage. The third, most often used method, is inverter regulation [21]. Regulation can be performed by pulse-width modulation (PWM), PWM with a controllable phase shift (PWM-PS), frequency variation (PFM) or combinations of these methods. PWM is the simplest and most often used method. In bridge inverter arm transistors are switched simultaneously at PWM. If arm transistors are switched with a time shift (PWM-PS) dynamic losses and interference can be reduced. At PWM application, variation of pulse duration is possible at constant duration of the pause or at its variation at constant pulse duration. Frequency method is most often used in budget or self-made sources [6, 11].

Source reliability and energy efficiency are strongly influenced by the processes of transistor switching. At the moments of switching a high power is released in the transistor crystal, which causes accelerated ageing of the crystals. Application of chains of capacitors, diodes and resistors (snubbers) allows directing transistor current to a capacitor at the moments of switching [21, 22]. In the pauses between switching, energy stored in the capacitor dissipates in the resistor, thus increasing the temperature inside the source. At short pauses between switching the capacitor does not have enough time to discharge, and snubber effectiveness decreases. More complicated chains with an additional inductance ensure energy recovery [4, 5, 21]. Efficient snubbers are quite cumbersome. The simplest method to improve transistor switching conditions and their operating safety is switching off supply voltage from the inverter at the moments of switching by an additional transistor. Modern IGBT transistors can briefly transmit maximum admissible

current at maximum admissible voltage drop in them. Therefore, no special devices are used in many sources to form the path of transistor switching. Often just one high-frequency capacitor is applied to power the inverter, located as close as possible to the transistors.

Transistor voltage should not exceed the maximum admissible value, even briefly. Switching overvoltages caused by wire inductances may reach hundreds of volts. Overvoltage drop is achieved by reduction of the area of current flowing circuit inside the inverter [20, 21, 23]. Limitation of switching overvoltages is achieved also by designing circuits of minimum area. Application of transistor-diode modules reduces overvoltages.

Another method to lower dynamic losses and overvoltages is application of resonance inverters, in which transistor switching occurs at zero current or voltage [5, 6, 21, 24–27]. High-frequency transformer primary winding is most often connected in series with capacitor C and inductance L. In this case transistor switching occurs at zero current. Capacitor also eliminates the direct component of magnetization current. Circuits with parallel connection of C, L and primary windings are applied less frequently. Inverter should provide a wide range of adjustment of voltage and current at load variation in the range from short-circuiting to open-circuit mode. Under such conditions it is difficult to ensure transistor switching without current in all the modes. Therefore, in some cases dynamic losses of resonance inverter can exceed the losses in regular inverters. Resonance inverters are the most often applied in sources with power supply from 220 V mains. Current is regulated by frequency method. Transistor switching at zero current occurs at maximum welding current and minimum frequency. At frequency increase circuit impedance rises, and welding current decreases. Capacitor voltage during the resonance can reach several kilovolts [6, 11]. Investigation and design of a resonance source by analytical methods is a challenge, it is more convenient to model it using MatLab, MicroCap and other packages [26].

Current consumed from the mains by welding inverter has a pulsed component, which is due to input capacitor charge. Pulsed currents are particularly significant at power supply from single-phase mains. This increases the mean-root-square value of the consumed current and distorts the mains voltage. Application of power factor correctors (PFC) reduces the mean-root-square current, and allows increasing the welding current at the same mains voltage. This is particularly urgent for power sources connected to a low-power network [4]. A simple enough and effectively operating PFC can be constructed by converter circuit with voltage increase (Figure 6). PFC output voltage is 400 V that allows application of current transformation coefficient 5/1 and reducing transistor current. The same circuit can be applied at power supply from three-phase mains. Further reduction of mains distortions requires more sophisticated control algorithms and circuits [4, 28]. Power correctors on the whole make the power source more complicated and increase the cost. Therefore, despite the advantages, they are seldom used.

For a good ignition of the arc and prevention of its extinction, source open-circuit voltage should be 60–80 V. At 200 A current arc voltage is not more than 24 V. If transformer transformation coefficient ensuring smooth voltage adjustment in the range from 0 up to 80 V is used, transistors will transmit higher current by short pulses in the operating mode. This increases energy losses and necessitates application of transistors with higher admissible current. Therefore, it is advantageous to apply transformers, in which maximum secondary voltage is equal to nominal arc voltage, and apply an additional low-power source with a steep-falling characteristic to increase the open-circuit voltage. To avoid using a separate inverter, increased voltage for low-power rectifier can be obtained from an additional winding of the main transformer. Another method is application of secondary voltage multiplier [6]. Pilot current in the arc will be maintained all the time that lowers the requirements to smoothing choke inductance.

Transistors and diodes fail at voltage exceeding the above limit values even for a short-time. Therefore, it is extremely important to provide high-speed overvoltage protection. Overvoltages develop during switching processes in the inverter proper, at arc extinction or may come from the mains. Overvoltages are smoothed using damping chains, and maximum value is limited

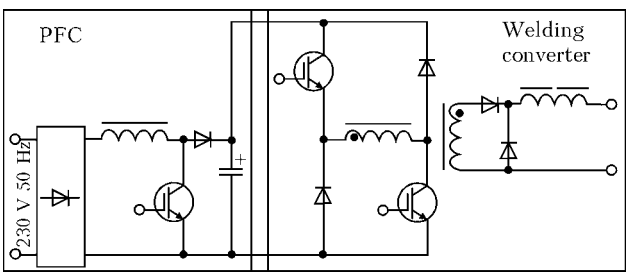

Figure 6. Circuit of source with PFC

by stabistors [21]. Stabistors are the most often used to protect the transistor gate, as voltage can rise uncontrollably at switching because of the capacitance between the gate and collector. Stabistors increase the capacitance of the control circuit that may lead to high-frequency generation. Much more seldom stabistors protect collector-emitter terminals, even though it improves the reliability. Quite often *RC* chains and stabistors protect welding current rectifier diodes [4, 6, 12]. Inverter power capacitors are charged at mains voltage connection. To prevent short-term current rise that may lead to malfunction of input rectifier diodes, a resistor is connected in series, which is shunted by relay contacts after capacitor charging. Such a circuit is used practically in all single-phase power sources.

In addition to overvoltages, exceeding current level, temperature, operation in active mode and high-frequency generations are hazardous for the transistor. It is rational to envisage partial protection from such hazardous impacts using drivers, which can be made in the form of one microcircuit or as a hybrid version. The latter type features greater functional capabilities [29]. One microcircuit case can contain drivers to control the inverter upper and lower arms. To simplify the circuit, upper arm driver is powered from the capacitor, charged from lower driver power source at closed lower transistor. Hybrid version drivers often have a built-in power source of upper arm circuit. Drivers provide a delay between switching on the upper and lower arm transistors, eliminating through currents. To prevent transistor operation in the active region, transistor voltage in off condition is monitored [30]. Driver can have built-in protection from current exceeding the admissible value. A shunt connected into emitter circuit of the lower transistor or additional transistor terminal can be used as current sensor. More advanced drivers can distinguish between a soft and hard short-circuit. Soft short-circuit occurs in the load, connected to inverter by a cable with inductance. Hard short-circuit runs inside the inverter and is much more hazardous. Drivers determine the short-circuit type, while changing the switching-off algorithm. The most functionally complete are drivers based on digital technology, providing adaptation for specific application conditions [31].

Inverter power sources enable controlling electrode metal melting and transfer. Lincoln Electric developed a method of metal transfer in CO_2 welding by surface tension forces (Surface Tension Transfer). Its main advantages are lower spatter, welding process stability, and less fumes. In Russia similar control is applied by Company «Tekhnotron» in welding root welds of pipelines [32]. Investigation of metal transfer by surface tension forces was earlier performed at PWI and Institute of Electrodynamics of the NAS of Ukraine [2, 3, 33].

Fronius Company developed a method to control metal transfer with CMT trademark (Cold Metal Transfer). During short-circuiting the wire is drawn back, current stops flowing, and the drop goes into the pool without spatter. Product heating and harmful substances evolution are reduced. Similar work on acceleration of metal transfer with pulsed wire feed was performed at PWI in 1970s [34]. In CMT Advanced voltage polarity on the electrode is changed during short-circuiting. Negative polarity increases electrode melting rate. At positive polarity controlled precision transfer of metal is ensured. Ratios of positive and negative polarities are determined individually [35].

Lorch Company combined several control algorithms under a common Speed trademark — SpeedMaster [36]. Compared to regular pulsed-arc welding SpeedPulse reduces drop diameter and increases their number. Metal transfer becomes similar to jet transfer. Penetration and efficiency increase by 48 %. SpeedArc technology is designed for narrow-gap single-pass welding of up to 15 mm thick metal. Increased electrode extension promotes wire preheating and increase of melting rate by 30 %. Similar investigations of automatic control systems in welding with longer extension were begun in 1970s [37, 38]. SpeedUp technology is used for vertical semi-automatic welding. In the hot phase of arcing increased current melts the material. At the cold stage low current ensures precise filling of the groove. A similar method is given in [39]. Holder movement path in vertical semi-automatic welding was studied and algorithms of feed rate control allowing achievement of an even lower spatter and greater efficiency, were proposed in the same work. SpeedRoot technology is designed for welding the weld root with up to 8 mm gap by MIG/MAG processes. Controlled oscillations of weld pool in electrode direction are induced. Drop transfer into the pool occurs at short-circuiting without any current at the moment of pool movement away from the electrode that lowers the metal temperature.

Kemppi Company presents their control algorithms under Wise trademark. Semi-automatic and automatic welding of weld root with a gap

is performed by WiseRoot technology with transverse oscillations of the electrode. Control system controls the entire pool volume and periodically switches wire feed off, allowing time for metal cooling down. WiseThin technology allows welding up to 0.6 mm metal.

In [40] it is shown that welder's hand movements may be imposed on the speed of wire movement to item surface, thus increasing metal losses and impairing weld formation. Stabilizing the real rate of wire feed into the arc allows lowering the spatter. A particularly pronounced effect of wire feed rate regulation can be achieved in vertical welding. Such a control technique is not used so far in batch production.

Development of automatic control systems is restrained by absence of more profound information on the welding process. Similar to many years ago, welding current and voltage still remain the main feedback signals. It is convenient to measure arc voltage in the power source case. In reality this signal includes voltage drops on inductances of cables supplying current from the source to the arc, voltage drop at the point of contact of the wire with the tip. At short-circuiting at the final stage of bridge breaking up voltage drop does not exceed several volts and its rapid changes are filled with interferences with a close frequency spectrum. Effective control of welding requires knowledge of instantaneous dimensions of the drop and pool, their temperature and composition of evolving gas. This information could be obtained using video sensors. However, the high temperature of the arc, spattering, portable torch and control system sophistication prevent their application. For control system operation it is necessary to know the speed of wire movement to the arc. Wire feed rate is often measured by motor armature emf. The error of such a measurement is equal to tens of percent. Real speed of wire movement into the arcing zone differs even more, because of elastic deformations of wire in the hose, periodical stopping as a result of electrode welding to the current conducting tip, and welder's hand motions. Not knowing the main welding parameters, it is impossible to make a good control system.

In the control system block-diagram inverter dynamic characteristics can be presented by a link with pure delay $T/2$, equal to half of output voltage period. Microprocessor control system can be also presented by a link with pure delay, the value of which depends on the control algorithm and microprocessor response speed. Choke in the welding circuit is used for smoothing the rectified voltage ripple. For good smoothing of current ripple, time constant of welding circuit should be significantly higher than T. Control system uses current and voltage feedbacks, the signals from which should be filtered with time constants, which are much higher than T. Therefore, the total time of links with pure delay and time constants of the block-diagram is equal to several milliseconds. Final stage of breaking up of the bridge between the electrode and pool proceeds in several milliseconds [2, 33]. Chaotic motions of the drop at electrode tip in MAG welding are in the kilohertz frequency range. Therefore, modern power sources are not capable of reacting to many fast processes in the arc.

Development of transistor power sources began in 1950s with appearance of crystals. During the Soviet period many developments were performed, which were ahead of their time. They are now being put into production by leading companies under various trademarks. As the component base is developed, power source capabilities will be enhanced. Promising directions for improvement are increase of reliability of transistor parallel connection, widening the range of transistor soft switching, reliable protection from all, even rare emergency situations. Dimensions of the drop and pool, their temperature and composition of arc gaseous evolutions with be used for feedbacks. Control algorithms will be introduced for operation in microsecond range. Wire feed rate will be regulated depending on welder's hand motions.

1. Drabovich, Yu.I., Lebedev, A.V., Kravchenko, V.V. et al. (1987) Regulation of mechanized CO_2 welding conditions at application of multioperator current sources. *Avtomatich. Svarka*, **10**, 70–71.
2. Lebedev, A.V. (1991) Study of controlled metal transfer in CO_2 welding. *Ibid*., **3**, 33–38.
3. Lebedev, A.V., Gritsenko, N.P., Dovbishchenko, I.V. et al. (1994) Transistor power source for arc welding. *Ibid*., **9**/**10**, 50–51.
4. Advanced circuitry of welding inverters. *http*://radiohobby.org/modules/news/article.php
5. Petrov, S. (2009) Advanced circuitry of welding inverters. *Sovr. Elektronika*, **1**, 36–45.
6. Negulyaev, V.Yu. (2005) *Welding inverter — this is simple*. Kiev.
7. Konev, Yu.I. (1957) Parallel connection of transistors: *Semiconductors and their application*, Issue 1, 41–52.
8. Abramov, A.S., Vigdorchik, V.G., Vedeneev, G.M. et al. (1969) Design of highly reliable power static converters. *Devices of converter engineering*, Issue 3, 82–93.
9. Lebedev, A.V. (1976) Rectification of rectangular voltage. *Problemy Tekhn. Elektrodinamiki*, **57**, 66–69.
10. Nazarov, V.I., Ryzhenko, V.I. (2008) *Welding inverter*. Rybinsk: Oniks.
11. Volodin, V.Ya. (2008) *Self-made up-to-date welding systems*. St.-Petersburg: Nauka i Tekhnika.
12. Borisov, D.A. Electric circuit of welding inverter. *http*://nanolife.info/svarochnoe-oborudovanie/

13. Petrov, S. (2007) Circuitry of industrial welding inverters. *Sovr. Elektronika*, **8**, 42–47.
14. (2002) *Parallel operation of dynex IGBT modules*: Dynex Semiconductor AN5505-1.3. July.
15. Roccaro, A., Filippo, R., Salato, M. (2003) *AC TIG welding: output inverter design basics*: VIR AN-1045. Oct. 2.
16. *Application characterization of IGBTs*: IR AN-990.
17. Drabovich, Yu.I., Ponomarev, I.G. (1974) Study of processes in bridge circuit of inverter at transistor failures. *Problemy Tekhn. Elektrodinamiki*, **45**, 56–62.
18. Kolpakov, A. (2005) Specifics of parallel connection of IGBT modules. *Komponenty i Tekhnologii*, **5**, 31–37.
19. Kolpakov, A. (2008) Switching of signal circuits in power converter systems. *Novosti Elektroniki*, **15**, 25–29.
20. Simkin, Ya., Kolpakov, A. (2002) Specifics of application of the Semikron IGBT power modules. *Elektron. Komponenty*, **6**, 18–16.
21. Lebedev, A.V. (1998) *Transistorized power sources for arc welding*. Harwood Acad. Publ.
22. Meleshin, V.I. (2005) *Transistorized converter devices*. Moscow: Tekhnosfera.
23. Lebedev, A.V., Kravchenko, V.V. (1986) *Lowering of switching overvoltages in pulse converters*: VINITI Dep. 18734. Moskow.
24. Dudrik, J., Dzurko, P. (2006) Arc welder with series-parallel resonant DC-DC converter. *Acta Technica CSAV*, **51**, 415–426.
25. Petrov, S. (2006) Prospects of application of resonance converters as the welding current sources. *Sovr. Skhemotekhnika*, **7**, 16–23.
26. Feldsher, I.F. (2007) Computer-assisted modeling of quasi-resonant inverter power source for arc load. *Matemat. Mashyny i Systemy*, **1**, 117–121.
27. Horvath, M., Borka, J. (2006) Up-to-date, integrated, multifunctional energy converters of welding technologies. In: *Proc. of EPE-PEMC Conf.* (Portoroz, Slovenia, 2006), Vol. 2-11, 70–75.
28. Kim, J.H., Kim, S.S., Won, C.Y. et al. (2001) Harmonic reduction of CO_2 welding machine using single-switch, three-phase boost converter with six order harmonic injection PWM. In: *IEEE ISIT Proc.*, 1526–1529.
29. Krapp, J. (2010) Safety functions of current IGBT drivers. *Silovaya Elektronika*, **5**, 40–48.
30. Nikitin, A. (2006) Up-to-date high voltage drivers of MOSFET- and IGBT transistors. *Novosti Elektroniki*, **6**, 23–31.
31. Hummer, R., Kwiz, P., Wend, M. (2010) IGBT-drivers with program-controlled characteristics. *Silovaya Elektronika*, **5**, 38–39.
32. Getskin, O.B., Getskin, B.L., Poloskov, S.I. (2009) Development of multifunctional inverter source for welding with controlled electrode metal transfer. *Tyazh. Mashinostroenie*, **2**, 16–20.
33. Paton, B.E, Lebedev, A.V. (1988) Control of melting and electrode metal transfer in CO_2 welding. *Avtomatich. Svarka*, **11**, 1–5.
34. Paton, B.E., Voropaj, N.M., Buchinsky, V.N. et al. (1977) Control of welding process by wire feed programming. *Ibid.*, **1**, 1–5.
35. (2009) More possibilities with CMT advanced. *Weld+Vision*, **23**.
36. (2011) *Quality principle*: Industrial Program of Lorch Company.
37. Lebedev, A.V. (1978) Structural diagram of process of arc self-adjustment in short-circuiting metal transfer. *Avtomatich. Svarka*, **5**, 7–12.
38. Lebedev, A.V. (1978) Effect of heat generation in electrode stick-out on arc self-adjustment process. *Ibid.*, **7**, 10–16.
39. Lebedev, A.V. (1986) Control of wire feed rate in mechanized welding of vertical welds. *Ibid.*, **3**, 34–39.
40. Lebedev, A.V., Suprun, S.A. (1978) Efficiency of welding current stabilization in semi-automatic welding. *Ibid.*, **10**, 37–42.

TECHNOLOGY OF REPAIR WELDING OF BOILER UNIT ASSEMBLIES WITHOUT POSTWELD HEAT TREATMENT

A.K. TSARYUK[1], V.D. IVANENKO[1], V.Yu. SKULSKY[1], S.I. MORAVETSKY[1], A.R. GAVRIK[1] G.N. STRIZHIUS[1], M.A. NIMKO[1], S.I. MAZUR[2], A.A. TROJNYAK[2], Yu.V. ODIN[3] O.V. DERKACH[3] and R.I. KURAN[4]

[1]E.O. Paton Electric Welding Institute, NASU, Kiev, Ukraine
[2]Tripolskaya HEPS, Ukrainka, Ukraine
[3]Kremenchugskaya HPP, Kremenchug, Ukraine
[4]OJSC «YuTEM», Bucha, Ukraine

The paper considers repair welding of the damaged assemblies of boiler equipment at heat electric power stations and heat power plants made from heat-resistant steels of the Cr–Mo and Cr–Mo–V systems (collectors, heating surface pipes, T-joints, steam piping elements etc.), which exhausted their life under severe service conditions (at high temperature and pressure) that caused damages in metal mainly in the form of cracks. The technology recommended for repair of such damages involves manual arc welding using the 06Kh1M type electrodes combined with the 09Kh1MF type electrodes. It includes for the use of preliminary and concurrent heating with subsequent thermal recovery of a welded joint. Welded joints made by the suggested technology have high crack resistance and required mechanical properties. Present technology successfully passed the tests in repair welding of boiler equipment assemblies.

Keywords: *repair welding, damages, heat-resistant steels, assemblies of boiler equipment, electrodes, preheating, thermal recovery, extension of life time*

Extension of life time of power equipment for HEPS and HPP with exhausted equipment service life is possible after technical diagnostics and detection of operation damages as well as investigation of metal state (structure and properties). Elements of boiler equipment (heating surface pipes, superheaters, collectors, T-joints, stem piping elements etc.) are manufactured from heat-resistant Cr–Mo or Cr–Mo–V steels. Tables 1–3 [1, 2] show the main grades of steel as for application at operating temperatures, their chemical composition and mechanical properties.

Chromium, molybdenum and vanadium are the main alloying elements of these steels. Molybdenum as one of the main elements determining the steel heat resistance is mainly in a solid solution. It reduces a diffusion mobility of atoms and rate of dislocation movement. Certain content of molybdenum allows obtaining an optimum combination of strength and ductility of steel. Participation of molybdenum in carbide formation is limited at that. Chromium and vanadium carbides are formed at its presence. Vanadium makes a positive effect on increase of long-term strength and creep strength due to formation of heat-resistant carbides. Steels of Cr–Mo system were virtually completely replaced by steels of Cr–Mo–V system in the power units with 545 °C vapor operating temperature at manufacture of boiler equipment and pipelines of domestic HEPS. At the same time the damages caused by operational, technological and structural factors [1, 3] are formed in the boiler units manufactured from indicated steels in a process of long-term operation at high temperature.

Cracks of different type are the most typical damage for the welded joints from heat-resistant steels. Welding and surfacing are the main methods of repair of the damaged parts and assemblies of boiler units. Repair of the damaged parts has specific difficulties related with the necessity of work performance under working conditions of electric power stations. Development of progressive welding technologies as the main method for repair of power equipment is, therefore, an im-

Table 1. Heat-resistant steels used for seamless pipes of collectors and steam piping elements in boiler unit manufacture

Steel grade	Standard		Limiting maximum temperature, °C
	Pipes	Steel	
12MKh	TU 14-3-610–75	GOST 20072–74	530
15KhM	TU 14-3-460–75	TU 14-3-460–75	550
12Kh1MF			570
15Kh1M1F			570

Table 2. Chemical composition of heat-resistant steels of Cr–Mo and Cr–Mo–V systems, wt.%

Steel grade	C	Si	Mn	Cr	Mo	V	Ni	Cu	S	P
							Not more			
12MKh	0.09–0.16	0.17–0.37	0.40–0.70	0.40–0.70	0.40–0.60	–	–	–	–	–
15KhM	0.11–0.16	0.17–0.37	0.40–0.70	0.80–1.10	0.40–0.55	–	–	–	–	–
12Kh1MF	0.08–0.15	0.17–0.37	0.40–0.70	0.90–1.20	0.25–0.35	0.15–0.30	0.25	0.20	0.025	0.025
15Kh1M1F	0.10–0.16	0.17–0.37	0.40–0.70	1.10–1.40	0.90–1.10	0.20–0.35	0.25	0.25	0.025	0.025

Table 3. Mechanical properties of pipes from heat-resistant steels at 20 °C temperature [1]

Steel grade	Heat treatment, °C	σ_t, MPa	σ_y, MPa	δ, %	ψ, %	KCU, J/cm^2
			Not more			
12MKh	Normalization at 910–930 + tempering at 670–690	≥ 410	235	21	45	60
15KhM	Same at 930–960 + 680–730	450–650	240	21	50	60
12Kh1MF	Same at 950–980 + 720–750	450–650	280	21	55	60
15Kh1M1F	Same at 1020–1050 + 730–760	500–700	320	18	50	50

portant and relevant task for extension of life and secure operation of the boiler units of HEPS [4].

Welding of heat-resistant steels of Cr–Mo–V system are as a rule performed using preliminary and concurrent heating as well as postweld heat treatment (PWHT) of the welded joints. Application of welding methods without PWHT is highly perspective considering that performance of the heat treatment of repaired parts and assemblies is not always possible under HEPS conditions. The aim of the present paper in this connection is a development of repair welding technology without PWHT providing high crack resistance and required properties of the welded joints of boiler unit assemblies.

Activities preventing formation of cold cracks in the welded joints are one of the main conditions of repair welding technology. It is well known [5, 6] that combination of three factors, i.e. formation of hardening structures in HAZ or weld metal, content of diffusible hydrogen, and level of residual welding stresses in the welded joints promotes formation of the cold cracks (delayed fracture).

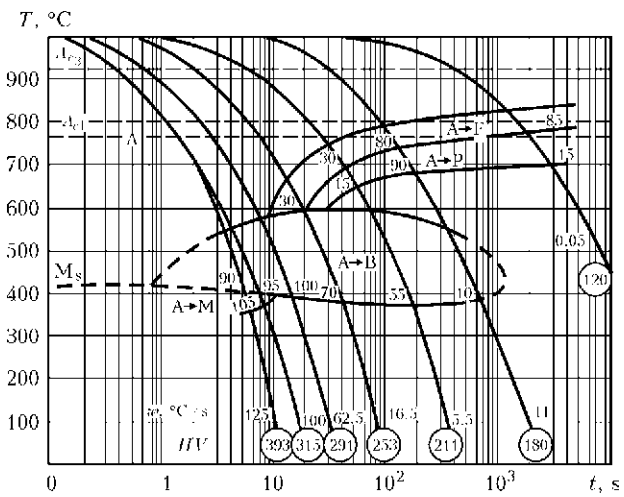

Figure 1. Thermal-kinetic diagram of austenite transformation in 12Kh1MF steel [3]

Selection of heat modes and welding conditions can provide absence of the hardening structures in the welded joint. This is achieved as a rule through application of the preliminary and concurrent heating, at which cooling rate will promote formation of HAZ metal structure stable to crack generation.

High sensitivity to cooling rates starting from austenite decay temperature (A_{c3}) is character for pearlite class heat-resistant steels. Therefore, influence of welding thermal cycle on structure and properties of widely used 12Kh1MF grade steel (Figure 1) under different welding conditions was investigated first of all. It can be seen from given diagram that austenite decay takes place in martensite area with 100 % martensite formation in 800–700 °C temperature interval at cooling rate more than 125 °C/s. Decrease of cooling rate results in formation of structures of intermediate transformation, i.e. bainite. Structure consisting of 30 % ferrite and 70 % bainite is formed already at 16.5 °C/s cooling rate. Thus, structures differing by sensitivity to delayed fracture and promoting obtaining of various mechanical properties of metal [7] can be obtained due to cooling rate regulation. Application of additional activities for regulation of process of welding zone cooling in a form of preliminary and

Table 4. Chemical composition and mechanical properties of metal of welded joints from steel of Cr–Mo–V system [3]

Electrode grade (type)	Chemical composition, wt.%						
	C	Si	Mn	S	P	Mo	Cr
				Not more			
TML-5 (E-06Kh1M) (for welding of root passes)	Requirements according to normative documents (weld metal)						
	0.065	0.025–0.40	0.5–0.7	0.025	0.025	0.45–0.60	0.55–0.80
	Actual values (weld metal)						
	0.044**–0.05***	0.25–0.34	0.56–0.70	0.017–0.021	0.021–0.020	0.51–0.50	0.69–0.72
TML-3U (09Kh1MF) (for groove filling)	Requirements according to normative documents (weld metal)						
	0.08–0.12	0.15–0.40	0.5–0.9	0.025	0.030	0.4–0.6	0.80–1.25
	Actual values (weld metal)						
	0.09	0.30	0.8	0.016	0.025	0.51	1.10

Table 4 (cont.)

Electrode grade (type)	Mechanical properties at 20 °C, not less				
	σ_t, MPa	σ_y, MPa	δ_5, %	ψ, %	*KCU*, J/cm^2
TML-5 (E-06Kh1M) (for welding of root passes)	Requirements according to normative documents (weld metal)				
	550	350	18	60	88
	Actual values (weld metal)				
	580	430	20	69	130****
	Requirements according to normative documents (welded joint)				
	500	–	–	40	–
	Actual values (welded joint)*				
	490	–	16	–	78.5
TML-3U (09Kh1MF) (for groove filling)	Actual values (weld metal)				
	569	481	17	40	160

*Fracture place — base metal (12Kh1MF) at 6–8 mm from the fusion line. **Diameter of electrodes — 3.0 mm. ***Diameter of electrodes — 4.0 mm. ****61 J/cm^2 at –20 °C, 40 J/cm^2 at –40 °C.

concurrent heating or usage of welding providing autoheating of the joint allows, therefore, formation of metal structure resistant to crack generation.

Application of welding consumables providing chemical composition and weld metal structure close to the base metal [8] is necessary for obtaining of the required properties of the welded joints from heat-resistant steels in repair of elements of power equipment operating under temperature above 540 °C. Thus, TML-5 electrodes of E-06Kh1M type (GOST 9467–75) [8–12] were recommended and implemented for repair welding of cast parts of turbine case equipment from steels of Cr–Mo and Cr–Mo–V systems without PWHT. Table 4 shows chemical composition and mechanical properties of metal deposited using TML-5 grade electrodes. These electrodes provide high crack resistance and optimum combination of strength and ductile characteristics of the deposited metal of welded joints from Cr–Mo steels. Therefore, they are also useful for welding of root welds and facing of edges, and electrodes of TML-3U grade (09Kh1MF type) are used for further groove filling in repair welding of the joints from steels of Cr–Mo–V system.

Investigations on Implant method (method of inserts) [13] were carried out for evaluation of Cr–Mo–V system steel resistance to cold crack formation and determination of the necessary preheating temperature in repair welding using TML-3U electrodes. The maximum (critical) stresses in the samples before fracture start were the criterion of welded joint crack resistance. Significant attention at that was also dedicated to investigation of effect of postweld heating (recovery) on crack resistance of the welded joints.

Influence of the conditions of recovery performance on diffusible hydrogen content $[H]_{dif}$ in the deposited metal was preliminary studied.

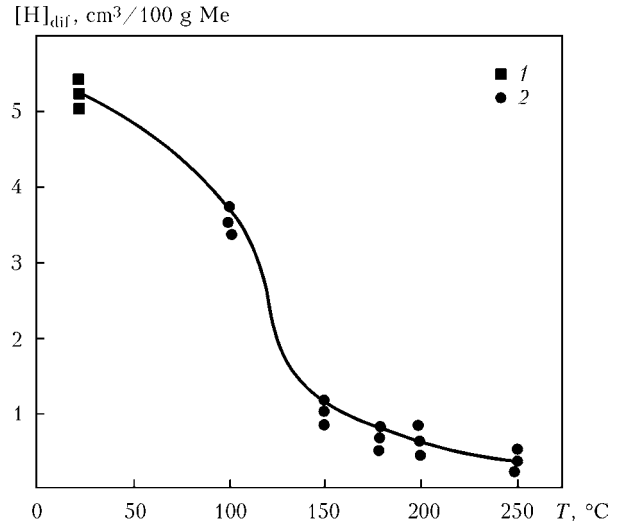

Figure 2. Dependence of content of diffusible hydrogen in deposited metal on heating temperature without recovery (*1*) and at 10 min recovery (*2*)

Considering that its content in the metal deposited using standard TML-3U electrodes has relatively low level (1.5–2.5 cm^3/100 g of metal based on alcohol test), evaluation of recovery effect on $[H]_{dif}$ content of initial higher concentration makes an interest. Pilot electrodes TML-3U were manufactured in this connection. Muscovite was specially included in their coating that provided increased concentration of the diffusible hydrogen. Concentration of $[H]_{dif}$ in the deposited metal made 5.3 cm^3/100 g of metal according to alcohol test after baking of the electrodes at 400 °C during 1.5 h. Holding of these samples of the deposited metal for 10 min at different recovery temperatures significantly reduces content of the diffusible hydrogen (Figure 2). $[H]_{dif}$ = 0.5 cm^3/100 g in thermal recovery at 250 °C that promotes increase of crack resistance of the welded joints.

Heating of pilot joint using electric resistance heater was performed after sample-to-plate welding in testing on insert method for evaluation of recovery effect on crack resistance. Temperature was controlled using chromel-alumel thermocouples in welded-in condition. The samples were hold under load for 24 h. The investigations were performed by stages. Firstly, the joints welded without preheating was tested for evaluation of the level of critical stresses, exceeding of which results in development of delayed fracture. Further a cycle of testing were performed with application of thermal recovery under conditions of load stress, which exceeded the critical one, in order to confirm efficiency of present procedure and determine the parameters of recovery mode necessary for delayed fracture resistance to be provided.

Figure 3 shows results of testing of the welded joints without preheating and further thermal recovery. Investigations performed allowed determining that critical level of stresses makes approximately 150 MPa. The result of study of effect of the postweld recovery showed that the load stress of 200 MPa from a supercritical area does not lead to development of fractures as a result of weakened influence of hydrogen factor (see Figure 2). Therefore, further investigations were performed with load corresponding to 400 MPa stress for fracture initiation. Such a load promotes a fracture. Generalizing dependence was build based on given data (Figure 4) which determines correspondence between the temperature and recovery duration necessary for providing delayed fracture resistance. Present dependence can be a basis for selection of thermal recovery mode.

Thus, obtained results verify high efficiency of the postweld recovery for providing delayed fracture resistance of the welded joints. No phase transformations are observed at that, and favorable conditions are developed in order to remove diffusible hydrogen from the zone of welding [14, 15].

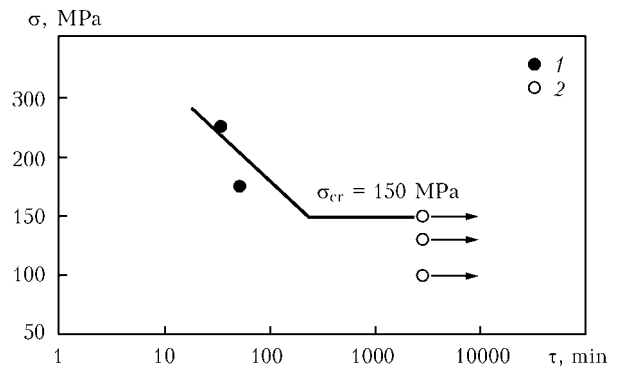

Figure 3. Effect of stresses on tendency of welded joints from 12Kh1MF steel to delayed fracture (*1*), and welded joints without fracture (*2*)

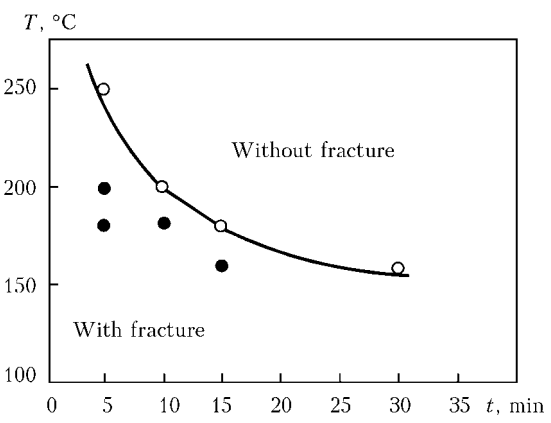

Figure 4. Influence of temperature and duration of thermal recovery on tendency of welded joints from 12Kh1MF steel to delayed fracture in load stress σ = 400 MPa

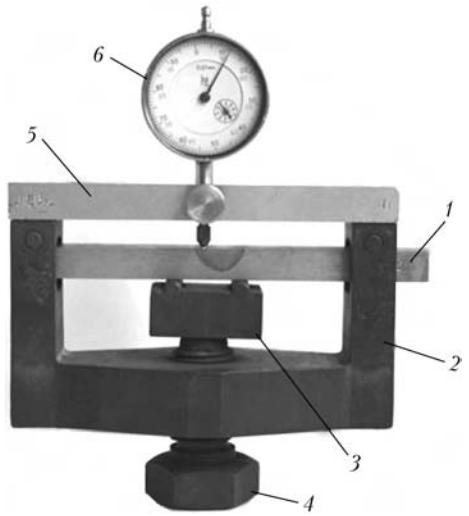

Figure 5. Scheme of device for loading of sample in relaxation tests: *1* — sample; *2* — welded base; *3* — support; *4* — loading screw; *5* — removable plate for indicator fastening; *6* — indicator

Since the level of residual welding stresses is one of the constituent factors determining welded joint cracking resistance, the investigations of influence of temperature of postweld heating (recovery and heat treatment) on a level of stress relaxation were performed. The investigations were carried out in accordance with a procedure proposed by OJSC «I.I. Polzunov SPA TsKT» [16]. The sample of the welded joint from 12Kh1MF steel of 12 × 14 × 210 mm size was set over a support of special device manufactured from heat-resistant nickel alloy, and load was applied up to obtaining specified stress in area of pure bending (Figure 5). The stress was measured depending on bending deflection f using an indicator being fastened over a removable plate. After loading and measurement of elastic bending deflection the device together with loaded sample was put in a furnace heated to specified temperature for defined time. The samples were cooled up to ambient temperature after holding in the furnace, and bending deflection f was repeatedly measured on them. Plastic strains in the samples and relaxation of the stresses depending on time of holding in the furnace at specified temperature and load were calculated on bending deflection differences. Figures 6 and 7 show the results of the investigations.

It was determined that thermal recovery of the studied samples independent on time of holding at 250–350 °C makes no influence on relaxation of the stresses. However, stress drop can be reduced up to 150 MPa level in the welded joint at operating temperature 545 °C. Such a tendency of the welded joints from steels of Cr–Mo–V system to relaxation at operating temperature

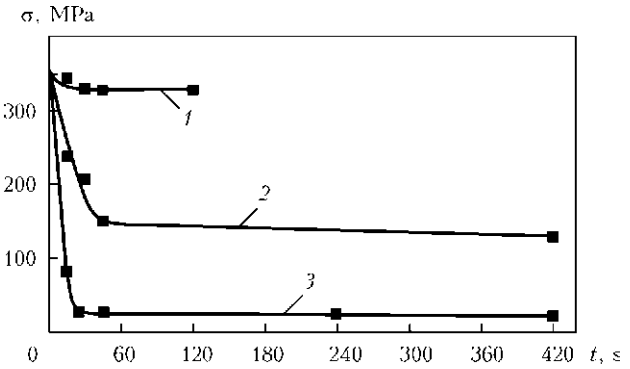

Figure 6. Dependence of stress relaxation in the welded joint samples on holding time and temperature of 250 (*1*), 545 (*2*) and 750 (*3*) °C

provides a real possibility to apply only thermal recovery in a case when performance of postweld high-temperature tempering (730–750 °C) is difficult.

Further operation of the boiler unit at 545 °C operating temperature promotes significant relieve of the residual welding stresses. However, relaxation of the residual stresses at operating temperature is significantly lower than after high-temperature tempering (see Figure 6). Therefore, repaired assemblies of the boiler units without postweld high-temperature tempering can operate with limited life. Decision about further operation is made after performance of routine examination and technical diagnostics.

The results of performed investigations allowed considering a question about the possibility of repair without PWHT during welding-up of the damages in parts of boiler units at the place of operation. Collector of heater from 12Kh1MF steel with outer diameter 273 mm and wall thickness 36 mm was taken as an object of repair using proposed welding technology. Damage in a form of circular crack was formed as a result of stress raiser action (in the corner of root in a backing ring) and propagated along the weld and coarse-grain HAZ up to appearance on the surface. Preliminary evaluation of the proposed technology was carried out in order to take a

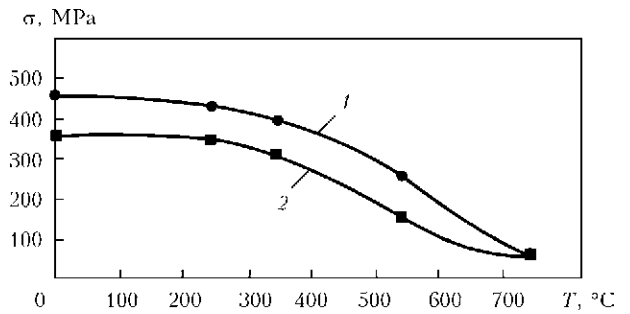

Figure 7. Dependence of stress relaxation on temperature in short-time loading ($\sigma = 0.8\sigma_y$) (*1*) and 60 min thermal recovery at $\sigma = 0.8\sigma_y$ (*2*)

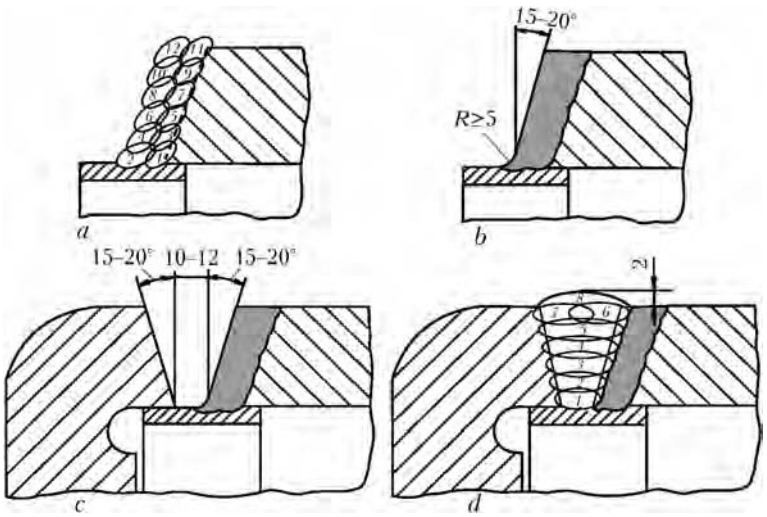

Figure 8. Scheme of order of collector repair performance: *a* — preliminary multilayer surfacing of collector end by circular beads with their successive performance; *b* — shape of groove after machining preliminary deposit; *c* — assembly for welding of bottom to collector joint; *d* — filling the groove by multilayer welding

technical decision about possibility of performance of repair welding without PWHT. Evaluation tests [17] were carried out on collector model with actual wall thickness. Magnetic particle testing of crack absence was carried out after machining end of the collector for preliminary surfacing of edge. The backing ring was tacked to the end edge from an outside with 250–300 °C preheating. Preliminary double layer surfacing of collector end (Figure 8, *a*) was carried out with 250–300 °C preheating by multilayer method using circular beads 4–5 mm thick and 15–20 mm width applying E-06Kh1M (TML-5) type electrodes. Electrodes of 3 mm diameter (I_w = 90–110 A) were used for the first layer, and electrodes of 4 mm diameter (I_w = 120–160 A) for the second one. After that the deposit surface was treated by an abrasive tool up to obtaining of the necessary size and shape of the edge (Figure 8, *b*) with quality evaluation using visual, ultrasonic and magnetic testing methods and hardness measurement. Than assembly of collector to bottom joint (Figure 8, *c*) over backing ring was carried out.

Preheating in the collector to bottom assembly and welding made 250–300 °C. The first two root welds were made using TML-5 electrodes of 3 mm diameter (I_w = 90–120 A). They allow obtaining more ductile deposited metal due to low content of carbon and chromium as well as absence of vanadium. This prevents possibility of lamellar tearing formation in the weld root and provides high crack resistance of the welded joints. TML-3U 4 mm electrodes (I_w = 130–180 A) were used for further groove filling (Figure 8, *d*). Complete thermal recovery of the welded joint at 250 °C during 2.5 h was performed immediately after welding for evacuation of diffusible hydrogen and increase of crack resistance. Slow cooling of zone of repair welding up to 50–70 °C was carried out after thermal recovery by means of wrapping of the repair place by asbestos cloth. Then outer surface of the circular weld was mechanically treated up to obtaining of the joint of required shape (see Figure 8, *d*). Non-destructive quality testing was the final stage. Visual and ultrasonic testing, and surface etching with 15 % solution of nitric acid were used for detection of surface defects in evaluation of repair quality. Performed testing of quality of evaluated joint showed no defects in the welded joint.

Investigations of the mechanical properties showed that tensile strength of the welded joint was in the limits of 490–560 MPa in tensile testing of the samples, and impact toughness of the deposited metal made 120–160 J/cm^2 that corresponds to the requirements to the base metal of this steel (σ_t = 440–588 MPa and $a_n \geq 98$ J/cm^2).

Carried out metallographic investigations of marco- and microstructure determined no defects in the weld metal and HAZ. Hardness of the weld metal makes *HB* 180 at allowable values of reduction of medium hardness up to *HB* 140 and increase not more than *HB* 270 for 12Kh1MF steel.

Thus, positive results were obtained after performed evaluation tests of repair welding of collector from 12Kh1MF steel using developed technology. This allowed making the technical decision and recommending the proposed technology of repair welding for the collector from 12Kh1MF steel.

CONCLUSIONS

1. Technology of repair welding of standard heat-resistant steel 12Kh1MF being widely used in manufacture of the boiler units of HEPS and HPP was developed and its weldability was investigated.

2. Preliminary and concurrent heating together with postweld low-temperature recovery can be used for repair of damaged assemblies and parts of the boiler units from heat-resistant steels in acting HEPS and HPP in the case when performance of high-temperature tempering is impossible. Further running at operating temperature 545 °C promotes reduction of the residual welding stresses (up to the level of around 150 MPa) that allows extending resource of the repaired boiler unit for limited period up to the next examination.

1. Khromchenko, F.A. (2002) *Service life of welded joints of steam pipelines*. Moscow: Mashinostroenie.
2. Melekhov, R.K., Pokhmursky, V.I. (2003) *Structural materials of power equipment*. Kiev: Naukova Dumka.
3. Anokhov, A.E., Korolkov, P.M. (2003) *Welding and heat treatment of case power equipment in repair*. Kiev: Ekotekhnologiya.
4. Anokhov, A.E., Khromchenko, F.A., Fedina, I.V. (1986) New technology of repair welding of chrome-molybdenum steel parts without heat treatment. *Svarochn. Proizvodstvo*, **10**, 15–17.
5. Makarov, E.L. (1981) *Cold cracks in welding of alloy steels*. Moscow: Mashinostroenie.
6. Shorshorov, M.Kh., Chernyshova, T.A., Krasovsky, A.I. (1972) *Weldability tests of metals*. Moscow: Metallurgiya.
7. Shorshorov, M.Kh., Belov, V.V. (1972) *Phase transformations and changes of steel properties in welding*. Moscow: Nauka.
8. Khromchenko, F.A. (2005) *Welding technology in repair works*. Moscow: Intermet Engineering.
9. *RD 108.021.112–88*: Repair of defects in cast case parts of turbines and fittings by welding-up methods without heat treatment. Moscow.
10. Anokhov, A.E., Ganiev, F.B., Korolkov, P.M. (2003) Improvement of technology of repair welding and heat treatment is the base of service life prolongation of vapor turbines. *Montazhn. i Spets. Raboty v Stroitelstve*, **7**, 7–11.
11. Anokhov, A.E., Korolkov, P.M. (2006) *Welding and heat treatment in power engineering*. Kiev: Ekotekhnologiya.
12. Tsaryuk, A.K., Ivanenko, V.D., Volkov, V.V. et al. (2009) Repair welding of turbine case parts from heat-resistant steels without subsequent heat treatment. *The Paton Welding J.*, **12**, 32–36.
13. Kasatkin, B.S., Brednev, V.I., Volkov, V.V. (1981) Procedure of examination of deformation kinetics at delayer fracture. *Avtomatich. Svarka*, **11**, 13.
14. Kozlov, R.A. (1969) *Hydrogen in welding of hull steels*. Leningrad: Sudostroenie.
15. Kozlov, R.A. (1986) *Welding of heat-resistant steels*. Leningrad: Mashinostroenie.
16. Demyantsevich, S.V., Zemzin, V.N. (1979) Procedure of evaluation of welded joint susceptibility to cracking in heat treatment. *Trudy TsKTI*, **169**, 22–27.
17. *RTM-1s–89 (RD 34 15.027–89)*: Welding, heat treatment and testing of pipe systems of boilers and pipelines in mounting and repair of power plant equipment. Moscow: Energoizdat.

MODERN METHODS OF SURFACING THE TOOLS OF AGRICULTURAL TILLERS AND HARVESTERS (Review)

V.S. SENCHISHIN and **Ch.V. PULKA**

Ternopol I. Puluj National Technical University, Ternopol, Ukraine

It is shown that application of induction surfacing is the most promising for flat parts of agricultural machinery with wall (BM) thickness of 2.0–6.0 mm and deposited metal (DM) thickness of 0.8–2.0 mm. In this case, minimum mixing of BM and DM, minimum equipment cost, possibility of mechanization and automation are provided.

Keywords: *surfacing processes, electric contact strengthening, agricultural machinery tools, thin parts, induction surfacing, automation*

Thin flat parts are widely applied in agriculture as tools of tilling and harvesting machinery, namely: plough shares, cultivator hoes, skim plough discs, shredder knives, etc. which operate under the conditions of abrasive wear and considerable static and dynamic loads. These parts should have high strength and wear resistance [1–4]. However, during operation the metal continuously contacts the soil and plants that, in its turn, leads to blade blunting. To ensure the cutting properties, the tools should sharpen themselves during operation. Bimetal (two-layer) working parts are the most suitable for these conditions. Their strength is ensured by base material from which the tool is made, and wear resistance and self-sharpening are provided by

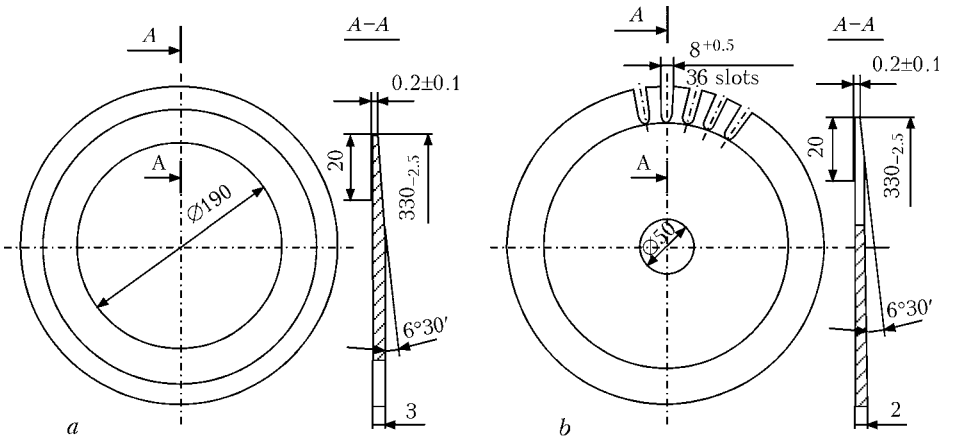

Figure 1. Schematic of disc cutter design [12]: *a* — nondriven; *b* — driven

the cladding layer deposited on the base metal. Self-sharpening depends on the ratio of thickness and wear resistance of base and cladding layers [5]:

$$\omega = \frac{\varepsilon_2 h_2}{\varepsilon_1 h_1},$$

where ε_1, ε_2 is the resistance of base and cladding layers, respectively; h_1, h_2 is the thickness of the base and cladding layers, respectively.

The best self-sharpening is provided at $\omega = 1.5$.

Various surfacing processes are applied for tool strengthening, namely: electric contact, plasma, electric arc, explosion cladding, induction and other strengthening techniques [4, 6–11].

Known is a method of surfacing agricultural machinery tools, using electric contact strengthening [4, 6 12, 13]. With this method the filler material can be powders, wires and strips. The principle of the technology is application on the part surface of a powder-like wear-resistant hard material (charge), strip and wire with their subsequent heating up to the temperature, at which their sintering and formation of a strong diffusion bond with the part take place. This technology is applied at strengthening of tiller disc cutters, which should have a wear-resistant cutting edge and should sharpen themselves in operation.

Figure 2. General view of machine for strip welding to skim plough disc based on up-graded MShPR-300/1200 machine [1]

Figure 1 shows disc knives, surfaced by powder-like hard alloy by electric contact method, and Figure 2 shows a machine for strip welding to skim plough disc [1, 12].

In [13] a technological process of electric contact surfacing of a share by flux-cored wire of segmented cross-section is proposed. In this case, the process of flux-cored wire surfacing runs in two stages: cold compacting of the powder core and, as a consequence, deformation of filler materials in the zone of contact with the part; surfacing process proper, which provides heating of flux-cored wire at the segment top, in the zone of intensive heat evolution, deformation propagation to peripheral zones, melting and welding of the shell to the base with simultaneous sintering of the powder core. Figure 3 shows a share surfaced by the above technology.

Advantages of this process are absence of base metal penetration, minimum deformations of surfaced parts, ability to deposit thin layers, high heating rate, which may reach several thousand degrees per second. A disadvantage is a low efficiency of the process, absence of batch-production of the equipment, and non-uniform quality of the deposited metal, as well as complexity of manufacturing flux-cored wire of segment section.

Figure 3. General view of surfaced plough [13]

To obtain bimetal tools, namely skim plough discs, it is proposed to apply the process of electric contact cladding by a wear-resistant strip [14]. To ensure the specified strength and elasticity disc knives are subjected to bulk quenching and tempering before cladding. Scale formed during rolling and heat treatment, is removed by etching in 20 % sulphuric acid solution with addition of 1 % inhibitor OP-1, heated up to the temperature of 70 °C. After etching, washing and drying, the disc is considered to be fit for strip cladding. The main disadvantages of this method are high labour consumption of preparatory operations, complexity of strip manufacturing from highly wear-resistant alloys, and low strength of welded layers.

Methods of cladding by explosion and rolling are used to strengthen the working surfaces of various flat parts, including tiller tools [15]. Advantages of explosion cladding include the high speed of the process, ability of joining metals, which cannot be produced or are difficult to produce by other methods, and relative simplicity of the technology (absence of the need for application of complex equipment) [15]. In Czechia explosion cladding technology was used in production of bimetal knives and other flat parts. Compared to traditional metallurgical process of casting cladding, explosion surfacing application is technically and economically substantiated

PWI developed and tried out a method of producing a wear-resistant bimetal at rolling of packets with powder PG-C1 [16], which is based on the principle of auto-vacuum pressure welding. In [17], this process was applied to produce tool bimetal with a cladding layer of PR 10R6M5 powder. The main disadvantage of the process is making a large-sized packet, related to the need for powder compaction to create a minimum volume of air in the packet cavity that is eliminated using powder pre-pressing. In [18] it is shown that at manufacture of bimetal sections for tiller tools cladding layer powder PG-S1 was first compacted by the method of hot isostatic pressing. However, industrial application of this technology is prevented by complexity and high labour consumption.

Works [7, 8, 19–21] describe the technology of plasma surfacing, which is applied in manufacturing of multiblade metal-cutting tools (end mills, etc.), as well as cutting edges of disc and flat cutters of various purpose. Powders of high-speed steels, as well as vanadium-containing alloys, are used as surfacing materials. This surfacing process allows comparatively easily controlling the energy, heat and gas-dynamic parameters of a plasma jet in wide ranges, that eventually allows obtaining a deposited layer with specified physico-chemical and mechanical properties.

Technology of plasma-powder surfacing of paper cutting machine knives was developed. Resistance of batch-produced knives without surfacing is determined by their wearing time, dependent on strength, hardness, mechanical properties and some other characteristics of steel [7, 8, 20]. Blank for surfacing has a groove, which allows practically eliminating deformation after surfacing and edge effect arising at edge surfacing. Paper-cutting knives were surfaced by plasma-powder method for several steel types and alloys. After surfacing the blank is subjected to two-times annealing at the temperature of 540–560 °C, cutting, straightening and machining.

The advantages of plasma-powder surfacing are slight penetration of base metal, high quality of deposited layer, and possibility of deposition of thin layers (1–5 mm), using a wide range of filler materials. The disadvantages include relatively low efficiency and need for complex and expensive equipment, as well as high requirements to size distribution and shape of powder granules that makes its cost much higher, and this limits the application of this process.

To improve the performance of tiller tools (shredder knives, cultivator hoes, plough shares and other parts) PWI proposed spot strengthening using arc surfacing with PP-AN170 flux-cored wire [22]. Height of strengthening spot is equal to 1–3 mm, and base metal penetration depth is 2–4 mm. Surfacing is performed at reverse polarity. Penetration depth at spot strengthening is regulated by changing the current, voltage and arcing time. Figure 4 shows the general view of a plough share surfaced by flux-cored wire, before and after service. A disadvantage of this process is high labour and material costs for manufacturing the parts.

In [10, 23–25] the technology of strengthening the working surfaces of cultivator hoes by local strengthening is proposed. The essence of this method consists in that beads are deposited on the hoe outer surface by arc surfacing with 40 mm step at 25° angle to the hoe blade. Figure 5 shows the general view of the strengthened hoe. A disadvantage of this method are high labour costs and non-uniformity of bead deposition, which depends on welder's qualifications.

Also known is the technology of improvement of tiller tool wear resistance by carbonization of

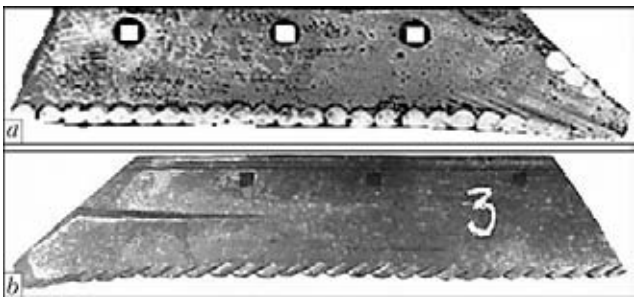

Figure 4. General view of surfaced share before (*a*) and after (*b*) service [22]

the surface layer by carbon electrode [26]. The principle of the method consists in that at carbon electrode contact with the part, carbon from the electrode goes into the base metal as a result of a spark discharge, forming on its surface a cementite layer, the hardness of which is much higher than that of base metal. This method was not widely accepted, because of the complexity of the technological process.

Works [11, 27] propose the technology of reconditioning and strengthening of plough shares by brazing on metal-ceramic plates. The essence of this method consists in that hard alloy plates in a continuous and intermittent arrangement are brazed-on from the face side of the share blade. To realize the process, a slot of 1.5–2.0 mm depth is milled out, then L63 braze alloy is placed into it, on which T15K6 and VK8 metal-ceramic plates are placed later on. Braze alloy heating is performed by the flame process, after brazing-on the share is placed into a thermo-insulating tank, heated up to the temperature of 620 °C, together with which it cools down to room temperature (Figure 6).

The main advantage of tool strengthening by metal-ceramic plates is lowering of draught resistance, which allows the machine working speed to be increased, thus increasing ploughing efficiency.

A disadvantage of this process are high cost and labour consumption related to the technology of part manufacturing.

Figure 6. General view of share strengthened by metal-ceramic plates [11]

Other methods of tiller tool strengthening were also developed. They include surfacing using electronic amplifier [28], laser surfacing [29–31], etc. However, because of the complexity of the technology and lack of equipment, its imperfection and high cost, these processes have not found any industrial application so far.

Induction surfacing method is widely used for strengthening thin flat parts, including agricultural machinery tools. In [32–34] a technology of simultaneous induction surfacing of thin shaped discs over the entire working surface is proposed. Surfacing is performed using a special charge, consisting of a mixture of wear-resistant powder-like hard alloy and flux. Charge is applied on the part surface in the form of a layer of the required thickness (Figure 7). After that the part is placed inside the inductor (Figure 8), in which the power source is a high-frequency generator. At passage of high-frequency currents through the inductor, eddy currents are induced in the surface layers of the part to be surfaced, which heat the part, and the charge melts from its surface [32]. Advantages of the method include ability of thin layer deposition, high efficiency, ability of mechanization and automation of the process. The disadvantages are a high energy consumption, base metal overheating, and filler materials should be lower-melting than the base metal. Despite the above-said, this method is the most widely accepted in the enterprises manufacturing agricultural machinery, ploughs, skim ploughs, cultivator hoes, etc. [32].

To improve the labour conditions and process efficiency at induction surfacing of thin flat parts, in particular bits and hoes of cultivators, the authors developed semi-automatic machines

Figure 5. General view of hoe after local strengthening [10]

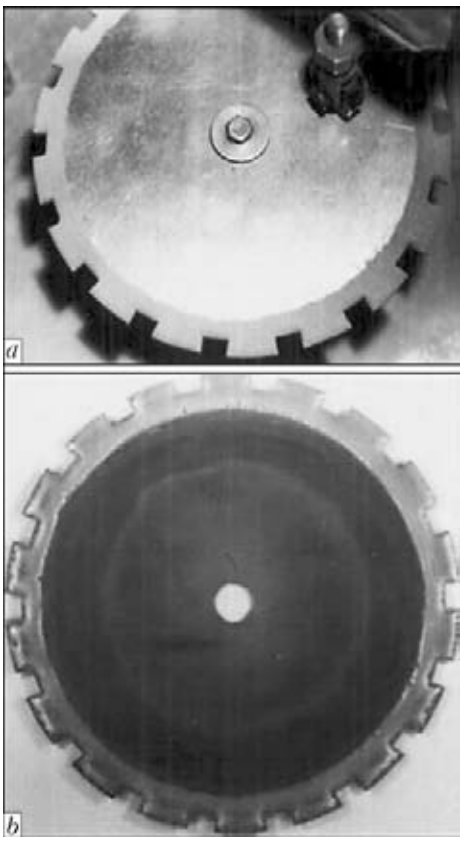

Figure 7. Device for charge filling (*a*) and surfaced disc (*b*) [34]

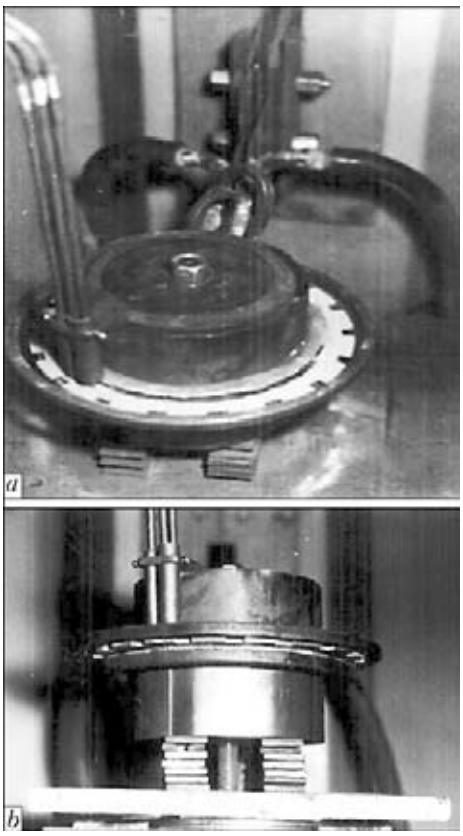

Figure 8. Device for surfacing the disc in two-turn circular inductor [34]: *a* — top view; *b* — side view

and automatic lines [33]. For surfacing of cultivator knives having a curvilinear cutting surface, carousel-type units are applied, in which wedge-shaped shears can be surfaced. The main disadvantage of these lines and machines is a low efficiency of the surfacing process proper, as well as low level of mechanization in terms of blank loading, charge filling and unloading.

To improve the efficiency of the process of induction surfacing of thin shaped discs — shedder knives of beet harvesters — by continuous-successive and simultaneous surfacing methods, production lines were developed and put into production [32], which allow mechanization and automation of the process, including loading and unloading of the blanks, and their movement in the rotor device, placing them in the positions of charge filling and surfacing and removal after surfacing.

Improvement of induction surfacing of thin flat parts is performed in the following directions: improvement of wear resistance of the deposited metal layer, optimization of the heating mode in order to save power, as well as design parameters of inductors and heating systems for surfacing discs of arbitrary diameters and surfacing zone dimensions, proceeding from technology needs, without allowing for shielding of electromagnetic fields and allowing only for electromagnetic shielding, as well as combined shielding of electromagnetic and thermal fields simultaneously; mathematical simulation of the surfacing process to determine residual stresses, strains and displacements of parts; mechanization and automation of surfacing processes taking into account ecological compatibility of the process and protection of man from the impact of electromagnetic and thermal fields [32].

To improve wear resistance of deposited metal of tillers, in [35–39] it is proposed to apply part vibration after surfacing. The essence of this method consists in that a large number of microshocks with the respective frequency and amplitude of 0.5 mm, which are caused by the impact of processing tool oscillations, are successively applied to the deposited layer for 20 s. The main advantage at application of this technology is development of a uniform and more fine-grained structure of the deposited layer, that leads to 25 % increase of deposited metal hardness. High labour consumption and cost related to application of additional technological operations after surfacing, should be regarded as the disadvantages of this process.

Works [40–42] describe the technology of vibration treatment of welded joints of oil and gas

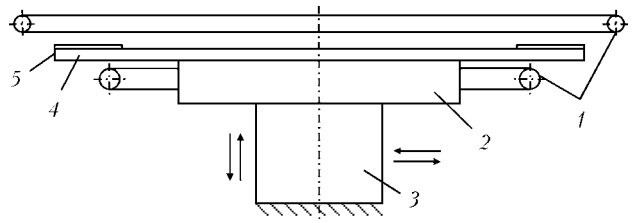

Figure 9. Schematic of induction surfacing of thin flat parts with vibration application during surfacing: *1* — inductor; *2* — table; *3* — vibrator (arrows show direction of vibration application); *4* — part; *5* — powder-like hard alloy

equipment. This technology allows lowering the level of residual stresses and strains, arising after welding. It, however, has not yet become widely accepted, because of the complex technological process and equipment.

Further improvement of induction surfacing technology is achieved using horizontal and vertical vibration to increase the wear resistance and lower the deformation of thin flat parts, which consists in that vibration at a certain frequency and amplitude (Figure 9) is introduced, when the powder-like wear-resistant hard alloy starts melting and it is continued up to its complete melting and solidification [43]. Wear resistance and lower deformations are achieved due to formation of a fine-grained structure and more favourable distribution of carbides in the deposited metal, compared to surfacing without vibration. The authors developed methods and devices for surfacing thin flat parts with application of horizontal and vertical vibrations. Conducted investigations of the structure, wear resistance and hardness of the deposited metal showed its advantages compared to the currently available methods of induction surfacing and need to develop a mathematical model of the process, which would allow assessment of the influence of mechanical vibrations on the physical essence of refinement of deposited metal structure and its service properties.

Results of improvement of the process of induction surfacing of agricultural machinery tools, conducted by the authors with introduction of horizontal and vertical vibration, were published in [43–46].

Thus, analysis of the modern surfacing methods showed that for thin flat parts of tillage agricultural machinery, including discs, with base metal and deposited layer thickness of 2.0–6.0 and 0.8–2.0 mm, respectively, the most widely accepted and promising method is induction surfacing without base metal mixing with the deposited metal. This method is the most readily adaptable to fabrication due to application of simple equipment, simplicity of the surfacing process proper, and no requirement of a high qualification of surfacing operators, and possibility of process mechanization and automation (that is important in batch production). It is being constantly improved in terms of increasing the efficiency, wear resistance, and uniformity of deposited metal layer thickness, power saving, as well as lowering part deformation.

1. Tkachev, V.N. (1971) *Wear and increase in service life of agricultural machine parts*. Moscow: Mashinostroenie.
2. Bol, A.A., Leskov, S.P. (1985) Induction surfacing of parts in agricultural machine-building. In: *Surfacing. Experience and efficiency of application*. Kiev: PWI.
3. Vishnevsky, A.A., Kostylev, Yu.A., Ostrov, D.D. (1978) Technology of fabrication of built-up disc cutters. In: *Surfacing of parts of metallurgical and mining equipment*: Coll. Moscow: NIIInformtyazhmash.
4. Pulka, Ch.V. (2003) Hardfacing the working components of tillage and harvesting agricultural machinery (Review). *The Paton Welding J.*, **8**, 35–40.
5. Rabinovich, A.Sh. (1962) *Self-sharpening plough shares and other tiller tool parts of machines*. Moscow: GOSNITI.
6. Nikolaenko, M.R., Rymorov, E.V. (1976) *New technological processes of arc and contact surfacing of rapidly wearing parts of building and road machines*. Moscow: TsNIITEstrojmash.
7. Gladky, P.V., Pereplyotchikov, E.F., Ryabtsev, I.A. (2007) *Plasma surfacing*. Kiev: Ekotekhnologiya.
8. Bouaifi, B., Gebert, A., Heinze, H. (1993) Plasmapulverauftragschweissung zum Veschleissschutz abrasiv beanspruchter Bauteile mit Kantenbelastung. *Schweissen und Schneiden*, **9**, 506–509.
9. Denisenko, M.I., Vojtyuk, V.D. (2011) Increase in service reliability of tools of tillage machines. Pt 1 *Nauk. Visnyk Nats. Univ. Bioresursiv*. Series Technique and power engineering of agricultural sector, Issue 166, 274–284.
10. Kobets, A.S., Pugach, A.M. (2010) Methods and processes of increase in wear resistance of tools of cultivators. *Visnyk Dnipropetr. DAU*, **1**, 61–63.
11. Kuznetsov, Yu.A., Goncharenko, V.V. (2007) Repair and strengthening of plough shares with cermet plates. *Vestnik Ros. GAZU*, **2**, 122–123.
12. Turkin, V.P., Putilin, V.G., Nikolaenko, M.P. et al. (1978) Electric contact surfacing of disk cutters. *Avtomatich. Svarka*, **2**, 74–76.
13. Volkov, D.A. (2012) *Improvement of technology of sparcelly-alloyed surfacing of wear-resistant alloy using flux-cored wire*: Syn. of Thesis for Cand. of Techn. Sci. Degree. Kramatorsk.
14. Mamuliya, G.E., Murov, G.F., Tyuleneev, V.P. et al. (1984) Contact cladding of tillage machine tools. *Svarochn. Proizvodstvo*, **2**, 37–39.
15. Gelman, A.S., Tsemakhovich, B.D., Chudpovsky, A.D. et al. (1978) *Explosion cladding of steel*. Moscow: Mashinostroenie.
16. Ryabtsev, I.A. (1981) Bimetallic rolled metal with clad layer of granular powder PG-S1. In: *Abstr. of 3rd Republ. Sci.-Techn. Conf. on Current Methods of Surfacing and Consumables* (Kharkov, 1981), 9–10.
17. Kalner, V.D., Goryushina, M.N., Sichuzhnikova, A.A. (1984) Processes of interaction in interface of bimetallic billets produced by method of nonsintered powder rolling. *Metallovedenie i Termich. Obrab. Metallov*, **3**, 28–29.
18. Fedorov, B.N., Osadchy, V.A., Tits, M.Yu. et al. (1975) Prospects of application of compact materials in bimetallic parts of agricultural machine tools. *Traktory i Selkhozmashiny*, **9**, 39–41.
19. Ryabtsev, I.A. (2004) *Surfacing of machine and mechanism parts*. Kiev: Ekotekhnologiya.

20. Pereplyotchikov, E.F., Ryabtsev, I.A., Gordan, G.M. (2003) High-vanadium alloys for plasma-powder cladding of tools. *The Paton Welding J.*, **3**, 14–17.
21. Pereplyotchikov, E.F. (2005) Plasma cladding. *Remont, Vosstanovlenie, Modernizatsiya*, **12**, 35–40.
22. Denisenko, M., Opalchuk, A. (2011) Wear and increase in service life of agricultural machine tools. Pt 2. *Visnyk Ternopil. NTU*, **2**, 201–210.
23. Kobets, A.S., Kobets, O.M., Pugach, A.M. (2011) Field investigations of wear of hoes with local strengthening. *Visnyk Khark. NTU im. P. Vasylenka.* Series Mechanization of agricultural production, **107**, 208–213.
24. Mikhalchenkov, A.M., Tyureva, A.A., Mikhalchenkova, M.A. (2007) Increase in wear resistance of plough shares by deposition of strengthening beads in zone of maximum wear. *Remont, Vosstanovlenie, Modernizatsiya*, **9**, 17–19.
25. Vasilenko, M.O. (2008) Prospects of local strengthening application in manufacturing and repair of tools. *Tekhnika APK*, **1**, 29–31.
26. Kirgizov, V.E., Shishkin, G.M., Baldanov, K.P. et al. (2010) Increase in service life of plough shares in repair by carbon electrode surfacing. *Vestnik IrGSKhA*, Issue 38, 65–70.
27. Goncharenko, V.V., Ferbyakov, A.V., Kuznetsov, Yu.A. et al. (2006) Repair and strengthening of share cutting edge by brazing of cermet plates. *Mekhanizatsiya i Elektrifikatsiya Selsk. Khoz.*, **11**, 21–22.
28. Fominsky, L.P., Levchuk, M.V., Bajsman, A.F. et al. (1987) Surfacing of agricultural machine tools using electron accelerator. *Svarochn. Proizvodstvo*, **11**, 4–6.
29. Ivashko, V.S., Yaroshevich, V.K., Luzan, P.G. et al. (2006) Strengthening of rapidly-wearing parts of tillage machines. *Mizhvidom. Nauk.-Tekhn. Zbirnyk Kirovograd. NTU*. Series Design, manufacturing and service of agricultural machines, Issue 39.
30. Kovalenko, V.S., Merkulov, G.V., Strizhak, A.I. (1981) *Laser beam strengthening of parts*. Kiev: Tekhnika.
31. Solovykh, E.K., Aulin, V.V., Bobrytsky, V.M. (2005) Analysis of wear pattern of tillage part edges and increase in their resource using laser technologies. *Design, manufacturing and service of agricultural machines*, Issue 35, 153–159.
32. Pulka, Ch.V. (2006) *Technological and power efficiency of induction melting of thin steel discs*: Syn. of Thesis for Dr. of Techn. Sci. Degree. Kiev.
33. Shably, O.M., Pulka, Ch.V., Korol, O.I. (2008) Main directions in induction surfacing of agricultural machine tools. *Visnyk Ternopil DTU*, 13(**4**), 100–109.
34. Shably, O.M., Pulka, Ch.V., Senchishin, V.S. et al. (2011) Development of energy-saving heating system for induction surfacing of agricultural machine parts. *Ibid.*, **4**, 107–120.
35. Bilovod, O.I., Dudnikov, A.A. (2007) To problem of wear resistance of tools of beet harvesters. *Visnyk Khark. DTU im. P. Vasylenka.* Series Mechanization of agriculture, Issue 59 (**1**), 288–293.
36. Dudnikov, I.A., Kivshik, A.P., Dudnikov, A.A. (2009) *To problem of influence of vibration treatment on material deformation of treated parts*: Transact. Issue 39, 167–169.
37. Dudnik, V.V. (2011) Evaluation of structure of strengthened layer of pough edge. *Vostochno-Evrop. Zhurnal Pered. Tekhnology*, **4/7**, 4–6.
38. Dudnikov, A.A., Gorbenko, O.V., Bilovod, O.I. (2006) Strengthening treatment with vibrating deformation. In: *Transact. of Lugansk NAU*, **68/91**, 86–88.
39. Babichev, A.P., Babichev, I.A. (2008) *Principles of vibration technology*. Rostov-na-Donu.
40. Sutyrin, G.V. (1975) Study of mechanism of low-frequency vibration impact on weld pool crystallization. *Avtomatich. Svarka*, **5**, 7–10.
41. Khafizova, O.F., Bolobov, V.I., Fajrushin, A.M. et al. (2011) To influence of vibration treatment on mechanical properties of dissimilar welded joints. *Neftegazovoe Delo*, **1**; *http://*www.ogbus.ru/authors/Khafizova/Khafizova_1pdf/
42. Salmin, A.N., Fajrushin, A.M., Ibragimov, I.G. (2010) Study of influence of vibratons during welding on operational strength and mechanical properties of 11Kh11N2V2MF steel welded joints. *Ibid.*; *http://*www.ogbus.ru/authors/Salmin/Salmin_1.pdf
43. Pulka, Ch.V., Shably, O.N., Senchishin, V.S. et al. (2012) Influence of vibration of parts on structure and properties of metal in surfacing. *The Paton Welding J.*, **1**, 23–25.
44. Pulka, Ch.V., Senchishin, V.S. *Device for surfacing of thin shaped discs*. Pat. 59994 UA. Int. Cl. V23K 13/00. Fil. 05.11.2010. Publ. 10.06.2011.
45. Pulka, Ch.V., Senchishin, V.S. *Method of surfacing of steel parts*. Pat. 64371 UA. Int. Cl. V23K 13/00. Fil. 18.03.2011. Publ. 10.11.2011.
46. Shably, O.N., Pulka, Ch.V., Senchishin, V.S. et al. *Method of surfacing of flat steel parts*. Pat. 54204 UA. Int. Cl. V23K 13/00. Fil. 28.05.2010. Publ. 25.10.2010.

EXPERIENCE IN HARDFACING OF PROPELLER SHAFTS AT THE PJSC KHERSON SHIPYARD

Zh.G. GOLOBORODKO
PJSC Kherson Shipyard, Kherson, Ukraine

The industrial experience in repair arc hardfacing of marine propeller shafts is described. Data on the upgraded hardfacing machine and on the peculiarities of selection of shafts with defects to repair them by the hardfacing technology are given.

Keywords: *arc hardfacing, modernized installation, propeller shaft, cyclic loading, wear, restoration, industrial experience*

At the marine and river ships the parts of many mechanisms and devices (propeller shafts, spindles, rudder pins etc.) operate under conditions of cyclic loading and effect of corrosion environment. Under the influence of aggressive environment and other factors the surfaces of the parts are subjected to corrosion, intensive wear, thus leading to coming out of order of parts. The propagation of surface cracks can result in unpredicted fractures at cyclic loading.

The ship propeller shafts, spindles, rudder pins relate to the category of critical ship parts which bear considerable alternating loadings during their service. They remain under supervision of the Russian Maritime Register of Shipping (RMRS) and high requirements are set to their restoration. This is the reason why NA «Mortekhsudoremprom» approved RD 31.52.82–88 «Ship propeller shafts. Restoration using electric arc hardfacing by pearlite and chromium-nickel steels».

At the «Kherson Shipyard» to make hardfacing of propeller shafts of diameter up to 400 mm under flux the installation is applied, mounted on the base of the machine RM 461E for gas cutting of pipes with smooth control of speed of shaft rotation and dependent movement of electrode along the element of a shaft (Figure 1).

Figure 1. Hardfacing installation on the base of machine RM 461E

The installation is equipped with hardfacing head from feeding mechanism of the semi-automatic machine PDG 508M and flux hopper (Figure 2, *a*). In capacity of power source the rectifier VS 630 is used. The hardfacing of the first (experimental) propeller shafts was carried out according to the program approved by RMRS.

Propeller shafts with wear, corrosion fractures, cracks and collapses around the cone, under linings and in the rest part of a shaft, as well as corrosion cavities and other surface defects which can be the sources of fatigue cracks initiation are subjected to restoration surfacing. The shafts having such defects of depth of not more than 5 % in the limits of calculative (according to RMRS regulations) diameter of a shaft are admitted to restoration. During the wear exceeding 15 mm per side the restoration of shafts using surfacing is not admitted. The surface of a shaft subjected to surfacing should be machined until complete elimination of defects and should not have traces of dents, corrosion fractures, cracks, laminations, non-metallic inclusions.

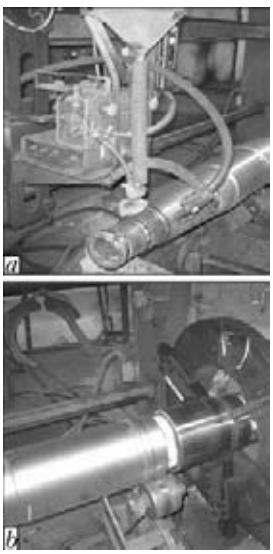

Figure 2. Hardfacing head of the installation (*a*) and shaft mounted in cartridge (*b*)

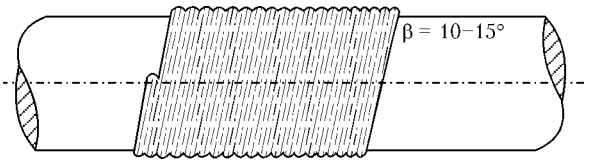

Figure 3. Scheme of one-pass hardfacing along the spiral line

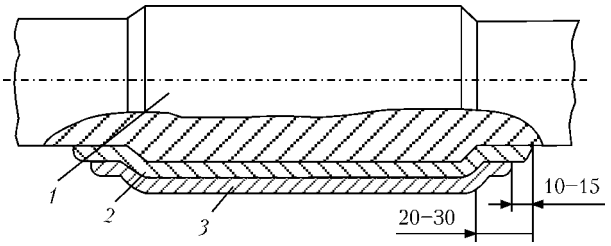

Figure 4. Scheme of performing anti-corrosion surfacing of shaft: *1* — base metal; *2* — low-carbon metal of deposited sublayer; *3* — high-alloyed austenitic deposited metal

The shaft prepared to surfacing is installed on wheel carriages, inserted into the cartridge (see Figure 2, *a*) and slightly clamped and then adjusted according to the level. After verification the shaft is finally clamped.

The run-out of deposited surfaces should not exceed 0.1 mm. The cartridge serves only for shaft rotation. The shaft should fit to wheeled carriages. It is prohibited to insert shaft into the cartridge using crane to prevent impacts of a shaft against the cartridge.

The restoration of worn surfaces is performed along the spiral line with overlapping of neighboring beads according to the scheme given in Figure 3.

To protect the propeller shafts and spindles, manufactured of conventional steels, from the influence of aggressive environment, their surface is deposited with lining of high-alloyed metal resistant against corrosion in sea water. The deposition of stainless corrosion-resistant layer of austenite steel on the propeller shafts, spindles and other parts should be performed only along the sublayer of low-alloyed steel (Figure 4). The sublayer of low-carbon steel is deposited using wire of grade Sv-08A, Sv-08AA under flux AN-348A or OSTs-45. The thickness of sublayer should be not less than 3–4 mm.

To obtain corrosion resistant layer the surfacing under the fluxes of grades AN-20 or AN-26 is applied using wire Sv-08Kh20N9G7T having high technological properties and providing high quality of deposited metal and, at their absence, the welding wires Sv-06Kh19N9T or Sv-04Kh19N11M3 are used. The thickness of corrosion-resistant deposited layer should be not less than 5.0–6.5 mm.

Figure 5. Propeller shaft as-assembled with screw

Chemical composition of wire Sv-04Kh19N11M3 and deposited metal, wt.%

Material	C	Mn	Si	Cr	Ni	Mo
Wire Sv-04Kh19N11M3	0.04	1.03	0.25	18.40	11.4	2.9
Deposited metal	0.07	–	–	16.07	10.0	2.9

To reduce the mixing of corrosion-resistant metal with low-carbon metal the first layer of austenite steel is deposited at the moderate conditions with low heat input at as lower as possible penetration depth of sublayer.

One of the deposited propeller shafts, as-assembled with a screw before mounting to the ship, is shown in Figure 5.

The investigation of stainless steel corrosion-resistant layer, deposited using wire Sv-04Kh19N11M3 under the layer of flux AN-26S to protect the propeller shaft of 200 mm diameter against corrosion in sea water, was carried out. The deposition was performed along the sublayer of low-carbon steel under the supervision of RMRS. To decrease mixing of corrosion-resistant metal with low-carbon metal of sublayer, the first layer was deposited using wire Sv-04Kh19N11M3 at moderate modes with low heat input at lower penetration depth of sublayer: I_w = 190 A; U_a = = 27 V; v_h = 24 m/h; electrode stickout 20 mm; shifting of electrode from zenith 14 mm; diameter of electrode is 2 mm.

During investigation of microstructure of fusion zone of corrosion-resistant deposited layer with sublayer of low-carbon steel no defects were detected. The results of chemical analysis of wire Sv-04Kh19N11M3 and the metal deposited by it are given in the Table.

The investigations showed that accepted technology allows conducting surfacing of propeller shafts with high quality and according to the requirements of RD 31.52.82–88.

In recent years at the «Kherson Shipyard» the hardfacing of more than 80 propeller shafts of different diameters of ships being in repair was performed.

EFFECT OF FLUX COMPOSITION ON THERMAL-PHYSICAL AND PHYSICAL-CHEMICAL PROCESSES IN LIQUID-METAL ELECTROSLAG SURFACING

O.G. KUZMENKO
E.O. Paton Electric Welding Institute, NASU, Kiev, Ukraine

The effect of fluoride silicon-free fluxes ANF-6, ANF-25 and ANF-1P, and low-silicon fluxes AN-15 and AN-15M on thermal-physical and physical-chemical processes occurring in liquid-metal electroslag surfacing (LMESS) of dies was assessed. Experimental results allow a conclusion that flux AN-15M is most preferable for LMESS of forming dies. It allows rapid and uniform melting of the surfaces of dies, as well as keeping the composition of the deposited metal almost unchanged, compared to the initial metal of steel 5KhNM chips at up to 50 % desulphurisation degree.

Keywords: *electroslag surfacing, dies, liquid metal, thermal-physical processes, carbonisation, desulphurisation*

The possibility of providing a sound joint in liquid-metal electroslag surfacing (LMESS) depends in many respects on thermal-physical properties of the applied flux, which determine stability of the electroslag process, character of distribution of the electric current in the slag pool, intensity of heat release in it and heat transfer to the metal pool, duration and uniformity of heating of the base metal surface, and degree of its cleaning from oxides [1].

In addition, during LMESS the slag, deposited metal and graphite of non-consumable electrodes, which support the electroslag process, interact between each other for quite a long time at high temperatures (up to 1900 °C). This may lead to a substantial change in composition and properties of both slag and deposited metal, which is inadmissible.

It is a known fact that the use of basic fluxes allows the liquid metal to be refined [2]. However, this may lead to carbonisation [3]. The degree of carbonisation grows with increase in the content of calcium oxide, and decreases with increase in the concentration of silica in slag [4, 5]. According to the data of study [4], when adding 15–20 % SiO_2 to slag of the CaF_2–Al_2O_3–CaO system no carbonisation takes place, and refining properties of the slag remain good. Also, it is noted that the equilibrium content of carbon in the liquid metal depends on its composition [6].

Therefore, the task of this study was to assess the effect of various fluxes on thermal-physical and physical-chemical processes in ESS that cause a change in the composition of metal and slag, as well as to determine the most suitable flux for the LMESS process.

Fluoride silicon-free fluxes ANF-6, ANF-25 and ANF-1P, as well as low-silicon fluxes AN-15 and AN-15M were chosen for the study (Table 1). Temperature dependences of viscosity and elec-

Table 1. Standard chemical composition of fluxes under investigation, wt.%

No.	Flux grade	CaF_2	CaO	$Al2O_3$	SiO2	MgO	MnO	Fe_2O_3	S	C
1	AN-15	20–23	14–18	22–25	24–29	8–11	1.5–2.5	≤ 0.85	≤ 0.05	–
2	AN-15M	16–20	29–33	36–40	6–10	≤ 2	≤ 0.9	≤ 0.8	≤ 0.07	–
3	ANF-1P	≥ 90	≤ 5	≤ 3	≤ 2.5	–	–	≤ 0.5	≤ 0.05	≤ 0.1
4	ANF-6	Base	≤ 8	25–31	≤ 2.5	–	–	≤ 0.5	≤ 0.05	≤ 0.1
5	ANF-25	50–60	10–15	12–20	2–7	10–15	–	≤ 0.5	≤ 0.07	≤ 0.1

Note. Flux AN-15M may contain 2.0–5.5 % NaF.

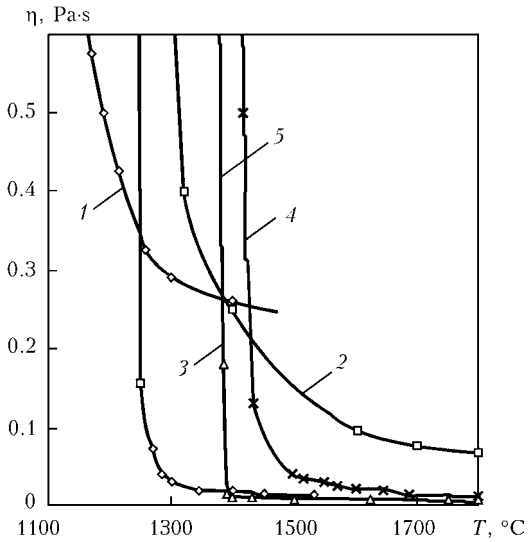

Figure 1. Dependence of viscosity of fluxes on temperature: *1–4* — here and below the grades of fluxes correspond to those given in Table 1

trical conductivity of these fluxes are shown in Figures 1 and 2 [7–9].

The experiments were conducted at the E.O. Paton Electric Welding Institute by using machine A-550 and at the Tokmaksky Press-Forging Factory by using machine OB-2213 for surfacing of 5KhNM steel billets of different standard sizes with liquid steel of the same grade.

Preliminarily the molten flux, i.e. slag, was poured on the surface of a solid billet (forging, worn-out die) placed in a copper water-cooled mould, and electroslag heating of the billet up to its incipient melting was performed by using graphitised electrodes. Then the liquid metal melted in an induction furnace was poured on the thus prepared surface through a layer of the molten slag. After pouring of the required amount of metal, it was solidified under the slag layer by gradually decreasing the power of the electroslag process.

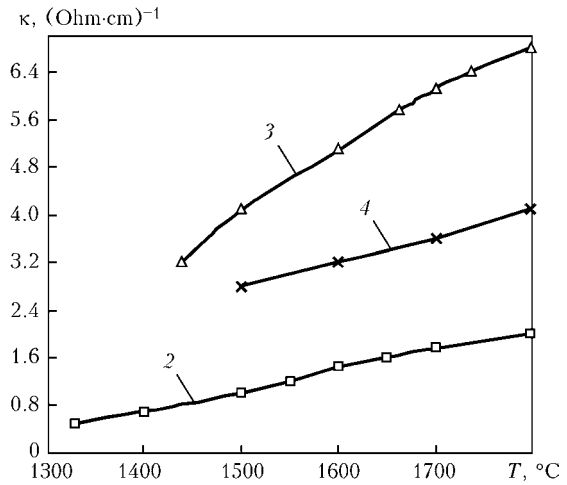

Figure 2. Dependence of electrical conductivity of fluxes on temperature

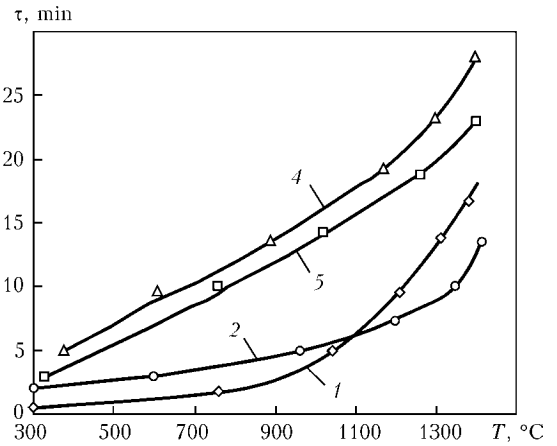

Figure 3. Intensity of electroslag heating of surfaces of dies measuring 210 × 210 × 50 mm (specific power $150 \cdot 10^4$ W/m^2, voltage 35 V)

In ESS the temperature of the slag was maintained within 1550–1800 °C, the depth of the slag pool being 50–60 mm. The slag temperature was measured by using a tungsten-rhenium thermocouple with a tip of boron carbonitride. The temperature of the billet being surfaced was measured at the centre and at the ends by using the similar thermocouples caulked under its surface at a depth of 5 mm. Samples for chemical analysis of metal and slag were taken before and after the experiment.

As shown by the experiments, in case of using more conducting fluoride fluxes ANF-1P, ANF-6 and ANF-25 the electroslag process performed under the same conditions as in case of using the low-silicon fluxes was unstable, and often changed into the arc one. This phenomenon aggravated with increase in voltage, and became particularly pronounced when using flux ANF-1P, which has the highest electrical conductivity. Moreover, it was hard to regulate gradually because of a dramatic change in the electric current with deepening of electrodes into the slag pool. Therefore, in the case of using the fluoride fluxes, to provide gradual regulation of the current and improve stability of the process it should be performed at a deeper slag pool than in the case of using the low-silicon fluxes.

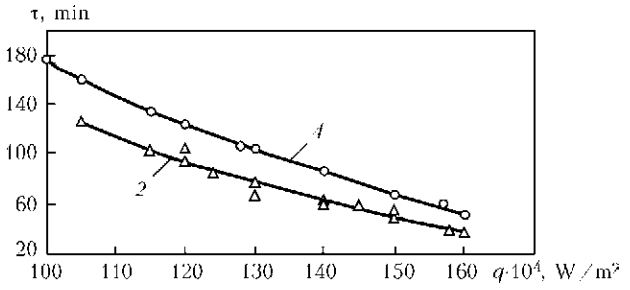

Figure 4. Effect of specific power q on duration of electroslag heating of die billets measuring 400 × 200 × 180 mm up to incipient melting

Table 2. Changes in chemical composition of deposited metal during the LMESS process depending on the flux grade

Type of deposited metal	Flux grade	Weight content of elements and its relative change η_E, %							
		C	η_C	Si	η_{Si}	Mn	η_{Mn}	S	η_S
Steel 5KhNM	AN-15	0.58 / 0.59	+1.7	0.41 / 0.53	+29.3	0.48 / 0.65	+35.4	0.025 / 0.020	−20
	AN-15M	0.55 / 0.56	+1.8	0.40 / 0.39	−2.5	0.52 / 0.53	+1.9	0.023 / 0.013	−43.5
	ANF-1P	0.55 / 0.63	+14.5	0.21 / 0.01	−95.2	0.55 / 0.19	−65.5	0.019 / 0.009	−52.6
	ANF-6	0.52 / 0.58	+11.5	0.37 / 0.16	−56.8	0.58 / 0.29	−50	0.025 / 0.015	−40.0
	ANF-25	0.52 / 0.55	+5.8	0.33 / 0.18	−45.5	0.61 / 0.29	−52.5	0.021 / 0.009	−57.1
Steel 5KhNM (DSTU 3953–2000)	–	0.5–0.6	–	0.1–0.4	–	0.5–0.8	–	≤0.03	–

Notes. 1. $\eta_E = \frac{([E_{end}] - [E_b])}{[E_{end}]} \cdot 100$ %, where $[E_b]$ and $[E_{end}]$ — contents of an element before the beginning and after the end of the process, respectively. 2. Values for $[E_b]$ are given in the numerator, and values for $[E_{end}]$ are given in the denominator. 3 η_C and η_S — degrees of carbonisation and desulphurisation, respectively. 4. Sign «+» means increase in the content of an element, and sign «−» — decrease. 5. As no significant decrease in the contents of chromium, nickel and molybdenum took place, they are not indicated in the Table.

Compared to the more conducting fluoride fluxes, when using the low-silicon fluxes the process of heating of the die surfaces was faster and less power-consuming (Figure 3). This difference was observed in heating over a wide range of specific power values (Figure 4). Lower electrical conductivity of the low-silicon fluxes requires that electrodes be immersed deeper into the slag pool to let pass the required amount of the current. So, it makes it possible to bring the zones of active heat release closer to the surface of the base metal being heated.

The fluxes investigated can be ranked as follows in uniformity of heating of the surface treated: AN-15M, AN-15, ANF-6, ANF-25 and ANF-1P. The difference in temperatures on the die surface (plane size 550 × 380 mm) in heating before melting under slag AN-15M is 240 °C, and under slag ANF-6 — 400 °C. This is related to the fact that a higher temperature of the slag pool is achieved, and a more intensive stirring of the latter occurs when using the less conducting low-silicon fluxes, thus providing increase in uniformity of heating.

The possibility of rapid and simultaneous setting of the electroslag process at all electrodes, which determines to a considerable degree the uniformity of heating of the billet surfaced, also depends on the thermal-physical properties and composition of a flux applied. When using refractory fluxes, after melting them and pouring into the mould the surface of the slag pool is rapidly covered with a crust, which hampers

Table 3. Change in chemical composition of slag during the LMESS process depending on the flux grade

Flux grade	CaF_2	CaO	$Al2O_3$	SiO2	MgO	MnO	Fe_2O_3	S	C
AN-15	21.0 / 18.9	17.3 / 18.7	22.7 / 22.4	26.9 / 24.9	9.5 / 9.3	2.40 / 2.30	0.51 / 0.44	0.007 / 0.006	0.030 / 0.025
AN-15M	20.8 / 19.8	29.2 / 29.7	39.3 / 37.5	9.3 / 9.9	0.6 / 0.4	0.20 / 0.16	0.28 / 0.37	0.008 / 0.019	0.040 / 0.035
ANF-1P	90.1 / 82.8	5.0 / 6.7	1.8 / 1.6	2.6 / 4.6	–	0.25 / 0.83	0.11 / 0.36	0.007 / 0.014	0.040 / 0.035
ANF-6	65.5 / 62.6	6.8 / 8.6	28.3 / 26.1	2.6 / 5.2	–	0.16 / 0.30	0.16 / 0.29	0.008 / 0.018	0.035 / 0.030
ANF-25	55.8 / 52.6	13.8 / 19.9	14.2 / 11.3	2.2 / 5.2	12.6 / 11.7	0.29 / 0.72	0.27 / 0.45	0.008 / 0.020	0.040 / 0.035

Note. The data before the beginning of the process are given in the numerator, and those after the end of the process — in the denominator.

Table 4. Effect of temperature and composition of slag on the processes of carbonisation and desulphurisation of metal in LMESS

Flux grade	Slag temperature, °C	Weight content of carbon and carbonisation degree η_C, %*				Weight content of sulphur and desulphurisation degree η_S, %**			
		Distance from surface, mm							
		Initial	3	10	90	Initial	3	10	90
ANF-6	1550	0.52	0.58 (11.5)	0.53 (1.9)	0.52	0.025	0.015 (40)	0.018 (28)	0.025
	1750	0.59	0.72 (22)	0.61 (3.4)	0.59	0.021	0.011 (47.6)	0.013 (38.1)	0.023
AN-15M	1550	0.55	0.56 (1.8)	0.55	0.55	0.023	0.013 (43.5)	0.016 (30.4)	0.023
	1800	0.58	0.60 (3.4)	0.59 (1.7)	0.58	0.020	0.010 (50)	0.012 (40)	0.020

*Values of carbonisation degree are given in brackets. ** Values of desulphurisation degree are given in brackets.

deepening of electrodes and inhibits setting of the electroslag process.

In case of using lower-melting point fluxes these operations are easier to perform. For the fluxes under investigation the possibility of rapid setting of the electroslag process grows in the following sequence: ANF-1, ANF-6, AN-15M and AN-15.

Analysis of the deposited metal shows that substantial changes in chemical composition of the deposited metal took place during the process as a result of interaction with fluoride fluxes ANF-1P, ANF-6 and ANF-25 (Table 2). For example, the compositions of sulphur, silicon and manganese decreased, and the composition of carbon increased. The most significant changes in composition of metal as to its content of carbon, silicon and manganese were noted in case of using flux ANF-1P containing 95 % CaF_2. When using flux AN-15, reduction of silicon and manganese takes place, and their contents in metal grows by 30–35 %. The degree of desulphurisation and carbonisation of metal is not high, which is in good agreement with the known data [4].

When using flux AN-15M, the contents of carbon, silicon and manganese in the deposited metal remain almost unchanged. At the same time, the content of sulphur decreases approximately by 44 %. The above changes in chemical composition of metal are in agreement with the corresponding changes in the composition of slag during the surfacing process (Table 3).

For instance, whereas with the fluoride fluxes the contents of silicon and manganese in metal decreased, in slag the contents of their oxides increased. The content of sulphur changed in a similar manner — it decreased in the metal and increased in the slag. An exception is carbon, the content of which always decreases compared to the initial one, which is related to its oxidation with air oxygen or slag components [5].

Increase in temperature of slag ANF-6 to 1800 °C is accompanied by intensification of the processes of carbonisation and desulphurisation of metal (Table 4). Desulphurisation of metal increases with increase in temperature of slag AN-15M as well, but in this case the trend appears to increase in the degree of carbonisation of metal.

Therefore, in LMESS of die tools it is indicated to use flux AN-15M, which makes it possible to rapidly and uniformly melt the die surface, as well as keep the composition of the deposited metal practically unchanged compared to the initial metal of 5KhNM steel chips at a desulphurisation degree of up to 50 %.

1. Kuskov, Yu.M., Skorokhodov, V.N., Ryabtsev, I.A. et al. (2001) *Electroslag cladding*. Moscow: Nauka i Tekhnologii.
2. Voinov, S.G., Shalimov, A.G., Kosoj, L.F. et al. (1970) *Refining of steel by synthetic slags*. Moscow: Metallurgiya.
3. Ponomarev, A.G., Kozlov, Yu.E. (1974) About solubility of carbon in slags. *Izvestiya AN SSSR.* Series Metally, **5**, 10–14.
4. Voronin, A.E., Latash, Yu.V., Nikolaev, V.A. et al. (1976) Investigation of carbonisation of metal in electroslag process with graphitized electrode. *Spets. Elektrometallurgiya*, Issue 32, 22–27.
5. Volkotrub, N.N., Lyuty, I.Yu., Voronin, A.E. et al. (1978) Specifics of the process of cast iron carbonisation in electroslag treatment. *Ibid*., Issue 37, 24–30.
6. Biktagirov, F.K. (2003) Carbon behaviour in electroslag treatment of metals. In: *Proc. of 8th Int. Conf. on Problems of Welding, Metallurgy and Related Technologies* (Tbilisi, Oct. 2003), 255–265.
7. Medovar, B.I., Tsykulenko, A.K., Shevtsov, V.L. et al. (1986) *Electroslag process metallurgy*. Kiev: Naukova Dumka.
8. Makara, A.M., Mosendz, N.A. (1971) *Welding of high-strength steels*. Kiev: Tekhnika.
9. Latash, Yu.V., Fetisova, T.Ya., Voronin, A.E. (1985) Study of electrical conductivity and viscosity of slags (fluxes) of CaF_2–CaO–Al_2O_3–SiO_2 system applied in electroslag technology: Report 3. *Spets. Elektrometallurgiya*, Issue 58, 11–17.

SUBSCRIPTION
FOR «THE PATON WELDING JOURNAL»

If You are interested in making subscription directly via Editorial Board, fill, please, the coupon and send application by fax or e-mail.

The cost of annual subscription via Editorial Board is $324.

Telephones and faxes of Editorial Board of «The Paton Welding Journal»:

Tel.: (38044) 200 82 77, 200 81 45

Fax: (38044) 200 82 77, 200 81 45.

«The Paton Welding Journal» can be also subscribed worldwide from catalogues of subscription agency EBSO.

SUBSCRIPTION COUPON

Address for journal delivery _____

Term of subscription since _____ **20** **till** **20**

Name, initials _____

Affiliation _____

Position _____

Tel., Fax, E-mail

Subscription to the electronic version of «The Paton Welding Journal» can be done at site: *www: rucont.ru*

РУКОНТ
НАЦИОНАЛЬНЫЙ ЦИФРОВОЙ РЕСУРС

We offer for the subscription all issues of the Journal in pdf format, starting from 2009. You can subscribe to individual issues or to the entire archive including all issues over a period of 2009–2011. The subscription is available for natural persons and legal entities.

ADVERTISEMENT
IN «THE PATON WELDING JOURNAL»

External cover, fully-colored:
First page of cover (190×190 mm) – $700
Second page of cover (200×290 mm) – $550
Third page of cover (200×290 mm) – $500
Fourth page of cover (200×290 mm) – $600

Internal cover, fully-colored:
First page of cover (200×290 mm) – $350
Second page of cover (200×290 mm) – $350
Third page of cover (200×290 mm) – $350
Fourth page of cover (200×290 mm) – $350

Internal insert:
Fully-colored (200×290 mm) – $300
Fully-colored (double page A3) (400×290 mm) – $500
Fully-colored (200×145 mm) – $150
Black-and-white (170×250 mm) – $80
Black-and-white (170×125 mm) – $50
Black-and-white (80×80 mm) – $15

- Article in the form of advertising is 50 % of the cost of advertising area
- When the sum of advertising contracts exceeds $1000, a flexible system of discounts is envisaged

Technical requirement for the advertising materials:
- Size of journal after cutting is 200×290 mm
- In advertising layouts, the texts, logotypes and other elements should be located 5 mm from the module edge to prevent the loss of a part of information

All files in format IBM PC:
- Corell Draw, version up to 10.0
- Adobe Photoshop, version up to 7.0
- Quark, version up to 5.0
- Representations in format TIFF, color model CMYK, resolution 300 dpi
- Files should be added with a printed copy (makeups in WORD for are not accepted)